REVIEW

Colloidal Self-Assembly

**ADVANCED
MATERIALS
TECHNOLOGIES**

www.advmattechnol.de

Self-Assembly of Colloidal Spheres toward Fabrication of Hierarchical and Periodic Nanostructures for Technological Applications

Xiaoguang Liang, Ruoting Dong, and Johnny C. Ho*

The current research status on the self-assembly of colloidal spheres for the fabrication of various hierarchical and periodic nanostructures is summarized, in which these structures exhibit unique properties for different technological applications in plasmonics, surface-enhanced Raman scattering, solar cells, and others. The fundamentals of colloidal self-assembly are first introduced. After which, the functions of the obtained monolayer of colloidal spheres (e.g., nanosphere monolayer) to act as the patterned mask for the subsequent pattern transfer onto underlying substrates are thoroughly discussed. In employing these nanosphere lithography techniques and fabrication templates, the focus switches to the successive construction of numerous nanostructures and their promising utilizations in a wide range of application domains. Finally, the current challenges and future opportunities of colloidal self-assembly are presented. This review not only aims to provide further insights for researchers to enable the ingenious designs of nanostructures, but also to facilitate the exciting research and development utilizing colloidal self-assembly for future manufacturing technologies.

1. Introduction

In the past decades, due to the cost-effectiveness, simple processing, high throughput, and excellent controllability, the self-assembly of colloidal particles, such as polystyrene (PS) and SiO$_2$ spheres, has been widely considered as a powerful tool

to potentially fabricate numerous hierarchical and periodic micro/nanostructure arrays in a large scale.[1–5] Importantly, these ordered micro/nanostructure arrays are essential active components for many technological applications, ranging from data storage,[6] solar cells,[7–9] plasmonics to functional coatings, and many others.[10–15] Combined with the recent advance in colloidal science, the colloidal spheres with uniform morphology and excellent disperse stability can be further realized by a number of methods, which include the suspension,[16,17] dispersion polymerization,[18,19] emulsion,[20,21] and Stöber techniques.[22] The diameter of colloidal spheres can also be precisely controlled in a wide range, spanning from several micrometers all the way to down to tens of nanometers. Uniquely, these colloidal spheres can be self-assembled into 2D monolayers and 3D periodic multilayers, where they are subsequently utilized as the versatile masks (e.g., optical lens) to achieve fabrication templates by simple surface patterning onto underlying substrates, facilitating the construction of micro/nanostructure arrays with excellent tunability.[23–25] Since then, these 2D monolayer colloidal crystals (MCCs) and 3D multilayers have attracted extensive attention for many of their further utilizations. For instance, by using the oxygen plasma and reactive ion etching (RIE) methods, the periodicity, the size, and the shape of individual spheres of MCCs are accurately controlled.[26,27] With further modification, etching, and decoration, the MCCs can be exploited as either the masks for metal catalyst deposition to generate hierarchical and periodic nanostructures on underlying substrates, or the templates for the growth of patterned nanostructures.[28,29] Furthermore, these MCCs can also be utilized as optical lens to construct the periodic nanostructures with photosensitive materials, broadening the preparing routes of hierarchical and periodic nanostructures.[30]

In order to prepare the periodic nanostructures, the fabrication process, including the self-assembly of MCCs, the morphological modification of MCCs, and the functionalized decoration, is commonly referred as the nanosphere lithography (NSL).[31–33] As compared with conventional lithographic techniques, such as photolithography,[34,35] electron beam lithography,[36] and focused ion beam lithography,[37] NSL can distinctively reduce the manufacturing cost and complexity,

Dr. X. Liang, R. Dong, Prof. J. C. Ho
Department of Materials Science and Engineering
City University of Hong Kong
Hong Kong 999077, P. R. China
E-mail: johnnyho@cityu.edu.hk

Dr. X. Liang, R. Dong, Prof. J. C. Ho
Shenzhen Research Institute
City University of Hong Kong
Shenzhen 518057, P. R. China

Prof. J. C. Ho
State Key Laboratory of Terahertz and Millimeter Waves (SKLTMW)
City University of Hong Kong
Hong Kong 999077, P. R. China

Prof. J. C. Ho
Centre for Functional Photonics (CFP)
City University of Hong Kong
Hong Kong 999077, P. R. China

The ORCID identification number(s) for the author(s) of this article can be found under https://doi.org/10.1002/admt.201800541.

Self-Assembly of Colloidal Spheres toward Fabrication of Hierarchical and Periodic Nanostructures for Technological Applications

Xiaoguang Liang, Ruoting Dong, and Johnny C. Ho*

The current research status on the self-assembly of colloidal spheres for the fabrication of various hierarchical and periodic nanostructures is summarized, in which these structures exhibit unique properties for different technological applications in plasmonics, surface-enhanced Raman scattering, solar cells, and others. The fundamentals of colloidal self-assembly are first introduced. After which, the functions of the obtained monolayer of colloidal spheres (e.g., nanosphere monolayer) to act as the patterned mask for the subsequent pattern transfer onto underlying substrates are thoroughly discussed. In employing these nanosphere lithography techniques and fabrication templates, the focus switches to the successive construction of numerous nanostructures and their promising utilizations in a wide range of application domains. Finally, the current challenges and future opportunities of colloidal self-assembly are presented. This review not only aims to provide further insights for researchers to enable the ingenious designs of nanostructures, but also to facilitate the exciting research and development utilizing colloidal self-assembly for future manufacturing technologies.

1. Introduction

In the past decades, due to the cost-effectiveness, simple processing, high throughput, and excellent controllability, the self-assembly of colloidal particles, such as polystyrene (PS) and SiO_2 spheres, has been widely considered as a powerful tool

to potentially fabricate numerous hierarchical and periodic micro/nanostructure arrays in a large scale.[1–5] Importantly, these ordered micro/nanostructure arrays are essential active components for many technological applications, ranging from data storage,[6] solar cells,[7–9] plasmonics to functional coatings, and many others.[10–15] Combined with the recent advance in colloidal science, the colloidal spheres with uniform morphology and excellent disperse stability can be further realized by a number of methods, which include the suspension,[16,17] dispersion polymerization,[18,19] emulsion,[20,21] and Stöber techniques.[22] The diameter of colloidal spheres can also be precisely controlled in a wide range, spanning from several micrometers all the way to down to tens of nanometers. Uniquely, these colloidal spheres can be self-assembled into 2D monolayers and 3D periodic multilayers, where they are subsequently utilized as the versatile masks (e.g., optical lens) to achieve fabrication templates by simple surface patterning onto underlying substrates, facilitating the construction of micro/nanostructure arrays with excellent tunability.[23–25] Since then, these 2D monolayer colloidal crystals (MCCs) and 3D multilayers have attracted extensive attention for many of their further utilizations. For instance, by using the oxygen plasma and reactive ion etching (RIE) methods, the periodicity, the size, and the shape of individual spheres of MCCs are accurately controlled.[26,27] With further modification, etching, and decoration, the MCCs can be exploited as either the masks for metal catalyst deposition to generate hierarchical and periodic nanostructures on underlying substrates, or the templates for the growth of patterned nanostructures.[28,29] Furthermore, these MCCs can also be utilized as optical lens to construct the periodic nanostructures with photosensitive materials, broadening the preparing routes of hierarchical and periodic nanostructures.[30]

In order to prepare the periodic nanostructures, the fabrication process, including the self-assembly of MCCs, the morphological modification of MCCs, and the functionalized decoration, is commonly referred as the nanosphere lithography (NSL).[31–33] As compared with conventional lithographic techniques, such as photolithography,[34,35] electron beam lithography,[36] and focused ion beam lithography,[37] NSL can distinctively reduce the manufacturing cost and complexity,

Dr. X. Liang, R. Dong, Prof. J. C. Ho
Department of Materials Science and Engineering
City University of Hong Kong
Hong Kong 999077, P. R. China
E-mail: johnnyho@cityu.edu.hk

Dr. X. Liang, R. Dong, Prof. J. C. Ho
Shenzhen Research Institute
City University of Hong Kong
Shenzhen 518057, P. R. China

Prof. J. C. Ho
State Key Laboratory of Terahertz and Millimeter Waves (SKLTMW)
City University of Hong Kong
Hong Kong 999077, P. R. China

Prof. J. C. Ho
Centre for Functional Photonics (CFP)
City University of Hong Kong
Hong Kong 999077, P. R. China

The ORCID identification number(s) for the author(s) of this article can be found under https://doi.org/10.1002/admt.201800541.

**ADVANCED
SCIENCE NEWS**

www.advancedsciencenews.com

**ADVANCED
MATERIALS
TECHNOLOGIES**

www.advmattechnol.de

and hence it can be widely utilized for the fabrication of periodic nanostructures in many manufacturing platform without the limitation of expensive and complex equipment. In this regard, the combination of lithographic methods based on colloidal self-assembly and other nanofabrication techniques can provide an alternative and intriguing strategy to create periodic nanostructures.[38] A great variety of 2D and 3D periodic micro/nanostructures, consisting of pillars, holes, rings, bowls, cones, disks, and other special structures, have been obtained based on these colloidal self-assembly assisted manufacturing schemes.[39–44] These hierarchical and periodic nanostructures with the well-controlled morphology, dimension, and intrinsic property are demonstrated to have the broad applications in solar cells, sensors, biology, photonics, and many others. Nevertheless, although substantial progresses in the appropriate design of these hierarchical and periodic micro/nanostructures are highly desired for the practical utilizations of colloidal self-assembly, there is still a lack of the comprehensive survey on these MCCs enabled nanostructures in the community.

In this work, we present a comprehensive review on the recent revolution in the fabrication of hierarchical and periodic nanostructures based on different nanosphere lithographic techniques. Special attentions are focused on the self-assembly of colloidal spheres, their morphological control and modification, as well as their functions in the fabrication process of nanostructures. Their applications in various technological domains will then be carefully emphasized. At the end, the current challenges and promising future prospects of these colloidal self-assembly are as well given. This survey does not only aim to provide further insights for researchers to enable the ingenious designs of nanostructures, but also facilitate the exciting research and development utilizing colloidal self-assembly for future manufacturing technologies.

2. Controllable Self-Assembly of Colloidal Spheres

In colloidal science, it is still a difficult task to achieve the controllable, uniform and large-scale self-assembly of colloidal spheres in a rapid and cost-effective manner. Until now, there are several key strategies developed to tackle the colloidal self-assembly issues, which can be divided into five different schemes, namely, (i) drop-coating, (ii) dip-coating, (iii) spin-coating, (iv) electrophoretic deposition, and (v) transferring self-assembly film at the gas/liquid interface to the gas/solid interface of substrate, as shown in **Figure 1**.[1] Specifically, during the drop-coating procedure (Figure 1A), the solvent evaporation rate is the primary parameter that affects the ordering and quality of the obtained monolayer film of colloidal spheres.[45] It is noted that the ordering and quality of these self-assembled arrays can be improved significantly by using dip-coating method for the accurate control of the solvent evaporation, as illustrated in Figure 1B.[46] For both of these two schemes, the capillary force and convective transport of the colloids (e.g., nanospheres) induced by the continuous solvent evaporation are the main process controlling factors. In order to obtain the large-area coating and high-throughput formation of these MCCs, spin-coating

Xiaoguang Liang received his B.E., M.E., and Ph.D. degrees from Hefei University of Technology in 2009, Kunming University of Science and Technology in 2012, and City University of Hong Kong in 2017, respectively. At present, he is a visiting scholar in the Department of Materials Science and Engineering at City University of Hong Kong under supervision of Professor Johnny C. Ho. His research interests are nanostructured arrays fabricated by the Langmuir-Blodgett method, and their applications in photovoltaic devices such as silicon and organometallic halide perovskite solar cells.

Ruoting Dong received her B.S. and M.S. degrees from South China Normal University in 2009 and 2013, respectively. Currently, she is a Ph.D. student under the supervision of Prof. Johnny C. Ho in the Department of Materials Science and Engineering at City University of Hong Kong. Her research interests are the controlled synthesis of nanomaterials and their applications in electronics and optoelectronics.
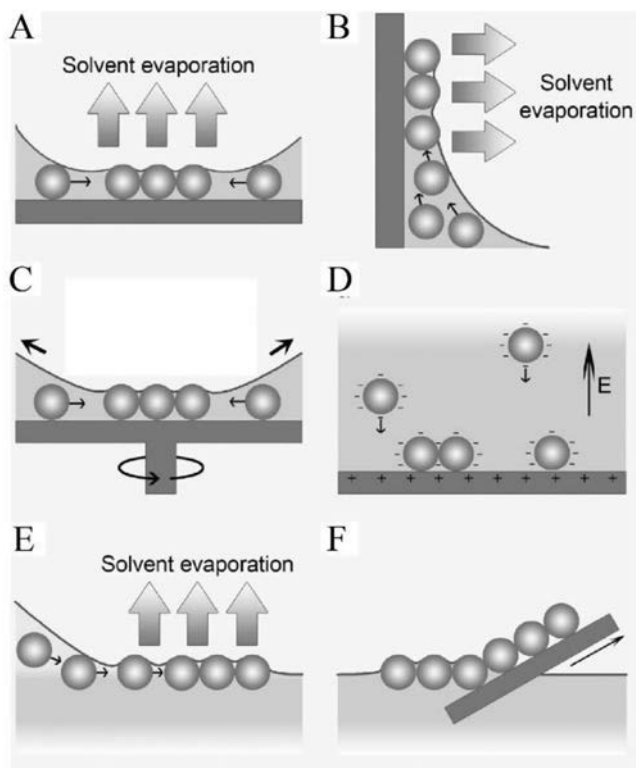
Johnny C. Ho received his B.S. with high honors in Chemical Engineering in 2002 and his M.S. and Ph.D. in Materials Science and Engineering from the University of California, Berkeley, in 2005 and 2009, respectively. From 2009 to 2010, he worked as a postdoctoral research fellow in the nanoscale synthesis and characterization group at Lawrence Livermore National Laboratory, California. Currently, he is an Associate Professor of Materials Science and Engineering at City University of Hong Kong. His research interests focus on the synthesis, characterization, integration, and device applications of nanoscale materials for various technological applications, including nanoelectronics, sensors, and energy harvesting.

method can be selected for the operation on any flat-surface substrate. For instance, the colloidal nanospheres can be densely deposited onto the substrate by spin-coating, while

**ADVANCED
SCIENCE NEWS**

www.advancedsciencenews.com

**ADVANCED
MATERIALS
TECHNOLOGIES**

www.advmattechnol.de

Figure 1. Schematic illustration of various colloidal self-assembly strategies. A) Drop-coating, B) dip-coating, C) spin-coating, D) electrophoretic deposition, E) self-assembly at the gas/liquid interface, and F) transfer from the gas/liquid to the gas/solid interface. Reproduced with permission.[1] Copyright 2011, Elsevier Ltd.
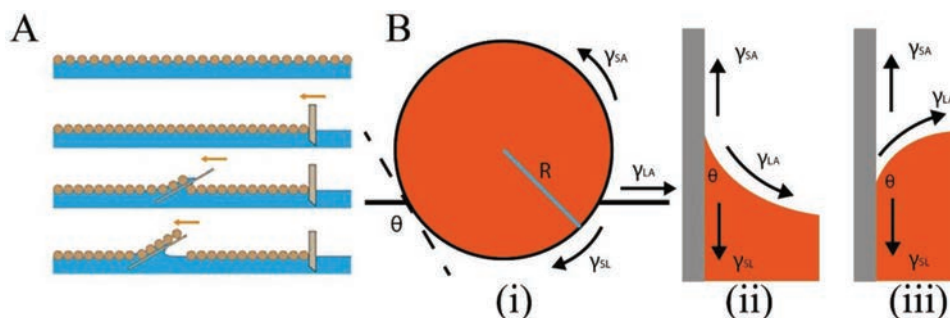
the quality of assembled colloidal film is mainly manipulated by the concentration of colloidal suspension, spin-coating speed, substrate wettability, etc (Figure 1C).[47] By using electrophoretic deposition, the charged nanospheres would move toward the electrodes under direct current fields or alternating current fields, leading to the self-assembly of colloidal spheres on the electrode surface, as displayed in Figure 1D.[48,49] Both Figure 1E and F show the self-assembly of colloidal spheres at the gas/liquid interface which is a facile and cost-effective route toward the large-area coatings.[3,50] These highly ordered and uniform nanosphere monolayers

can be obtained via the spreading of colloidal suspension onto a liquid surface, and then these floating monolayers are readily transferred onto varied substrates. After the evaporation of solvent in the suspension, the dense nanosphere existed in a single monolayer format without any variation in its thickness would remain on the substrate surface. In particular, utilizing this technique, MCCs can be efficiently synthesized by the self-assembly of PS nanospheres at the gas/ deionized water (DI water) interface, in which they are subsequently transferred onto other substrates. Nevertheless, there is not a champion method for the self-assembly of colloidal spheres, where the colloidal materials and their dimensions as well as the substrate materials and their surface roughness would dictate the proper method for the controllable formation of large-scale MCCs.

On the other hand, Langmuir–Blodgett (LB) assembly method is a very simple and powerful technique for the fabrication of highly ordered monomolecular films with a densely packed structure, a high reproducibility, and a large-area uniformity.[51–53] In this method, the colloidal nanoparticles (e.g., silica and PS nanospheres) are usually employed to form self-assembled monolayers with the hydrophobic surface as shown in **Figure 2**A. The general working principle is quite straightforward and commonly used with surfactants, such as oil. Importantly, this method can be applied to colloidal materials as well, as long as they allow the formation of a monolayer at an interface. When a colloidal suspension is dispersed onto a surface, the colloids would spread as far as possible, forming a spaced monolayer on the surface. The film is then compressed through a barrier, which reduces the available surface area, resulting in an increased surface tension. When a substrate is then "scooped" through this compressed film, the lower surface tension provided by the substrate would then cause the colloids to transfer onto it from the interface.

It is interesting that the assembled films can only be picked up on the upstroke of the substrate. In order to figure out and quantify this phenomenon of hydrophobic particles assembled film, researchers have provided expressions to describe the energy required by extracting a particle from the air/water interface in the upward direction and forcing a particle into the water, separately.

These expressions can be described as follows with details given in Figure 2B[54]

Figure 2. Fluidic deposition of the colloidal self-assembly: Langmuir–Blodgett (LB) method. A) Schematic demonstration of the LB method. Reproduced with permission.[51] Copyright 2018, Elsevier Ltd. B) Forces at the solid/liquid/air interface, (i) a particle at the air/water interface, (ii) hydrophilic surface (θ is acute angle), (iii) hydrophobic surface (θ is obtuse angle), γ_{SA}, γ_{LA}, and γ_{SL} are interfacial tensions between solid, liquid, and air, respectively. Reproduced with permission.[50] Copyright 2010, Wiley-VCH Verlag GmbH & Co. KGaA.

$$E_{OUT} = \pi R^2 \gamma_{LA} \left(1 + \cos\theta\right)^2 \qquad (1)$$

$$E_{IN} = \pi R^2 \gamma_{LA} \left(1 - \cos\theta\right)^2 \qquad (2)$$
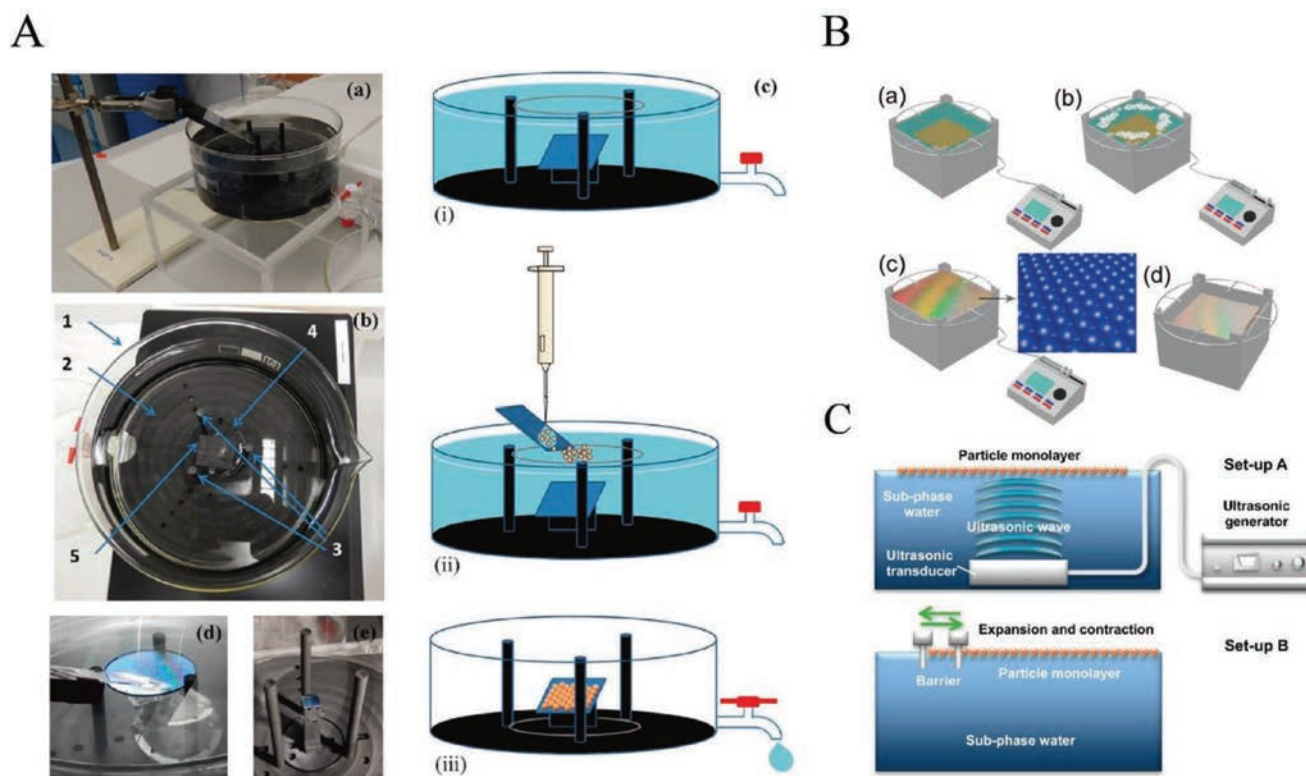
where R is the radius of the particle, γ_{LA} is the interfacial tension between liquid and air, and θ is the obtuse angle. Furthermore, the ratio of E_{OUT}/E_{IN} can be presented by Equation (3)[55]

$$E_{OUT} / E_{IN} = \cot^4\left(\theta/2\right) \qquad (3)$$

This ratio is quite small for any value of θ, which indicates that the required energy to move a particle upward is much less than the required energy to move a particle downward. These investigations can evidently provide a theoretical basis for the fact that the nanospheres based monolayer is only deposited on the upstroke.

Figure 3 demonstrates several improved methods of LB assembly schemes. A container with a hole and a tap for water discharge can be designed to dispense the colloidal spheres using a tilted glass slide and allow the self-assembly formation of monolayers at the air/water interface (Figure 3A).[56] The nitrile butadiene rubber ring floating on the water surface is then employed to confine the self-assemble area, avoiding the monolayer damage or disruption during transfer. The self-assembly of colloidal spheres process is also sketched in Figure 3A(c) in details. After water draining out in the glass container, a dense monolayer is left on the substrate. At the same time, Figure 3B presents a low-cost and high-throughput micropropulsive injection (MPI) method based on a large-area self-assembly of colloidal PS nanospheres.[57] The self-assemble process is shown as the following series of steps: (i) presetting the substrates underneath the water and connecting the injectors with the MPI system (Figure 3B(a)); (ii) self-assembly of colloidal PS nanospheres on the water surface fabricated via the MPI system (Figure 3B(b)); (iii) formation of a dense self-assembled PS monolayer consisting of colloidal crystals on the entire water surface (Figure 3B(c)); transferring of PS monolayer onto the preset substrates (Figure 3B(d)). In order to decrease the defect concentration of the MCCs fabricated by LB method, two

Figure 3. A) Self-assembly of colloidal spheres at air/water interface by surface confinement and water discharge. (a) Photograph of the overall setup. (b) Detail of (1) glass container with tap, (2) circular plate, (3) cylindrical rods, (4) nitrile butadiene rubber ring, and (5) sample holder. (c) Sketch of the procedure: (i) installation of the substrate in the container, (ii) dispensation and self-assembly of colloidal spheres, and (iii) monolayer transfer onto the substrate after water discharge. (d) Photograph of the self-assembly monolayer at air/water interface confined within the area of the ring. (e) Photograph of a sample after transfer. Reproduced with permission.[56] Copyright 2016, American Chemical Society. B) Schematics of the micro-propulsive injection (MPI) systems and the formation processes for large-area PS nanosphere arrays. (a) An MPI system with one injector and four nozzles. A substrate is preset underneath the water. (b) Initial stage for the injection of PS colloids over the water surface. (c) The formation of hexagonally arranged PS monolayer upon the water surface once a defect-less and colorful interference pattern occurred under white light illumination. The inset image schematically shows the arranged PS monolayer. (d) Transfer of the PS monolayer onto the preset substrates by slowly declining the water level or raising the substrate. Reproduced with permission.[57] Copyright 2015, American Chemical Society. C) Schematic illustrations of the setup of Langmuir–Blodgett trough. Setup "A": ultrasonic irradiation to the particle monolayer. Setup "B": Barrier-sway process to the particle monolayer. Reproduced with permission.[58] Copyright 2015, American Chemical Society.

ADVANCED
SCIENCE NEWS
www.advancedsciencenews.com

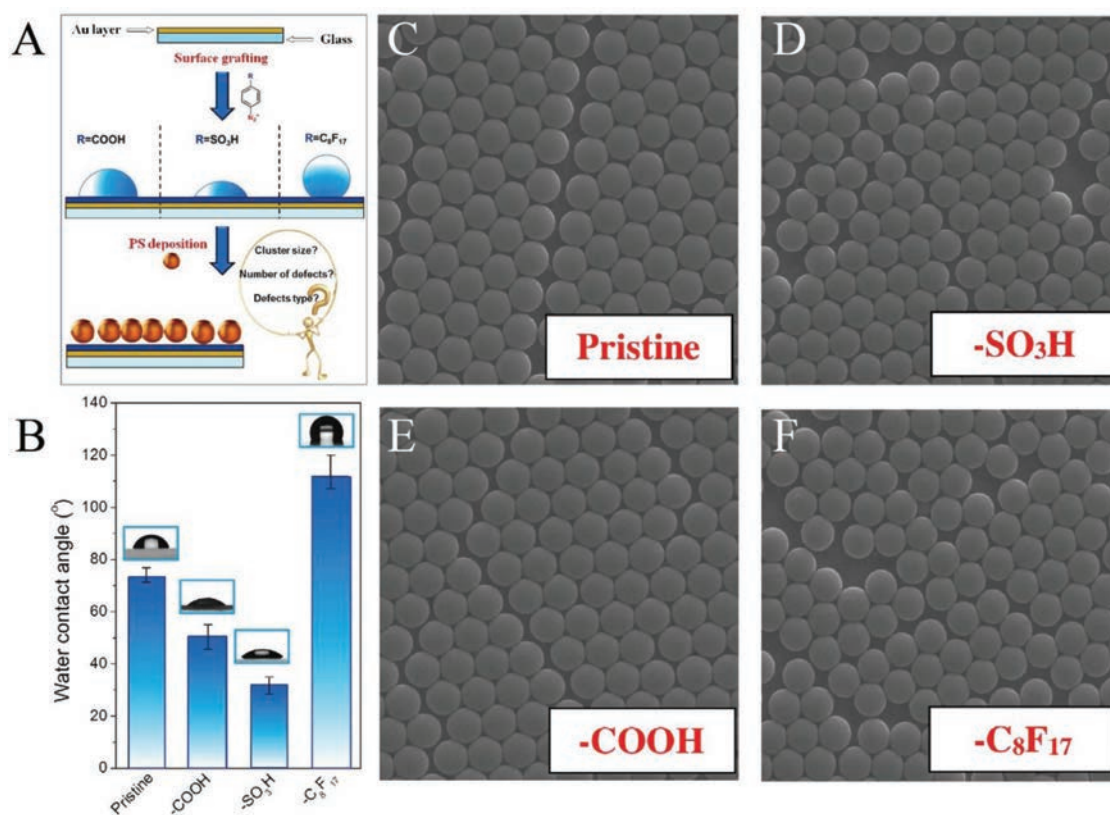**ADVANCED**
MATERIALS
TECHNOLOGIES
www.advmattechnol.de

different techniques of the ultrasonic annealing and the barrier-sway can be employed as illustrated in Figure 3C.[58] The setup of "ultrasonic annealing" is consisted of an ultrasonic generator and a transducer. 1.2 to 1.5 MHz oscillation is irradiated from the transducer head to the water surface for 30 min at 20 °C. Meanwhile the colloidal silica spheres are dripped, and then spread on the water surface (Figure 3C, setup "A"). By contrast, the "barrier-sway" is a physical treatment process, leading to a sway forward and backward of the silica spheres on the water alternately at a frequency rate of 0.2 to 0.5 Hz with an amplitude of 25–35 mm at 20 °C by manipulating the barrier of LB trough (Figure 3C, setup "B"). All of these demonstrate the unique characteristics of different LB methods for the formation of controllable, uniform and large-scale monolayers of self-assembled colloids for practical utilizations.

Moreover, the hydrophilic or hydrophobic functional groups can be used to modify the quality of MCCs on the Au surface.[59] **Figure 4**A shows a thin Au layer, which can be covalently modified by different organic functional groups via diazonium chemistry with the aim to introduce hydrophilic or hydrophobic properties. The impact of the surface grafting on the wettability (i.e., contact angle) is systematically demonstrated in Figure 4B, while Figure 4C shows the colloidal PS spheres deposited onto the pristine Au surface with the dislocation-like defects. The same type of defects is also observed in the case of 4-carboxyphenyl-modified surface (Figure 4E). In the case of 4-sulfophenyl
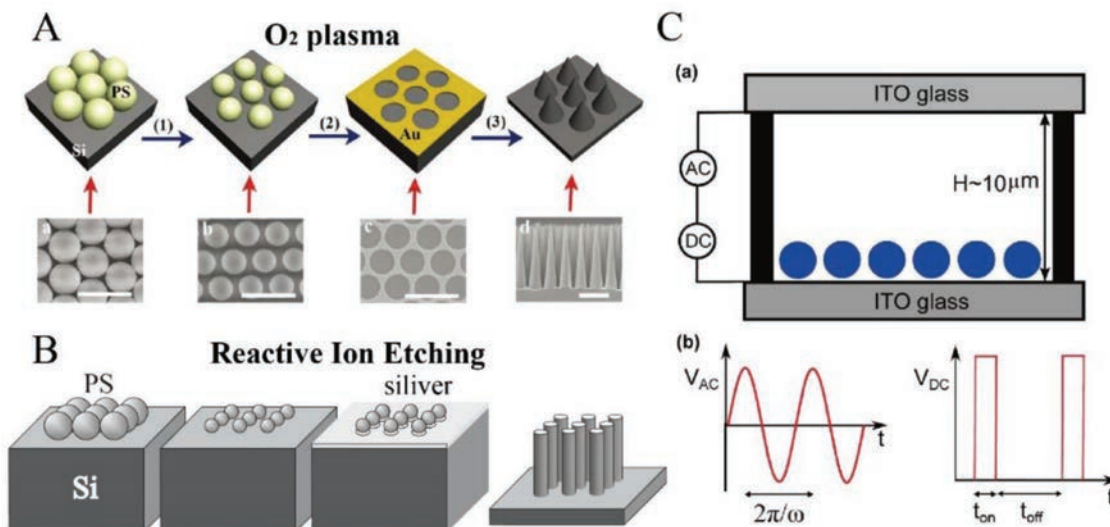
functional groups, the Schottky-like defect becomes dominant (Figure 4D). The surface grafting by arenediazonium tosylates-C_8F_{17} can also significantly disrupt the ordering of PS sphere arrays (Figure 4F). Thus, the colloidal spheres cannot self-assemble into a perfect monolayer on the substrate surface with a high hydrophilicity. These findings can clearly indicate that controlling the surface hydrophobicity is crucial for the formation of high-quality self-assembled colloidal monolayer.

3. Construction of Various Large-Scale, Hierarchical, and Nanostructured Arrays

Once the large-scale and high-quality MCCs are obtained, they can then be acted as the mask for metal deposition after processing of O_2 plasma, reactive ion etching or combinations of various electric fields. In specific, the PS monolayer was subjected to O_2 plasma in order to reduce the diameter of PS spheres, and then Au film was deposited onto the substrate via thermal evaporation as shown in **Figure 5**A.[60] After removal of the PS spheres, nanocone arrays could be generated by using the method of metal-assisted chemical etching (MaCE), which is a well-developed chemical etching scheme to obtain highly anisotropic nanostructure in Si, GaAs, and others with designated metal catalysts.[63–65] Reactive ion etching process is another technique to reduce the diameter of the PS spheres, leading to

Figure 4. Au surface grafting and their properties tuning with the aim to investigate further the deposited PS array quality. A) Process schematics. B) Water contact angles measured on pristine Au surface and Au surfaces grafted with organic compounds (−SO₃H, −COOH, and −C₈F₁₇). C–F). Scanning electron microscope (SEM) images of PS spheres deposited on the pristine and grafted samples with organic compounds of −SO₃H, −COOH, and −C₈F₁₇, respectively. The scan area is 6 × 6 µm². Reproduced with permission.[59] Copyright 2018, Elsevier B.V.

ADVANCED
SCIENCE NEWS
www.advancedsciencenews.com

ADVANCED
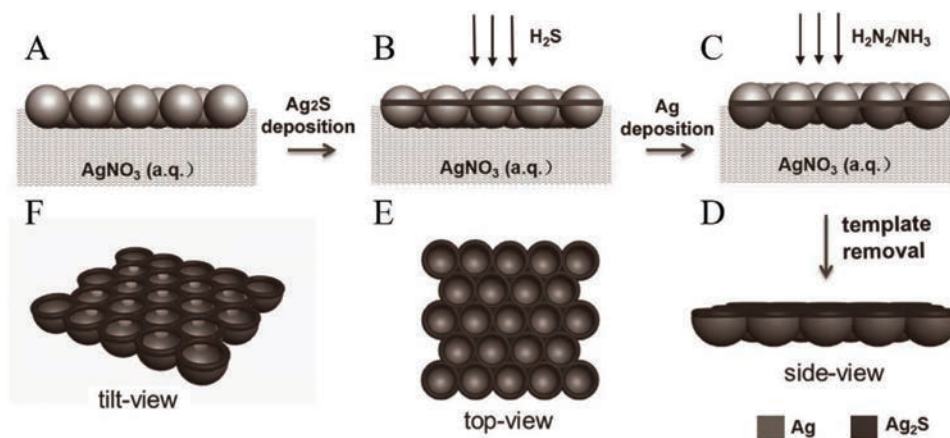**MATERIALS**
TECHNOLOGIES
www.advmattechnol.de

Figure 5. A) Oxygen plasma processed PS spheres for the fabrication of periodic nanocone arrays and their corresponding SEM images. The scale bar represents 1 μm. Reproduced with permission.[60] Copyright 2017, The Royal Society of Chemistry. B) Reactive ion etching processed PS spheres for the fabrication of periodic nanopillar arrays. Reproduced with permission.[61] Copyright 2007, Wiley-VCH Verlag GmbH & Co. KGaA. C) Cross-sectional view of the experimental setup (a). The electric field applied combines both a continuous alternating current and pulses of direct currents (b). Reproduced with permission.[62] Copyright 2017, American Chemical Society.
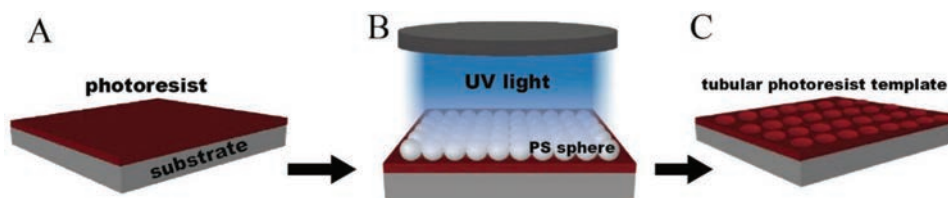
an unclose-packed array of colloidal PS spheres as presented in Figure 5B.[61] A silver film was next evaporated onto the silicon substrate as a catalyst. Simultaneously, Figure 5C presents an electric-field assisted self-assembly of colloidal spheres into the unclose-packed array due to the dipolar repulsion. The cross-sectional view of the setup is shown in Figure 5C(a). In explicit, a droplet of colloidal suspension was placed between two indium tin oxide (ITO) slides. First, an alternating-current (AC) electric field was applied between the two electrodes using a function generator. Then, a sequence of direct-current (DC) pulses together with a programmable DC power supply were applied, resulting in the separation of colloidal spheres

from each other at a constant distance because of the induced dipolar repulsion. Obviously, combining with different fabrication schemes, these MCCs can be utilized as the masks for the effective construction of various hierarchical nanostructured arrays.[62]

In addition, **Figure 6** shows that the unique $Ag_2S–Ag$ heterostructured nanobowl arrayed structure can also be realized by the nanosphere lithography method.[66] In details, the MCCs self-assembled on the surface of aqueous $AgNO_3$ solution was employed as the template as presented in Figure 6A. Next, the Ag_2S nanonet film was obtained due to the preferential deposition of Ag_2S at gas–liquid interface under the H_2S gas

Figure 6. The template of PS monolayer for the fabrication of $Ag_2S–Ag$ heterostructured and periodic nanobowl arrays by two-step nanosphere lithography at the gas–liquid interface. A) Self-assembly of PS spheres on the surface of aqueous $AgNO_3$ solution. B) Ag_2S nanonet film was obtained under the H_2S gas. C) Introducing the N_2H_4/NH_3 gas mixture would lead to the reduction of Ag^+ ions while the preferential deposition of metallic Ag is taken place at the bottom of each PS spheres. D) Formation of 2D ordered arrays of $Ag_2S–Ag$ heterostructured nanobowls after the template removal. E,F) Top- and tilt-schematic view of the obtained arrays which consist of Ag_2S nanonets lying on Ag nanobowl arrays. Reproduced with permission.[66] Copyright 2017, Wiley-VCH Verlag GmbH & Co. KGaA.

**ADVANCED
SCIENCE NEWS**
www.advancedsciencenews.com

**ADVANCED
MATERIALS
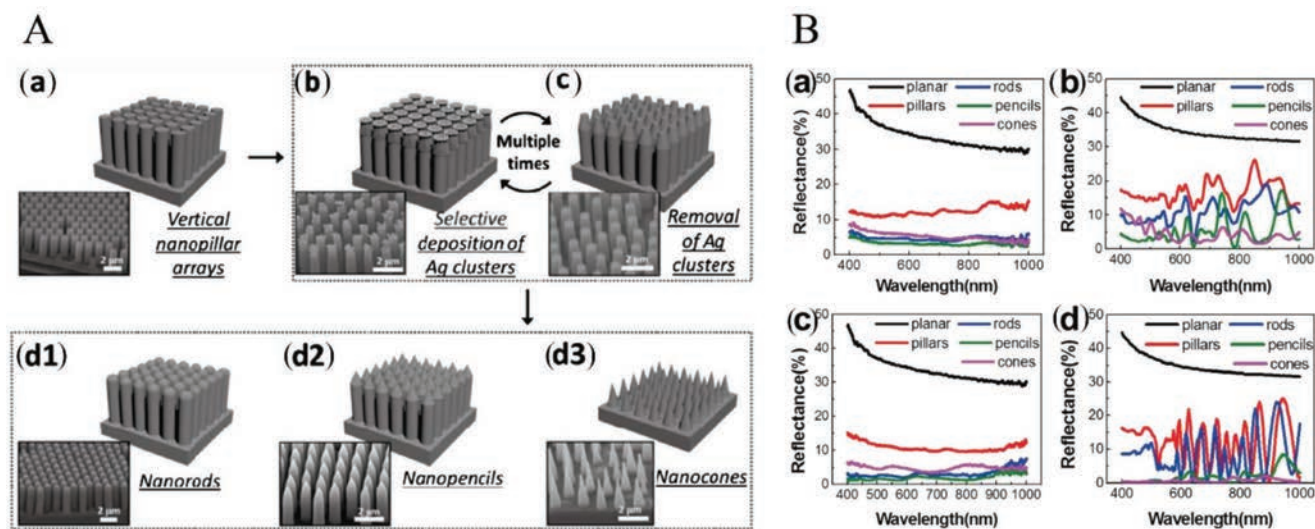TECHNOLOGIES**
www.advmattechnol.de

Figure 7. A schematic illustration of the photolithography-assisted process for the fabrication of periodic nanoarrays: A) spin-on deposition of photoresist on a substrate, B) a monolayer of silica or PS spheres formed on top of the photoresist under UV light exposure. C) The patterned photoresist nanohole obtained after removing the spheres and developing of photoresist.

(Figure 6B). Subsequently, when the N_2H_4/NH_3 gas mixture is diffused into the system, it would lead to the reduction of Ag^+ ions and the preferential deposition of metallic Ag at the bottom of each PS spheres (Figure 6C). After removal of the MCC template, the periodic and heterostructured Ag_2S–Ag nanobowl arrays were obtained with a high uniformity in a large scale, consisting of connected Ag_2S rings lying on the edge of Ag bowls with some cavities on the lateral walls (Figure 6D–F). These unique Ag_2S–Ag heterostructured nanobowl arrays have already been demonstrated with the effective resistance switching characteristics and superior photoresponses, being promising for potential utilizations in both electronic devices and photocatalysis, etc.[66,67]

Except functioning as the masks and the templates, the MCCs deposited on the photosensitive materials, such as photoresist, could also be served as the optical lens.[68] Explicitly, photoresists could be spun onto substrates, and then dipped into the developer solution for a few seconds after soft bake (**Figure 7**A). In this case, the hydrophilic surface of photoresist was obtained, which could facilitate the subsequent self-assembly of the colloidal silica or PS spheres on top of the photoresist (Figure 7B). After that, the samples were exposed under ultraviolet (UV) irradiation by using a conventional photolithography technique. Notably, the exposure profile of the

photoresist could be precisely controlled by the size of spheres, the thickness of photoresist layer and the duration of irradiation. Eventually, the nanohole arrays were simply obtained on the photoresist layer after removal of colloidal spheres and development in the developer solution (Figure 7C).

Apart from the pattern obtained in the photoresist layer, various hierarchical and periodic silicon nanostructures with the excellent optical properties could also be fabricated by employing the MCCs as the mask.[69–71] **Figure 8**A shows the fabrication procedures of silicon (Si) nanopillar, nanorod, nanopencil, and nanocone arrays constructed by using the MaCE method. Briefly, MCCs were assembled on boron-doped p-type Si (100) substrates by using the LB approach. The substrates were first pretreated with mild oxygen plasma to induce hydrophilic surfaces for the facilitation of uniform nanosphere coating. Utilizing these colloidal spheres as the mask, a 1.5/20 nm thick Ti/Au was then deposited through thermal evaporation. Subsequently, the hierarchical and periodic Si nanopillars with a controllable diameter and periodicity could be achieved via metal catalytic etching in HF/H_2O_2 solution (Figure 8A(a)). These Si nanopillars were used as the template, which could be further treated with a mixture of $AgNO_3$, HF, and HNO_3 or H_2O_2. Ag clusters in this mixture would preferentially deposit on the tips of nanopillars and at the same
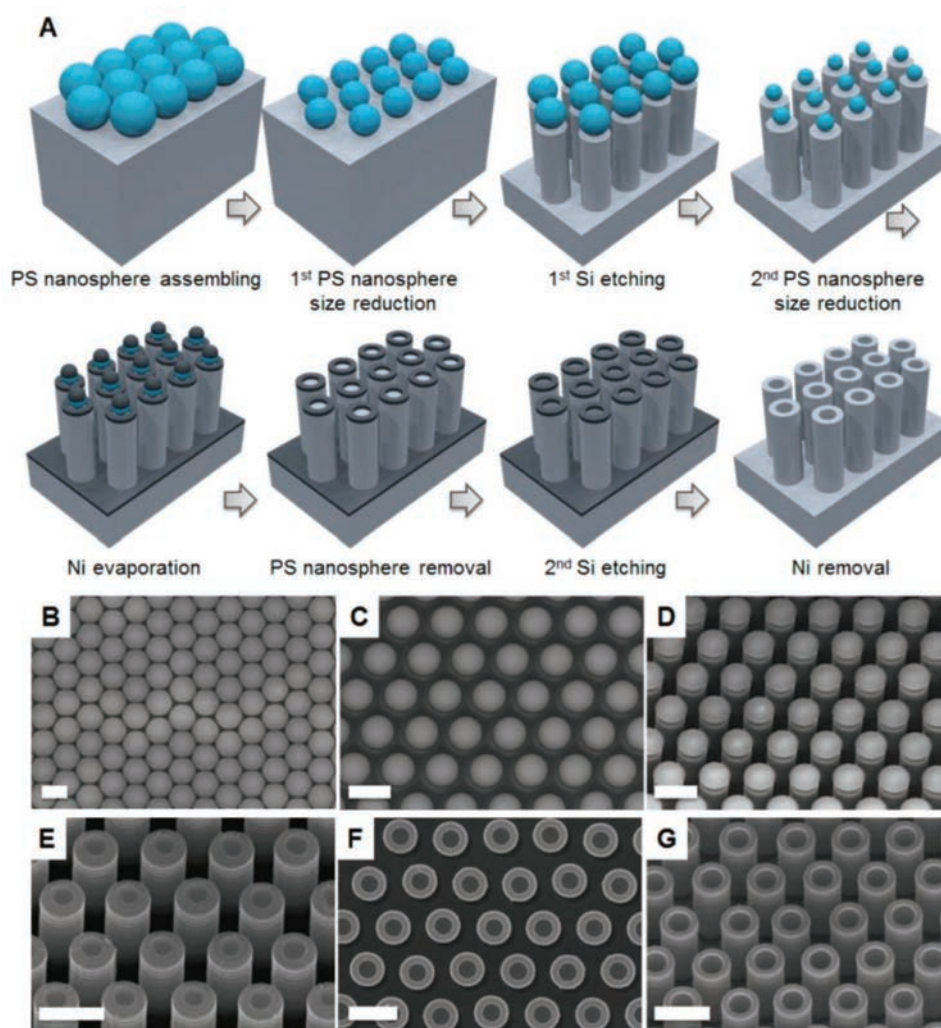

Figure 8. A) Schematics for the fabrication of different morphological Si nanoarrays. The insets show the representative SEM images of the correspondingly obtained nanoarrays. Reproduced with permission.[69] Copyright 2013, The Royal Society of Chemistry. B) Comparison of the reflectance spectra of various nanostructured arrays between experimental measurement and optical simulation. (a) Experimental and (b) simulated spectra of different nanostructures with the geometrical pitch of 1.27 µm. (c) Experimental and (d) simulated spectra of different nanostructures with the geometrical pitch of 0.6 µm. Reproduced with permission.[72] Copyright 2014, American Chemical Society.
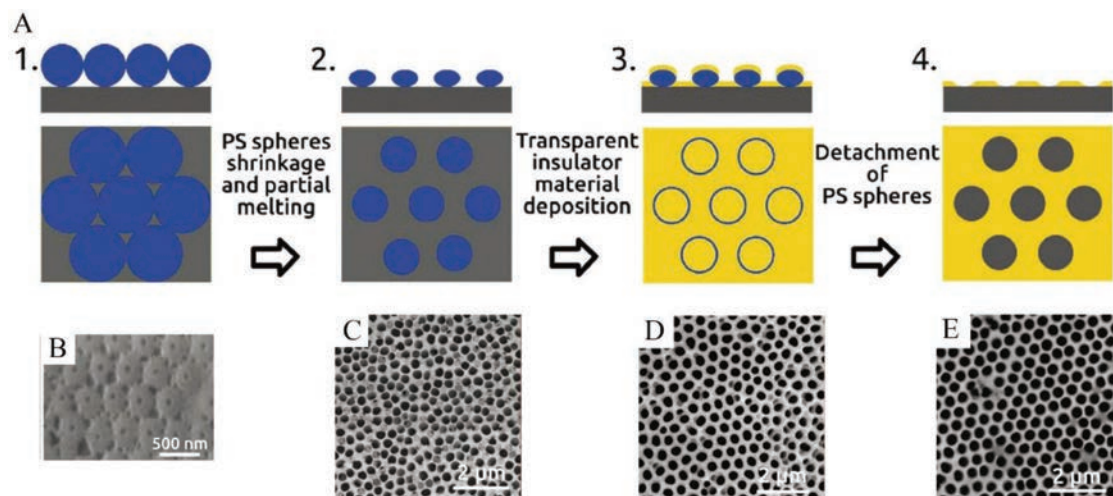
**ADVANCED
SCIENCE NEWS**

www.advancedsciencenews.com

**ADVANCED
MATERIALS
TECHNOLOGIES**

www.advmattechnol.de

time perform Si etching. This way, the subsequent removal of Ag clusters by HNO₃ washing would give fresh nanopillar tips as shown in the process schematic in Figure 8A(b),(c). Due to the repeated deposition and removal processes of these Ag clusters, different morphological nanopillar arrays (i.e., nanorods, nanopencils, and nanocones) tailored under well-controlled chemical conditions were generated (Figure 8A(d1)–(d3)). It is noted that the morphologies, dimensions, and aspect ratios of these hierarchical and periodic nanostructures could be controlled accurately with this simple wet-chemistry anisotropic etching technique. Impressively, these Si hierarchical and periodic nanostructures also demonstrated with the superb antireflection performance under ultraviolet–visible (UV–vis) spectroscopy, where the pencil and cone nanostructured arrays exhibited the best optical absorption characteristics

here among all samples, as shown in Figure 8B. These excellent broadband optical absorption behaviors could be attributed to the increasing material filling ratio changing from the tip to the basal plane of the nanoarrays, enhancing the mean free time of photons and trapping the photons within the hierarchical structure.[72] All of these hierarchical structures would contribute to the ideal configuration for next-generation photovoltaic devices.

Furthermore, **Figure 9**A presents the fabrication steps of the 3D Si nanotube arrays in large scale by multiple-patterning NSL (MP-NSL) based on the PS MCCs.[73] The SEM images of the products processed right after several key steps are shown as Figure 9B–G. First, a monolayer act as the mask for MP-NSL was formed at water/air surface by using the drop cast method, and then transferred to a 2 cm × 2 cm Si substrate underneath

Figure 9. Self-aligned multiple-patterning nanosphere lithography for Si nanotube arrays. A) A schematic illustration of the process. Step 1: the monolayer of close-packed (PS) nanospheres formed at water/air interface, and then transferred onto a Si wafer. Step 2: oxygen plasma processing. Step 3: Si nanopillars fabricated by deep reactive ion etching with the nanospheres as masks. Step 4: a second oxygen plasma processing. Step 5: deposition of Ni on PS nanospheres and Si nanopillars. Step 6: removal of PS nanospheres by oxygen plasma etching. Step 7: Si holes formed by deep reactive ion etching Step 8: 3D Si nanotube arrays achieved after the removal of Ni by HCl. SEM images of key intermediates: B) monolayer of closed-packed PS nanospheres formed on a Si wafer, C) PS nanospheres on Si wafer after first oxygen plasma processing, D) PS nanospheres on top of periodic Si nanopillar arrays, E) PS nanospheres after the second oxygen plasma processing, F) Ni nanorings on top of Si nanopillars, and G) Si nanotube arrays with the Ni nanorings. All Scale bars are 1 μm. Reproduced with permission.[73] Copyright 2017, American Chemical Society.
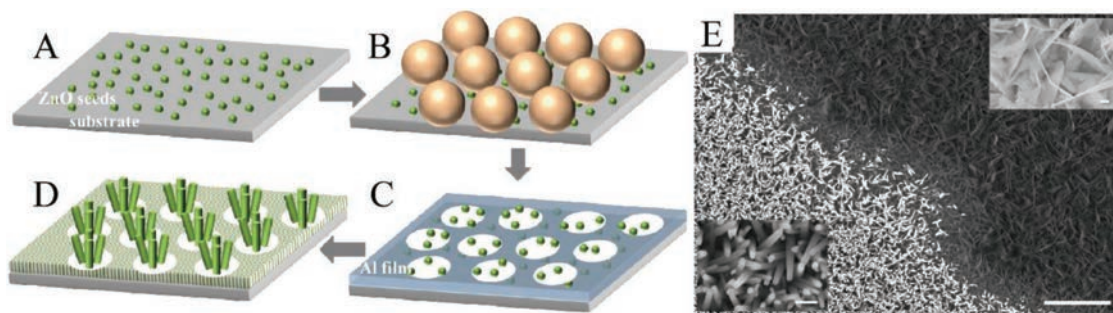
Figure 10. A) Schematic illustration of the four fabrication steps of the SiO$_2$ patterned Al foil. B) Hexagonally patterned SiO$_2$ layer with distances of 460 and 600 nm on the Al foil after detaching the PS spheres. Top-view SEM images of the AAO film grown in a 0.1 M phosphoric acid electrolyte applying 195 V after: C) first anodization of electropolished Al foil, D) second anodization, E) anodization of Al foil with prepatterned structures. Reproduced with permission.[76] Copyright 2018, The Royal Society of Chemistry.
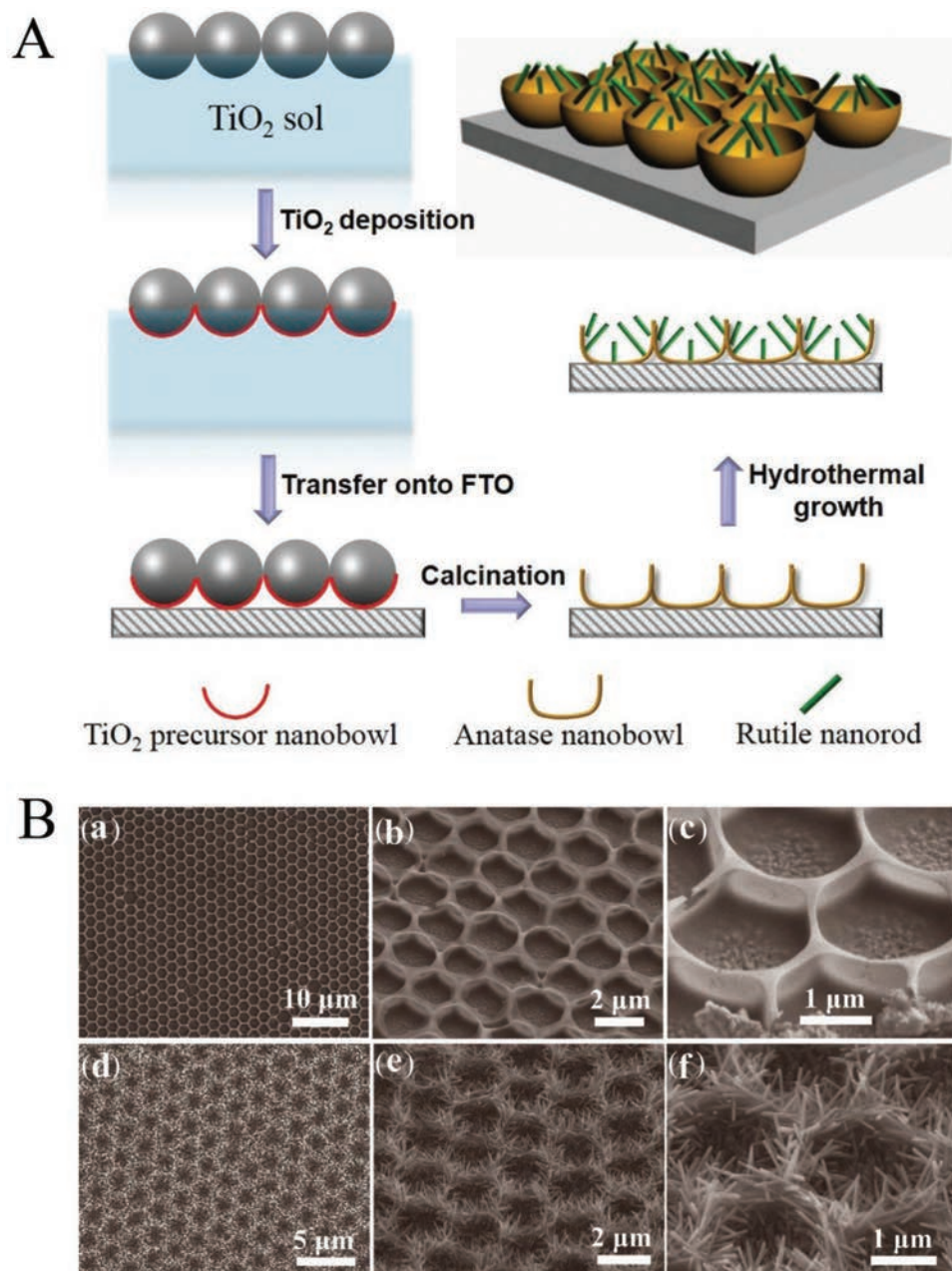
the water/air interface by gently removing the liquid as illustrated in Figure 9B. It is noted that the pitch of the final Si nanotube arrays can be tailored from several hundred nanometers to several micrometers depending on original size of the PS nanospheres. Next, the diameters of the polystyrene nanospheres are reduced by the oxygen plasma etching, which can define the outer diameter of the Si nanotubes as given in Figure 9C. By using the deep reactive ion etching (DRIE) technique, Figure 9D presents the fabricated Si nanopillar arrays with high-aspect ratio, while the PS nanospheres still remain on the top of these nanopillars. Then, a second oxygen plasma etching was employed to reduce the size of PS nanospheres on top of the pillars as illustrated in Figure 9E. Similarly, the smaller nanospheres remained on the center of Si nanopillars would serve as masks for the subsequent DRIE. Furthermore, the Ni layer with the thickness of 20 nm was deposited on the sample surface by electron-beam evaporation, acting as the anti-etching layer during the DRIE process. After removal of PS nanospheres, the Ni nanorings with the exposed Si surface at the central part were obtained as shown in Figure 9F.

Finally, Figure 9G displays the finished Si nanotube arrays achieved after the removal of Ni by the chemical etch treatment (5% HCl).

Besides the MaCE method and DRIE technique, the nanosphere lithography based on the MCCs could as well be combined with the bottom-up technique to fabricate periodic anodic aluminum oxide (AAO), which was usually employed as the template to prepare various nanostructures. The porous AAO with the uniform dimension of nanopores was successfully synthesized on different substrates, such as glass or ITO surface.[74,75] However, it was rarely reported the fabrication of periodic AAO. **Figure 10**A shows the fabrication process of the SiO$_2$ nanohole arrays on Al foil. The top-view SiO$_2$ monolayer on the Al foil after the removal of PS spheres was presented in Figure 10B. For comparison, an electropolished Al foil without any pre-patterning and an Al foil submitted to a preliminary first anodization for 24 h anodized under the same conditions were selected. The top-view SEM images of first anodization of electropolished Al foil and second anodization with preliminary first anodization were presented in Figure 10C,D

Figure 11. Schematic illustration of ZnO nanowire/nanosheet synthesis. A) ZnO seeds were formed on the substrate. B) A monolayer of PS spheres was deposited on top of the ZnO seeds. The size of the sphere can be adjusted with dry etching. C) Al nanohole arrays were fabricated using the PS spheres as the masks. D) Patterned ZnO nanowires/nanosheets grown from the same growth solution. E) SEM image of the boundary between the ZnO nanowire area (bottom-left) and nanosheet area (top-right). The scale bar is 5 μm in length. Inset: magnified SEM images of nanowires (bottom-left) and nanosheets (top-right). The scale bar in either inset is 200 nm. Reproduced with permission.[81] Copyright 2015, The Optical Society.
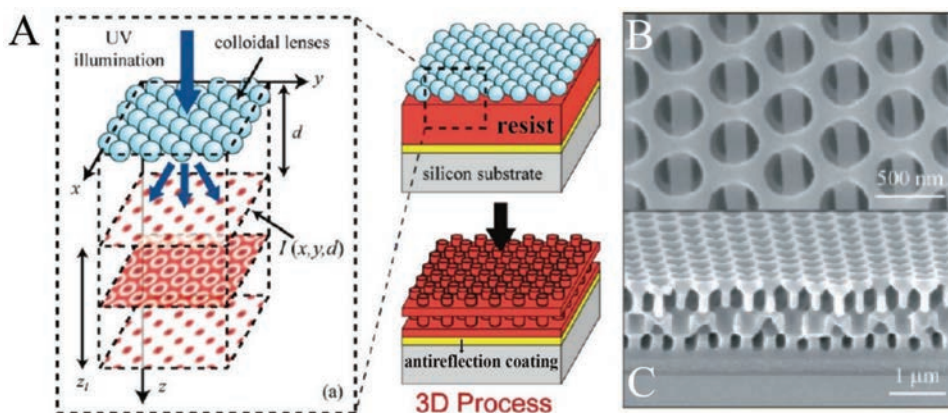
Figure 12. A) Schematic illustration of the preparation process of TiO$_2$ NR@NB arrays. B) SEM images of (a–c) TiO$_2$ NB arrays and (d–f) TiO$_2$ NR@NB arrays obtained after 5 h of hydrothermal growth. Reproduced with permission.[82] Copyright 2016, Wiley-VCH Verlag GmbH & Co. KGaA.

respectively. Obviously, the periodic AAO nanostructures with well-controlled and large interpore distances were obtained by the nanospheres lithography prepattering and one-step anodization process (Figure 10E). This unique hierarchical structure can open up lots of potential applications in various technology domains.[76]

It is noted that the hydrothermal method is one of the most popular approaches in the nanomaterial synthesis due to its simplicity and flexibility in the morphology control.[77–80] The nanosphere lithography with MCCs can then be combined with the hydrothermal method to generate numerous interesting hierarchical and periodic nanoarrays.[81] **Figure 11** demonstrates

the ZnO nanowire/nanosheet arrays synthesized on ITO glass substrates by hydrothermal method combined with nanosphere lithography scheme. In particular, the ZnO seed layer was first synthesized on the ITO glass substrates by spin-coating of the Zn precursor colloidal suspension as presented in Figure 11A. After drying and annealing of the seed layer in ambient air, a monolayer of PS spheres was prepared on top of the ZnO seeds/ITO glass substrates (Figure 11B). Then, the Al film of 50 nm in thickness was deposited onto the PS monolayer by using electron-beam deposition. After removal of the PS monolayer, the periodic Al nanohole arrays were obtained with the Zn seeds in the holes (Figure 11C). Finally, the hierarchical

**ADVANCED
SCIENCE NEWS**

www.advancedsciencenews.com

**ADVANCED
MATERIALS
TECHNOLOGIES**

www.advmattechnol.de

Figure 13. A) Schematic illustration of the proposed approach, where a hexagonal array of nanospheres is illuminated by an UV laser to generate a 3D intensity distribution. The x–y intensity pattern is a function of propagation distance d (right). The volumetric intensity distribution can be recorded by assembling the nanospheres directly on a substrate spin-coated with thick photoresist (left). B) The structure contains alternating 2D hexagonal holes array and 1D grating lines due to laser polarization. C) Cross-section view of fabricated nanostructure with $\lambda = 351$ nm, $D = 350$ nm, and $\gamma = 0.67$. Reproduced with permission.[89] Copyright 2011, American Chemical Society.
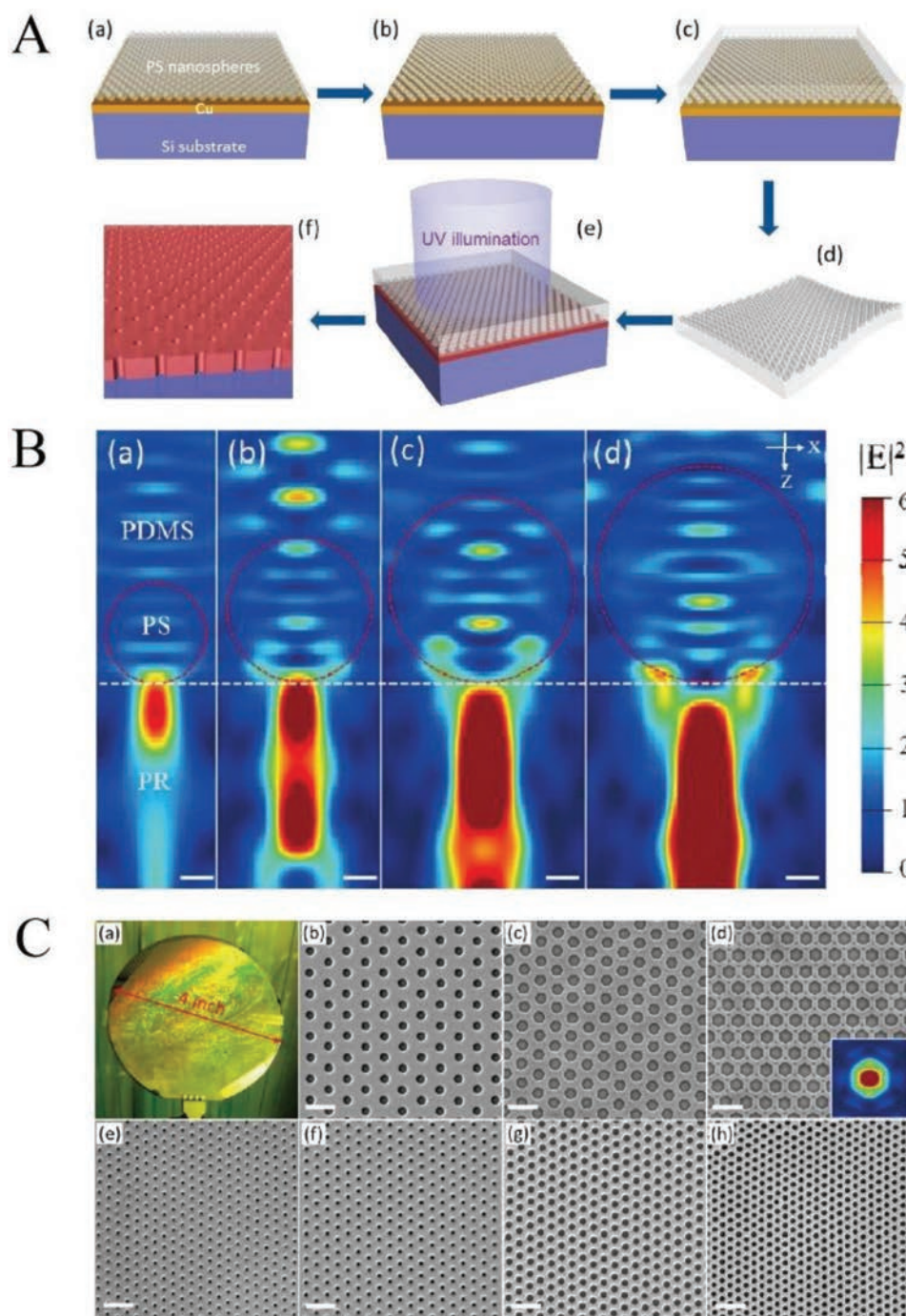
and periodic ZnO nanowires/nanosheets were prepared on the ITO glass substrate via hydrothermal routes (Figure 11D). Figure 11E shows an SEM image of the ZnO nanowire area, the nanosheet area, and the boundary between them. The nanowires were directly grown on cleaned ITO substrate because of the ZnO seed. By contrast, the ZnO nanosheets were grown onto the Al thin film.

Similarly, **Figure 12**A presents the fabrication process of hierarchical and periodic TiO_2 nanorod@nanobowl (NR@NB) arrays synthesized by combinations of nanosphere lithography and hydrothermal growth.[82] The MCCs based template was first self-assembled onto the surface of TiO_2 sol–gel, leading to the deposition of a thin layer of amorphous TiO_2 precursor onto the bottom of each PS sphere. Then, the as-formed MCCs with TiO_2 on the bottom was transferred to the fluoride-doped tin oxide (FTO) substrate. After removal of PS spheres via calcination process, the anatase TiO_2 nanobowl arrays were achieved with excellent electrical properties.[83–85] Furthermore, the TiO_2 nanobowl arrays on FTO were successively employed as a patterned substrate for the hydrothermal growth of rutile TiO_2 nanorods, resulting in the formation of hierarchical and periodic TiO_2 NR@NB arrays. These hierarchical TiO_2 NR@NB arrays with large surface area and the rutile/anatase phase junction were demonstrated with the significantly enhanced photocatalytic properties for water splitting.[86–88] In order to confirm their structural details, Figure 12B shows the SEM images of obtained TiO_2 NB arrays and NR@NB arrays on the FTO substrate. The top-view image of the NB arrays indicates that the formation of large area and periodic nanobowl arrays was achieved, retaining the periodic structure of the MCCs based template as given in Figure 12B(a). The corresponding tilt-view and high-magnification SEM images are also shown in Figure 12B(b),(c), while construction of hierarchical and periodic TiO_2 NR@NB arrays is evidently confirmed on FTO as presented in the SEM images in Figure 12B(d)–(f).
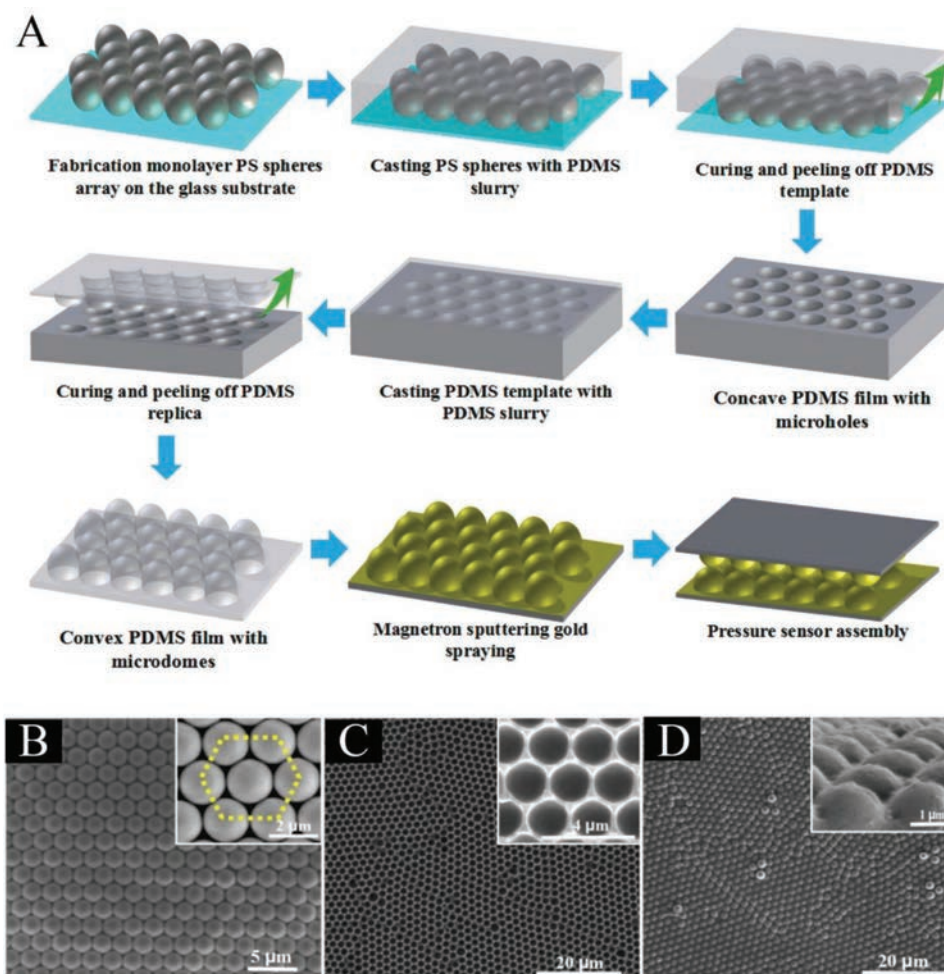
In addition to perform as masks and templates for 2D patterning, the MCCs can also be employed as the optical lens to generate 3D hierarchical and periodic nanostructures directly.[24,89] As presented in **Figure 13**A, the MCCs assembled

on the photoresist could serve as optical lens and then were illuminated with normal incident UV light. Because the self-assembled PS spheres is periodic, the diffracted light passing through the spheres would exhibit the Talbot effect, resulting in a repeated intensity with an axial period along the propagation distance.[90] The right schematic in Figure 13A shows the fabrication process of 3D nanostructures. The top-view SEM image of hierarchical and periodic 3D nanostructure with alternating layers of nanohole arrays and grating lines is also depicted in Figure 13B. The grating lines could be attributed to the polarized incident light during the exposure process. Figure 13C gives the cross-section geometry of the obtained 3D periodic nanostructures. It is obvious that these periodic nanostructures can be easily obtained and their dimensions can be precisely tuned by this simple colloidal self-assembly enabled fabrication process, which facilitate lots of practical utilizations requiring high surface-to-volume ratio, including energy storage, catalysis, and others.

However, in most cases, during the processing, the colloidal spheres are served as the sacrificial masks and cannot be reused as the optical lens, which is highly unfavorable for scalable cost-effective fabrications.[2,91] To shed light solving this problem, a novel photolithographic method by first replicating the geometrical features of self-assembled nanospheres onto the surface of a soft polymer film and then employing the film as reusable photomasks for nanopattern generations was developed.[92,93] In this special technique, highly ordered micro-/nanosphere arrays were interlinked and confined by a soft transparent polymer (e.g., polydimethylsiloxane, PDMS), and then acted as photomasks for area-selective exposures of photoresist in contact.[94] The fabrication process of soft photomask is illustrated in **Figure 14**A. First, a thin layer (30 nm) of Cu was coated on the surface of silicon wafer by magnetron sputtering. Then, a thin layer of Ti (3–5 nm) was sputtered under the same condition before the Cu deposition for the enhancement of the adhesion between the Cu and the Si substrate (Figure 14A(a)). The PS MCCs were assembled on the substrate via the LB method, and then etched by oxygen plasma to reduce the size of PS nanospheres (Figure 14A(b)).

**ADVANCED
SCIENCE NEWS**

www.advancedsciencenews.com

**ADVANCED
MATERIALS
TECHNOLOGIES**

www.advmattechnol.de

Figure 14. A) Deposition of PS nanospheres based monolayer on the Cu-coated Si substrate (a). Shrinking the nanospheres by oxygen plasma etching (b). Casting PDMS prepolymer over the nanospheres (c). Peeling off the cured PDMS film with the confined nanospheres monolayer (d). Attaching the PDMS soft mask to a photoresist layer and illuminating with flood UV light (e). Detaching the PDMS mask and developing the exposed photoresist to obtain nanopatterns (f). B) FDTD calculations of the electric field intensity ($|E|^2$) distributions. The diameters of the PS spheres in (a), (b), (c), and (d) are 500, 700, 900, and 1100 nm, respectively; and the corresponding pitches are 600, 800, 1000, and 1200 nm, respectively. The regions inside the red dashed circles denotes PS spheres; the outside circles and above the white dashed-dotted lines are PDMS matrix. The regions below the white dashed-dotted lines are photoresist (PR). All scale bars are 200 nm. C) Colloidal mask assisted optical patterning using positive photoresist (AZ5206E). (a) Digital photograph and (b)–(d) SEM images of photoresist patterns fabricated using an 1150/1280 (diameter/pitch, nm) colloidal mask. Exposure time for (b), (c), and (d) are 1, 3, and 5 s, respectively. Inset: calculated electric field intensity distribution at a depth of 300 nm under the photoresist surface. (e)–(g) SEM images of patterns fabricated using a 700/800 colloidal mask, with exposure time of 1, 2, and 4 s, respectively. (h) SEM image of pattern fabricated using a 500/600 colloidal mask, with exposure time of 4 s. Scale bars in (b)–(h) are 2 μm. Reproduced with permission.[92] Copyright 2014, American Chemical Society.

**ADVANCED
SCIENCE NEWS**
www.advancedsciencenews.com

**ADVANCED
MATERIALS
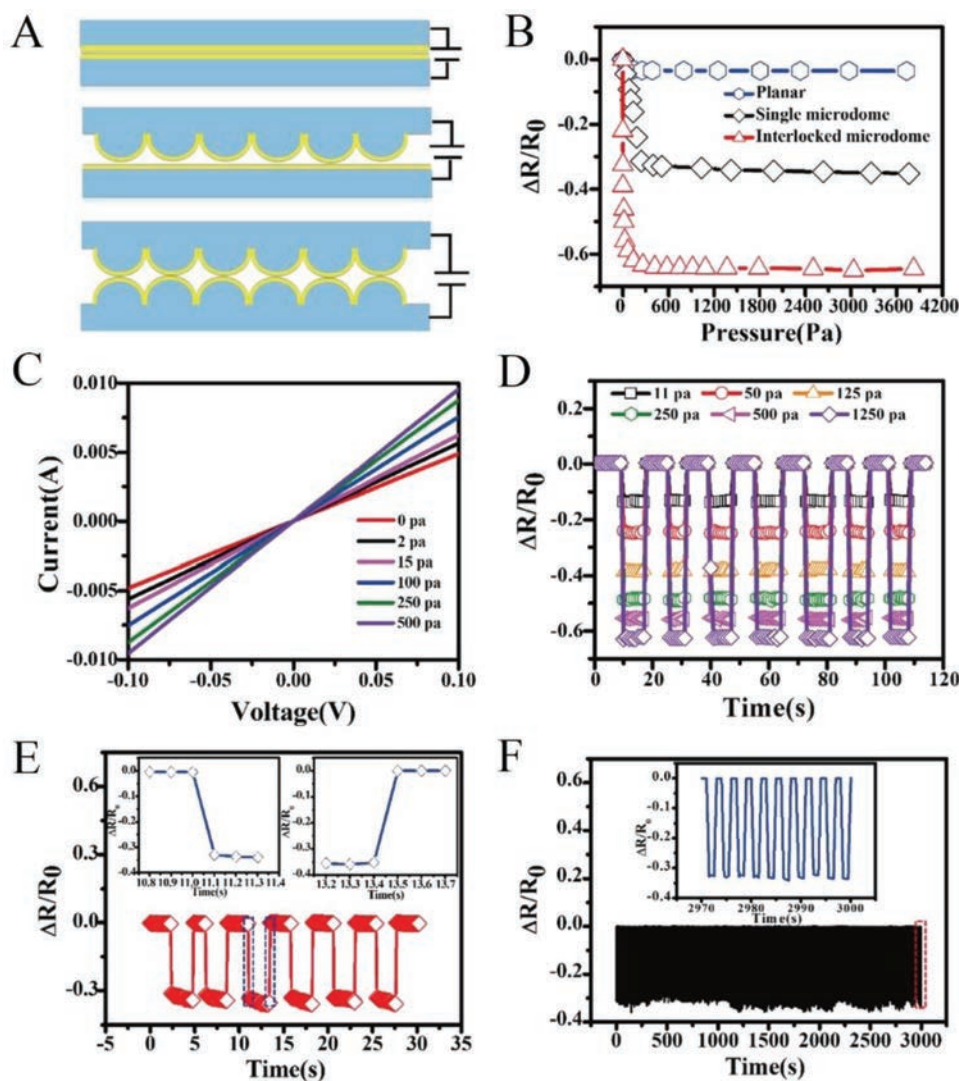TECHNOLOGIES**
www.advmattechnol.de

Figure 15. A) Schematic illustration of the fabrication process of PDMS films with microdome arrays and the corresponding pressure sensors. B) SEM image of the PS MCCs with a diameter of 2 µm. C) SEM image of the concave PDMS film with microbowls. D) SEM image of the convex PDMS film with microdome arrays. The inset shows the enlarged image of the corresponding microstructures. Reproduced with permission.[95] Copyright 2017, American Chemical Society.

PDMS prepolymers were casted over the sample in a Petri dish and cured at 60 °C for 2 h, as shown in Figure 14A(c). Finally, the cured PDMS film was peeled off manually from the substrate as shown in Figure 14A(d). Then, the PDMS soft mask was gently pressed against the surface of the photoresist layer to allow the conformable contact, and then was illuminated by UV light to fabricate the photoresist nanoholes, as presented in Figure 14A(e–f). The finite difference time-domain (FDTD) simulations were employed to further investigate the optical properties of the as-fabricated composite films. Figure 14B presents the intensity profile of the simulated UV light (365 nm) for the masks and the photoresist layer with PS sphere diameters from 500 to 1100 nm. It is clearly noted that the incident light can be efficiently focused underneath the PS nanospheres, demonstrating that these soft polymer films can serve as photomasks to produce subwavelength patterns.

After the exposure, the soft mask was detached from the substrate, rinsed with DI water and dried with nitrogen gas. These soft masks could be reused for many times without any geometrical degradation because of the mechanical robustness of embedded PS sphere within the tip region of the soft mask. Evidently, Figure 14C(a) shows the photograph of the fabricated photoresist nanoholes on a 4-in. wafer by using a 1150/1280 (diameter/pitch) soft colloidal mask. Figure 14C(b)–(d) presented the photoresist nanoholes by using positive photoresist. The inset of Figure 14C(d) shows the FDTD calculated light-intensity distribution in a horizontal plane at the depth of 300 nm below the photoresist surface. Moreover, the feature size and geometry can be finely tuned by changing the exposure time. With the increase of the exposure time, the size of holes became enlarged, and meanwhile, the shape changed from round to hexagonal. The shape change may result from the multiple light scattering among the spheres that were well-packed in a hexagonal lattice. Figure 14C(e)–(h) displays the SEM images of patterns fabricated using the masks of smaller colloidal particle sizes (700/800 and 500/600, diameter/pitch, nm) and different exposure parameters, showing excellent control of sizes/pitches of the features over wide dimension ranges. All these results can clearly reveal the versatility and the reproducibility of this unique fabrication scheme.
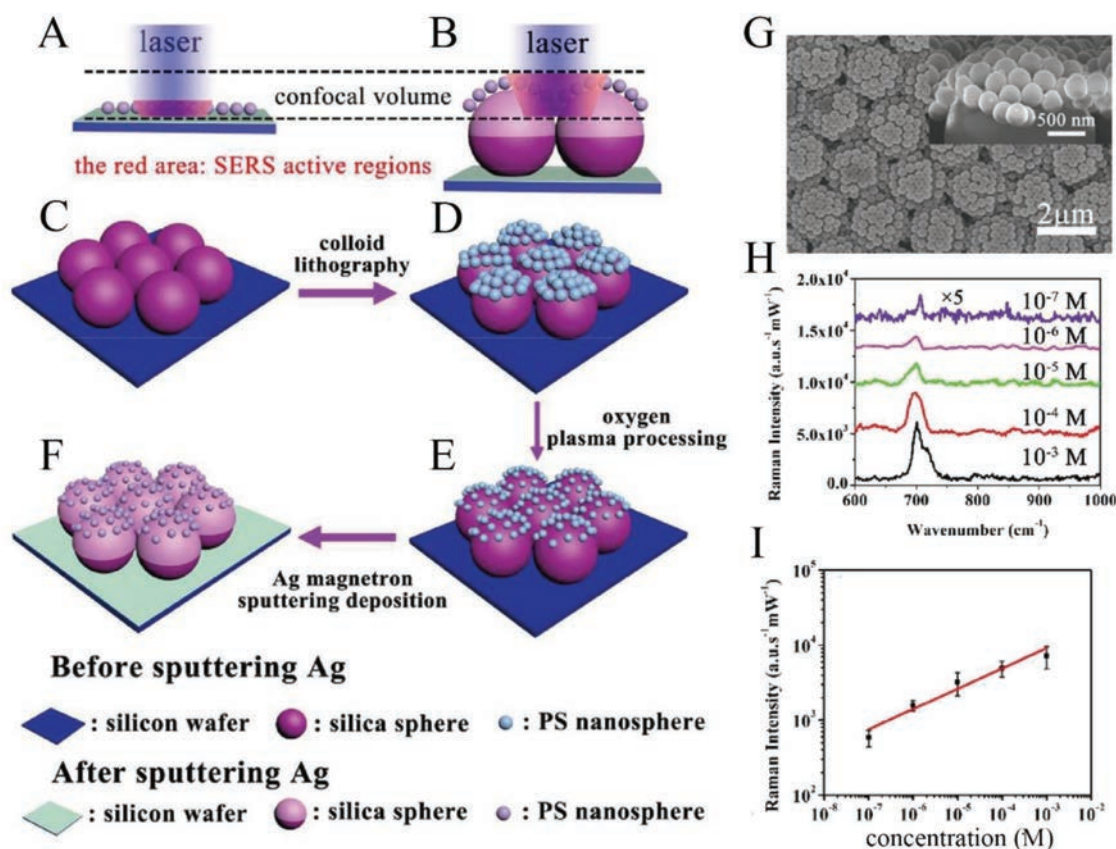
Figure 16. A) The diagram of three different sensor structures. B) The comparison of pressure sensitivities of different sensor structures: the planar film, single microdome film, and the interlocked microdome film. C) Current–voltage (I–V) curves of the pressure sensor with different applied pressures. D) Time-resolved static resistance change response of the sensor under repeated mechanical loads with pressures ranging from 11 to 1250 Pa. E) Response time of the pressure sensor with an applied pressure of 100 Pa. The insets show the section of the curve within the dashed lines which corresponds to the loading of pressure. F) Relative resistance changes of the sensor with repetition of 1000 loading/unloading cycles by 100 Pa. The inset shows the resistance change curves of the sensor extracted from the red part. Reproduced with permission.[95] Copyright 2017, American Chemical Society.

4. Other Practical Utilizations for Various Application Domains

Due to the features of simplicity, cost-effectiveness and well-controlled morphology, the self-assembly of colloidal spheres has been extensively applied to fabricate hierarchical and periodic 2D or 3D nanostructures, and subsequently applied in many technological fields such as the sensors and surface-enhanced Raman scattering (SERS).[95–98] **Figure 15**A shows the fabrication process of a flexible pressure sensor based on self-assembly of colloid PS microspheres and PDMS–PDMS pattern transfer technology. The 2 μm PS microspheres were self-assembled on glass to form MCCs and then covered with PDMS slurry (Figure 15B, SEM image of PS monolayer). After

peeling off from the glass substrate, the concave PDMS layer was obtained and acted as a template for the casting of PDMS slurry (Figure 15C, the corresponding SEM image). Finally, the convex PDMS with microdomes was achieved after the PDMS slurry form the concave PDMS layer. The SEM image of corresponding PDMS film with convex microdomes replicated from the concave PDMS is shown as the Figure 15D. The flexible pressure sensor is consisted of two pieces of PDMS films with microdome arrays, as displayed in Figure 15A.

The flexible pressure sensor with interlocking microdomes based on 2 μm PS spheres is presented in **Figure 16**A. As compared with the planar type and the planar/single microdome type, the response of the interlocked microdome sensor is very sensitive as illustrated in Figure 16B. The remarkable sensing

**ADVANCED
SCIENCE NEWS**
www.advancedsciencenews.com

**ADVANCED
MATERIALS
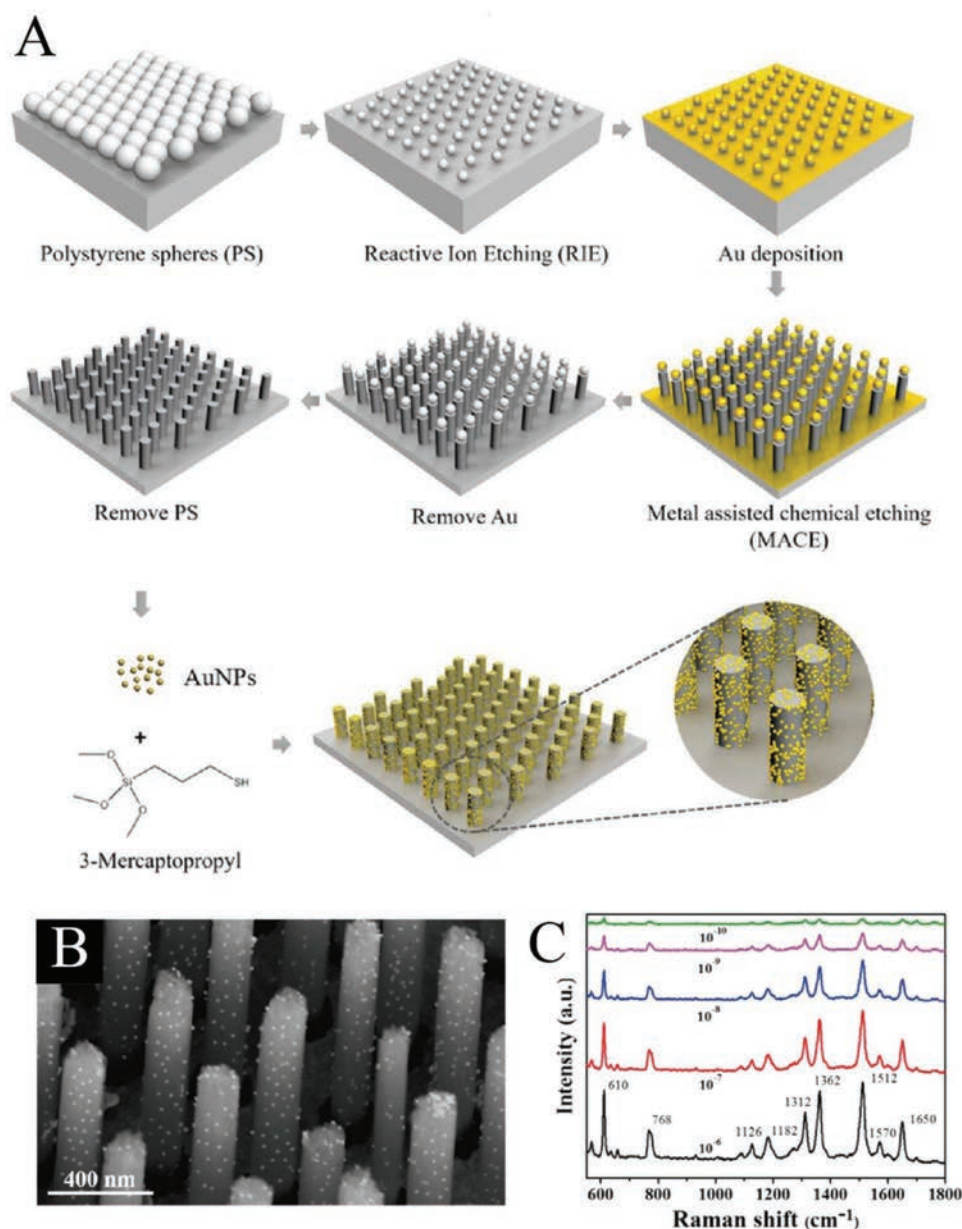TECHNOLOGIES**
www.advmattechnol.de

Figure 17. Schematic illustration of the preparation of SLNAs-Ag on clean Si wafers. A,B) The comparison between the planar and 3D microstructures. The "SERS active regions" were marked respectively with the red shadows. C) The silica spheres templates (denoted with red big spheres) prepared by spin-coating. D) A monolayer close-packed hexagonal structure of polystyrene (PS) particles (denoted with blue spheres) transferred onto the surface of silica spheres using colloid lithography. E) PS nanospheres were etching via oxygen plasma etching. F) Ag film deposition on etched PS nanospheres templates. G) SEM images of sunflower-like" nanoarrays decorated with Ag nanoparticles under the etching time of 5 min. H) SERS spectra of melamine with various concentrations ranging from 10^{-3} to 10^{-7} M. I) The calibration curve of normalized Raman intensity at 701 cm^{-1} versus the concentration of melamine. Reproduced with permission.[99] Copyright 2017, The Royal Society of Chemistry.

performance of this interlocked microdome sensor can be attributed to the change of the contact area, caused by the deformation of the microstructure. In addition, the electrical characteristics of the pressure sensor were also investigated. As given in Figure 16C, the current–voltage (*I–V*) curves of the pressure sensor under different weights were recorded. It is noted that the slope of the *I–V* curves increases with the increasing of the applied load under the constant voltage, indicating the resistance decrease as the external pressure rises. This linear characteristic of the *I–V* curves demonstrates that the device behavior obeys Ohm's contact behaviors. The reproducibility and stability properties of the pressure sensor under series of external pressures ranging from 11 to 1250 Pa were as well investigated. As depicted in Figure 16D, it is obvious that relative changes in resistance repeatedly take place under various external pressures, indicating the stable sensing performance and the great reproducibility of the pressure sensor upon various pressures regardless of low pressure, medium pressure, or high pressure. It also demonstrates that the pressure sensor can rapidly respond to the loading/unloading applied force without hysteresis. Figure 16E shows the response and relaxation time upon the application of a repeated pressure of 100 Pa. The similar

relative changes in resistance for the 6 cycles indicates a cycling stability of the flexible sensor under the pressure of 100 Pa. The insets indicate that the instant response time of sensor is impressively less than 100 ms. Meanwhile, the same value of relative resistance changes after 1000 loading/unloading cycles (Figure 16F) further demonstrate a high durability of the pressure sensor, which can be attributed to the excellent elasticity of the PDMS microdomes. This finding would confirm the double layer PDMS structure serving as a good preliminary platform for the fabrication of highly efficient pressure sensors.

Beside pressure sensors, **Figure 17** presents the application of self-assembly of colloidal spheres in the field of SERS.[99] The 3D hierarchical sunflower-like nanoarrays decorated with Ag nanoparticles (SLNAs-Ag) could be obtained by combining binary colloidal spheres (i.e., SiO$_2$ and PS spheres) and then decorating with Ag nanoparticles. First, Figure 17A,B shows the comparison of SERS active regions between the planar and 3D microstructures. The fabrication procedures of 3D SLNAs-Ag is then schematically illustrated in Figure 17C–F. Particularly, the monolayer of silica spheres was prepared on the substrate, and then acted as the basement for deposition of PS nanospheres via a spin-coating method (Figure 17C,D.

**ADVANCED
SCIENCE NEWS**

www.advancedsciencenews.com

**ADVANCED
MATERIALS
TECHNOLOGIES**

www.advmattechnol.de

Figure 18. A) Schematic illustration of Au nanoparticles (AuNPs)-conjugated Si nanorod (Si NR) arrays fabricating process. B) SEM images of AuNPs conjugated SiNR array. C) Raman spectra of Rhodamine 6G (R6G) molecules from 10^{-6} to 10^{-10} M on AuNPs@SiNR substrates. Reproduced with permission.[100] Copyright 2017, American Chemical Society.

After oxygen plasma etching, the Ag film was evaporated onto the sunflower-like nanoarrays consisting of silica nanospheres and PS nanospheres to generate an SERS substrate (Figure 17E,F), followed by the deposition of Ag on the SLNAs with etching time of 5 min. The SEM image of the SLNAs-Ag was presented in Figure 17G, and it can be clearly seen that there are obvious gaps between the adjacent PS nanospheres. After that, the SLNAs-Ag was dipped into different melamine water solutions with concentrations ranging from 10^{-3} to 10^{-7} M for SERS measurement. Figure 17H shows the SERS spectrums of various concentration levels of melamine from 10^{-3} to 10^{-7} M. The characteristic SERS spectra peaks at 701 cm^{-1} of melamine can be evidently observed for all concentration levels

of melamine. It is also noted that the SERS sensitivity at 701 cm^{-1} increases linearly with the increasing of the concentration of melamine (Figure 17I), demonstrating a high performance and low-cost SERS sensor of the SLNAs-Ag. The excellent control in the dimension of obtained hierarchical and periodic nanostructures enabled by colloidal self-assembly assisted fabrication techniques can further manipulate the detection peak and other SERS features for lots of other related applications.

The Si nanorod arrays fabricated by nanosphere lithography and metal-assisted chemical etching also can be applied in the area of SERS as shown in **Figure 18**.[100] As schematically depicted in Figure 18A, the SiNR arrays can be obtained from the following process: (i) self-assembly of a PS monolayer on

**ADVANCED
SCIENCE NEWS**
www.advancedsciencenews.com

**ADVANCED
MATERIALS
TECHNOLOGIES**
www.advmattechnol.de

the Si surface, (ii) reduction of diameter of PS nanospheres by RIE processing; (iii) deposition of the Au layer on the substrate; (iv) metal-assisted chemical etching; (v) removal of Au and PS nanospheres; (vi) conjugation of AuNPs. In order to achieve the conjugation with AuNPs, 3-mercaptopropyltrimethoxysilane (MPTS) was used due to its simple structure, easily removed by photolysis and no disturbance in the Raman spectra of target molecules.[101] The MPTS consists of three $-OCH_3$ and sulfhydryl, the former can be connected with silicon hydroxyl by a chemical reaction, while the latter can link to AuNPs on the other side. Therefore, abundant AuNPs (diameter 20 nm) can be decorated on the surface of SiNRs as displayed in Figure 18B. The SERS measurement of the AuNPs@SiNR was further investigated by varying the concentration of R6G molecules from 10^{-6} to 10^{-10} M. As presented in Figure 18C, the Raman intensity increases gradually with the increasing of R6G concentration. It can be seen that the distinguishable signals at the concentration of 10^{-10} M can still be observed, in which all these demonstrate an excellent Raman sensitivity of AuNPs@SiNR.

5. Conclusions and Outlook

In summary, nanosphere lithography enabled with self-assembly of colloidal spheres, modification of monolayer colloidal crystals and other lithographic processes can evidently serve as a cost-effective and large-scale surface patterning method as well as a straightforward one-step 3D fabrication scheme. In this review, the current up-to-date status on the research and development of self-assembly of colloidal spheres for the fabrication of various hierarchical and periodic nanostructures are summarized. To be specific, we focus on the fundamentals of colloidal self-assembly, the functions of obtained monolayers of colloidal spheres and the successive construction of numerous nanostructures. The applications of as-fabricated hierarchical and periodic nanostructures are also introduced. In spite of the great success of self-assembly of colloidal spheres and the subsequent fabrication of nanostructures, there are still several issues associated with nanosphere lithography, which remains to be addressed in the near future for their practical utilizations. First, the defects in the monolayer colloidal crystals will be entailed to the subsequent nanostructures, resulting the deterioration of the devices based on these nanostructures. Thus, the defects-free of these self-assembled colloids in large-scale should be further achieved. Second, although there are various assembly methods developed, such as the Langmuir–Blodgett scheme, their processing time is somewhat longer than required. Therefore, continual development of rapid assembly of monolayer colloidal crystals would be essential for their successive deployments to the industry. Third, the polystyrene or silica spheres are frequently used to function as masks, templates or optical lens. More colloidal materials configured in spherical shapes with the better dimension, surface and mechanical property control should be developed in order to fulfill different requirements for other technological domains. Fourth, these nanosphere lithography techniques can also be combined with two or more different fabrication techniques to generate more sophisticated hierarchical and periodic

nanostructures, especially for 3D configured geometries. This would enable the simple fabrication approach for the realization of complex structures, which cannot be easily achieved by various newly developed 3D printing schemes. Finally, substantial efforts should be input into the practical applications of hierarchical and periodic nanostructures facilitated by these nanosphere lithography enabled fabrication routes. All these fabricated structures would contain unexceptionally large surface-to-volume ratio, which are advantageous for lots of utilizations in photovoltaics, photonics, energy storage, catalysis, and others. With all the reviewed features and promising properties of nanolithography based on these self-assembly of colloidal spheres, we anticipate this technique bringing promising applications in the near future.

Conflict of Interest

The authors declare no conflict of interest.

[1] X. Ye, L. Qi, *Nano Today* **2011**, *6*, 608.
[2] J. Zhang, Y. Li, X. Zhang, B. Yang, *Adv. Mater.* **2010**, *22*, 4249.
[3] S. M. Yang, S. G. Jang, D. G. Choi, S. Kim, H. K. Yu, *Small* **2006**, *2*, 458.
[4] J. Tian, J. Jin, F. Zheng, H. Zhao, *Langmuir* **2010**, *26*, 8762.
[5] U. C. Fischer, H. P. Zingsheim, *J. Vacuum Sci. Technol.* **1981**, *19*, 881.
[6] K. Satoh, M. Matsuda, K. Nagai, M. Kamigaito, *Nat. Nanotechnol.* **2007**, *2*, 145.
[7] Z. Ning, O. Voznyy, J. Pan, S. Hoogland, V. Adinolfi, J. Xu, M. Li, A. R. Kirmani, J. P. Sun, J. Minor, *Nat. Mater.* **2014**, *13*, 822.
[8] X. Liang, Y. Cheng, X. Xu, R. Dong, D. Li, Z. Zhou, R. Wei, G. Dong, S. W. Tsang, J. C. Ho, *Appl. Surf. Sci.* **2018**, *451*, 250.
[9] X. Liang, L. Shu, H. Lin, M. Fang, H. Zhang, G. Dong, S. Yip, F. Xiu, J. C. Ho, *Sci. Rep.* **2016**, *6*, 34139.
[10] D. S. Dolzhnikov, H. Zhang, J. Jang, J. S. Son, M. G. Panthani, T. Shibata, S. Chattopadhyay, D. V. Talapin, *Science* **2015**, *347*, 425.

**ADVANCED
SCIENCE NEWS**

www.advancedsciencenews.com

**ADVANCED
MATERIALS
TECHNOLOGIES**

www.advmattechnol.de

[11] Y. Shirasaki, G. J. Supran, M. G. Bawendi, V. Bulović, *Nat. Photonics* **2013**, *7*, 13.

[12] B. Kowalczyk, I. Lagzi, B. A. Grzybowski, *Curr. Opin. Colloid Interface Sci.* **2011**, *16*, 135.

[13] Y. Hu, Y. Liu, H. Qian, Z. Li, J. Chen, *Langmuir* **2010**, *26*, 18570.

[14] S. Nie, S. R. Emory, *Science* **1997**, *275*, 1102.

[15] K. Kneipp, Y. Wang, H. Kneipp, L. T. Perelman, I. Itzkan, *Phys. Rev. Lett.* **1997**, *78*, 1667.

[16] P. J. Dowding, B. Vincent, *Colloids Surf., A* **2000**, *161*, 259.

[17] R. J. Ansell, K. Mosbach, *J. Chromatogr., A* **1997**, *787*, 55.

[18] S. Omi, M. Saito, T. Hashimoto, M. Nagai, G. H. Ma, *J. Appl. Polym. Sci.* **1998**, *68*, 897.

[19] J. M. Desimone, E. E. Maury, Y. Z. Menceloglu, J. B. Mcclain, T. J. Romack, J. R. Combes, *Science* **1994**, *265*, 356.

[20] M. Peer, A. Qajar, R. Rajagopalan, H. C. Foley, *Carbon* **2013**, *51*, 85.

[21] Z. Z. Gu, H. Chen, S. Zhang, L. Sun, Z. Xie, Y. Ge, *Colloids Surf., A* **2007**, *302*, 312.

[22] Q. He, X. Cui, F. Cui, L. Guo, J. Shi, *Microporous Mesoporous Mater.* **2009**, *117*, 609.

[23] T. Qiu, B. Luo, M. Giersig, E. M. Akinoglu, L. Hao, X. Wang, L. Shi, M. Jin, L. Zhi, *Small* **2015**, *10*, 4136.

[24] X. A. Zhang, J. Elek, C. H. Chang, *ACS Nano* **2013**, *7*, 6212.

[25] Y. Wang, N. Lu, H. Xu, G. Shi, M. Xu, X. Lin, H. Li, W. Wang, D. Qi, Y. Lu, *Nano Res.* **2010**, *3*, 520.

[26] J. Yoo, *Sol. Energy* **2010**, *84*, 730.

[27] C. J. Heo, S. H. Kim, S. G. Jang, S. Y. Lee, S. M. Yang, *Adv. Mater.* **2009**, *21*, 1726.

[28] R. Walter, A. Tittl, A. Berrier, F. Sterl, T. Weiss, H. Giessen, *Adv. Opt. Mater.* **2015**, *3*, 398.

[29] J. C. Li, Y. L. Chen, S. Y. Lu, *U.S. Patent Application 14/791*, 241, **2015**.

[30] Y. Zhang, T. Wei, Z. Xiong, L. Shang, *Appl. Phys. Lett.* **2014**, *105*, 013108.

[31] C. L. Haynes, R. P. Van Duyne, *J. Phys. Chem. B* **2001**, *105*, 5599.

[32] J. C. Hulteen, R. P. Van Duyne, *J. Vac. Sci. Technol., A* **1995**, *13*, 1553.

[33] J. H. Moon, W. S. Kim, J.-W. Ha, S. G. Jang, S. M. Yang, J. K. Park, *Chem. Commun.* **2005**, 4107.

[34] M. H. Wu, C. Park, G. M. Whitesides, *J. Colloid Interface Sci.* **2003**, *265*, 304.

[35] A. Douvas, P. Argitis, K. Misiakos, D. Dimotikali, P. S. Petrou, S. E. Kakabakos, *Biosens. Bioelectron.* **2002**, *17*, 269.

[36] C. Vieu, F. Carcenac, A. Pépin, Y. Chen, M. Mejias, A. Lebib, L. Manin-Ferlazzo, L. Couraud, H. Launois, *Appl. Surf. Sci.* **2000**, *164*, 111.

[37] J. Taniguchi, K. Koga, Y. Kogo, I. Miyamoto, *Microelectron. Eng.* **2006**, *83*, 940.

[38] A. Kosiorek, W. Kandulski, H. Glaczynska, M. Giersig, *Small* **2005**, *1*, 439.

[39] L. Ji, Y. F. Chang, B. Fowler, Y. C. Chen, T. M. Tsai, K. C. Chang, M. C. Chen, T. C. Chang, S. M. Sze, E. T. Yu, *Nano Lett.* **2014**, *14*, 813.

[40] H. Ceylan, M. Urel, T. S. Erkal, A. B. Tekinay, A. Dana, M. O. Guler, *Adv. Funct. Mater.* **2013**, *23*, 2100.

[41] S. Cataldo, J. Zhao, F. Neubrech, B. Frank, C. Zhang, P. V. Braun, H. Giessen, *ACS Nano* **2012**, *6*, 979.

[42] S. W. Lee, K. S. Lee, J. Ahn, J. J. Lee, M. G. Kim, Y. B. Shin, *ACS Nano* **2011**, *5*, 897.

[43] W. Wu, M. Hu, F. S. Ou, Z. Li, R. S. Williams, *Nanotechnology* **2010**, *21*, 255502.

[44] B. Cui, T. Veres, *Microelectron. Eng.* **2007**, *84*, 1544.

[45] A. S. Dimitrov, K. Nagayama, *Langmuir* **1996**, *12*, 1303.

[46] X. Li, J. Wang, J. Zhang, X. Yan, X. Zhang, D. Zhu, W. Li, X. Zhang, B. Yang, *Langmuir* **2010**, *26*, 2930.

[47] P. Jiang, M. J. McFarland, *J. Am. Chem. Soc.* **2004**, *126*, 13778.

[48] S. O. Lumsdon, E. W. Kaler, O. D. Velev, *Langmuir* **2004**, *20*, 2108.

[49] M. Trau, D. Saville, I. Aksay, *Science* **1996**, *272*, 706.

[50] M. Bardosova, M. E. Pemble, I. M. Povey, R. H. Tredgold, *Adv. Mater.* **2010**, *22*, 3104.

[51] R. van Dommelen, P. Fanzio, L. Sasso, *Adv. Colloid Interface Sci.* **2018**, *251*, 97.

[52] L. J. Cote, F. Kim, J. Huang, *J. Am. Chem. Soc.* **2009**, *131*, 1043.

[53] H. Du, Y. Bai, Z. Hui, L. Li, Y. Chen, X. Tang, T. Li, *Langmuir* **1997**, *13*, 2538.

[54] J. H. Clint, S. E. Taylor, *Colloids Surf.* **1992**, *65*, 61.

[55] M. Bardosova, P. Hodge, V. Smatko, R. Tredgold, D. Whitehead, *Acta Phys. Slovaca* **2004**, *54*, 409.

[56] V. Lotito, T. Zambelli, *Langmuir* **2016**, *32*, 9582.

[57] P. Gao, J. He, S. Zhou, X. Yang, S. Li, J. Sheng, D. Wang, T. Yu, J. Ye, Y. Cui, *Nano Lett.* **2015**, *15*, 4591.

[58] K. Shinotsuka, Y. Kajita, K. Hongo, Y. Hatta, *Langmuir* **2015**, *31*, 11452.

[59] V. Burtsev, V. Marchuk, A. Kugaevskiy, O. Guselnikova, R. Elashnikov, E. Miliutina, P. Postnikov, V. Svorcik, O. Lyutakov, *Appl. Surf. Sci.* **2018**, *433*, 443.

[60] F. Teng, N. Li, D. Xu, D. Xiao, X. Yang, N. Lu, *Nanoscale* **2017**, *9*, 449.

[61] Z. Huang, H. Fang, J. Zhu, *Adv. Mater.* **2007**, *19*, 744.

[62] J. Gong, N. Wu, *Langmuir* **2017**, *33*, 5769.

[63] X. Li, *Curr. Opin. Solid State Mater. Sci.* **2012**, *16*, 71.

[64] Z. Huang, N. Geyer, P. Werner, J. de Boor, U. Gosele, *Adv. Mater.* **2011**, *23*, 285.

[65] C. Chartier, S. Bastide, C. Lévy-Clément, *Electrochim. Acta* **2008**, *53*, 5509.

[66] Y. Li, X. Ye, Y. Ma, L. Qi, *Small* **2015**, *11*, 1183.

[67] L. Xu, Z. Yin, S. W. Cao, Z. Fan, X. Zhang, H. Zhang, C. Xue, *Chem. - Eur. J.* **2014**, *20*, 2742.

[68] W. Wu, A. Katsnelson, O. G. Memis, H. Mohseni, *Nanotechnology* **2007**, *18*, 485302.

[69] H. Lin, H. Y. Cheung, F. Xiu, F. Wang, S. Yip, N. Han, T. Hung, J. Zhou, J. C. Ho, C. Y. Wong, *J. Mater. Chem. A* **2013**, *1*, 9942.

[70] H. Lin, M. Fang, H. Y. Cheung, F. Xiu, S. Yip, C. Y. Wong, J. C. Ho, *RSC Adv.* **2014**, *4*, 50081.

[71] F. Xiu, H. Lin, M. Fang, G. Dong, S. Yip, J. C. Ho, *Pure Appl. Chem.* **2014**, *86*, 557.

[72] H. Lin, F. Xiu, M. Fang, S. Yip, H. Y. Cheung, F. Wang, N. Han, K. S. Chan, C. Y. Wong, J. C. Ho, *ACS Nano* **2014**, *8*, 3752.

[73] X. Xu, Q. Yang, N. Wattanatorn, C. Zhao, N. Chiang, S. J. Jonas, P. S. Weiss, *ACS Nano* **2017**, *11*, 10384.

[74] A. Pakes, G. Thompson, P. Skeldon, P. Morgan, *Corros. Sci.* **2003**, *45*, 1275.

[75] S. Z. Chu, K. Wada, S. Inoue, S. Todoroki, *J. Electrochem. Soc.* **2002**, *149*, B321.

[76] I. Minguez-Bacho, F. Scheler, P. Buttner, K. Bley, N. Vogel, J. Bachmann, *Nanoscale* **2018**, *10*, 8385.

[77] N. T. Suen, S. F. Hung, Q. Quan, N. Zhang, Y. J. Xu, H. M. Chen, *Chem. Soc. Rev.* **2017**, *46*, 337.

[78] Z. W. Seh, J. Kibsgaard, C. F. Dickens, I. Chorkendorff, J. K. Norskov, T. F. Jaramillo, *Science* **2017**, *355*, eaad4998.

[79] M. Fang, G. Dong, R. Wei, J. C. Ho, *Adv. Energy Mater.* **2017**, *7*, 1700559.

[80] M. Fang, W. Gao, G. Dong, Z. Xia, S. Yip, Y. Qin, Y. Qu, J. C. Ho, *Nano Energy* **2016**, *27*, 247.

[81] K. Chen, D. D. Thang, S. Ishii, R. P. Sugavaneshwa, T. Nagao, *Opt. Mater. Express* **2015**, *5*, 353.

[82] W. Wang, J. Dong, X. Ye, Y. Li, Y. Ma, L. Qi, *Small* **2016**, *12*, 1469.

[83] G. K. Mor, K. Shankar, O. K. Varghese, C. A. Grimes, *J. Mater. Res.* **2004**, *19*, 2989.

[84] J. R. Jennings, A. Ghicov, L. M. Peter, P. Schmuki, A. B. Walker, *J. Am. Chem. Soc.* **2008**, *130*, 13364.

[85] N. Negishi, K. Takeuchi, T. Ibusuki, *J. Mater. Sci.* **1998**, *33*, 5789.

1800541 (18 of 19)

**ADVANCED
SCIENCE NEWS**

www.advancedsciencenews.com

**ADVANCED
MATERIALS
TECHNOLOGIES**

www.advmattechnol.de

[86] J. Buckeridge, K. T. Butler, C. R. A. Catlow, A. J. Logsdail, D. O. Scanlon, S. A. Shevlin, S. M. Woodley, A. A. Sokol, A. Walsh, *Chem. Mater.* **2015**, *27*, 3844.

[87] D. O. Scanlon, C. W. Dunnill, J. Buckeridge, S. A. Shevlin, A. J. Logsdail, S. M. Woodley, C. R. Catlow, M. J. Powell, R. G. Palgrave, I. P. Parkin, *Nat. Mater.* **2013**, *12*, 798.

[88] L. W. Zhang, Y. J. Wang, H. Y. Cheng, W. Q. Yao, Y. F. Zhu, *Adv. Mater.* **2009**, *21*, 1286.

[89] C. H. Chang, L. Tian, W. R. Hesse, H. Gao, H. J. Choi, J. G. Kim, M. Siddiqui, G. Barbastathis, *Nano Lett.* **2011**, *11*, 2533.

[90] C. R. Worthington, J. T. Winthrop, *J. Opt. Soc. Am.* **1965**, *55*, 373.

[91] J. Zhang, B. Yang, *Adv. Funct. Mater.* **2010**, *20*, 3411.

[92] M. Fang, H. Lin, H. Y. Cheung, F. Xiu, L. Shen, S. Yip, E. Y. Pun, C. Y. Wong, J. C. Ho, *ACS Appl. Mater. Interfaces* **2014**, *6*, 20837.

[93] M. Fang, H. Lin, H. Y. Cheung, S. Yip, F. Xiu, C. Y. Wong, J. C. Ho, *Adv. Opt. Mater.* **2014**, *2*, 855.

[94] T. Y. Jeon, H. C. Jeon, S. Y. Lee, T. S. Shim, J. D. Kwon, S. G. Park, S. M. Yang, *Adv. Mater.* **2014**, *26*, 1421.

[95] Y. Zhang, Y. Hu, P. Zhu, F. Han, Y. Zhu, R. Sun, C. P. Wong, *ACS Appl. Mater. Interfaces* **2017**, *9*, 35968.

[96] Y. Luo, X. Jiang, L. Liu, G. Si, *Nanosci. Nanotech. Let.* **2018**, *10*, 1.

[97] H. S. Lee, J. Chung, G. T. Hwang, C. K. Jeong, Y. Jung, J. H. Kwak, H. Kang, M. Byun, W. D. Kim, S. Hur, *Adv. Funct. Mater.* **2014**, *24*, 6914.

[98] C. Pang, G. Y. Lee, T. I. Kim, S. M. Kim, H. N. Kim, S. H. Ahn, K. Y. Suh, *Nat. Mater.* **2012**, *11*, 795.

[99] X. Zhang, X. Xiao, Z. Dai, W. Wu, X. Zhang, L. Fu, C. Jiang, *Nanoscale* **2017**, *9*, 3114.

[100] D. Lin, Z. Wu, S. Li, W. Zhao, C. Ma, J. Wang, Z. Jiang, Z. Zhong, Y. Zheng, X. Yang, *ACS Nano* **2017**, *11*, 1478.

[101] I. Choi, Y. S. Huh, D. Erickson, *Microfluidics Nanofluidics* **2012**, *12*, 663.

**ADVANCED
SCIENCE NEWS**
www.advancedsciencenews.com

**ADVANCED
MATERIALS
TECHNOLOGIES**
www.advmattechnol.de

and hence it can be widely utilized for the fabrication of periodic nanostructures in many manufacturing platform without the limitation of expensive and complex equipment. In this regard, the combination of lithographic methods based on colloidal self-assembly and other nanofabrication techniques can provide an alternative and intriguing strategy to create periodic nanostructures.[38] A great variety of 2D and 3D periodic micro/nanostructures, consisting of pillars, holes, rings, bowls, cones, disks, and other special structures, have been obtained based on these colloidal self-assembly assisted manufacturing schemes.[39–44] These hierarchical and periodic nanostructures with the well-controlled morphology, dimension, and intrinsic property are demonstrated to have the broad applications in solar cells, sensors, biology, photonics, and many others. Nevertheless, although substantial progresses in the appropriate design of these hierarchical and periodic micro/nanostructures are highly desired for the practical utilizations of colloidal self-assembly, there is still a lack of the comprehensive survey on these MCCs enabled nanostructures in the community.

In this work, we present a comprehensive review on the recent revolution in the fabrication of hierarchical and periodic nanostructures based on different nanosphere lithographic techniques. Special attentions are focused on the self-assembly of colloidal spheres, their morphological control and modification, as well as their functions in the fabrication process of nanostructures. Their applications in various technological domains will then be carefully emphasized. At the end, the current challenges and promising future prospects of these colloidal self-assembly are as well given. This survey does not only aim to provide further insights for researchers to enable the ingenious designs of nanostructures, but also facilitate the exciting research and development utilizing colloidal self-assembly for future manufacturing technologies.

2. Controllable Self-Assembly of Colloidal Spheres

In colloidal science, it is still a difficult task to achieve the controllable, uniform and large-scale self-assembly of colloidal spheres in a rapid and cost-effective manner. Until now, there are several key strategies developed to tackle the colloidal self-assembly issues, which can be divided into five different schemes, namely, (i) drop-coating, (ii) dip-coating, (iii) spin-coating, (iv) electrophoretic deposition, and (v) transferring self-assembly film at the gas/liquid interface to the gas/solid interface of substrate, as shown in **Figure 1**.[1] Specifically, during the drop-coating procedure (Figure 1A), the solvent evaporation rate is the primary parameter that affects the ordering and quality of the obtained monolayer film of colloidal spheres.[45] It is noted that the ordering and quality of these self-assembled arrays can be improved significantly by using dip-coating method for the accurate control of the solvent evaporation, as illustrated in Figure 1B.[46] For both of these two schemes, the capillary force and convective transport of the colloids (e.g., nanospheres) induced by the continuous solvent evaporation are the main process controlling factors. In order to obtain the large-area coating and high-throughput formation of these MCCs, spin-coating

Xiaoguang Liang received his B.E., M.E., and Ph.D. degrees from Hefei University of Technology in 2009, Kunming University of Science and Technology in 2012, and City University of Hong Kong in 2017, respectively. At present, he is a visiting scholar in the Department of Materials Science and Engineering at City University of Hong Kong under supervision of Professor Johnny C. Ho. His research interests are nanostructured arrays fabricated by the Langmuir-Blodgett method, and their applications in photovoltaic devices such as silicon and organometallic halide perovskite solar cells.

Ruoting Dong received her B.S. and M.S. degrees from South China Normal University in 2009 and 2013, respectively. Currently, she is a Ph.D. student under the supervision of Prof. Johnny C. Ho in the Department of Materials Science and Engineering at City Universi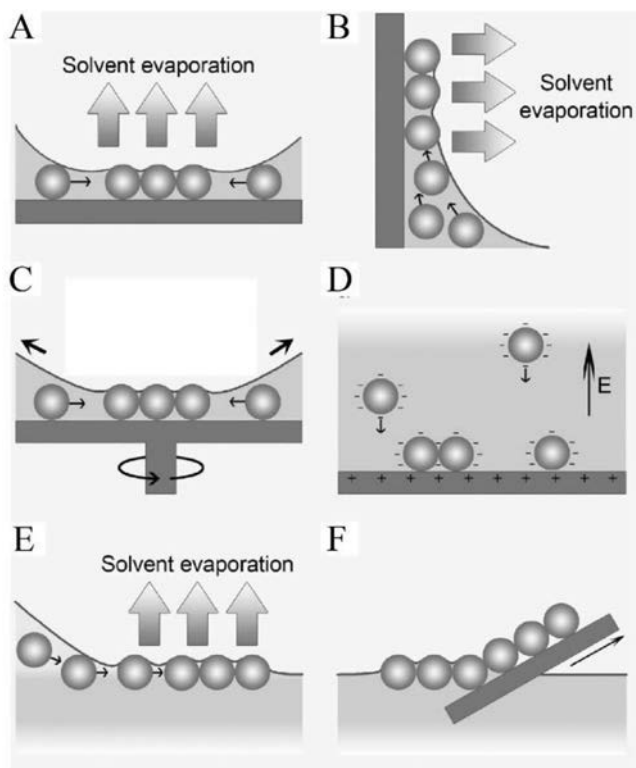ty of Hong Kong. Her research interests are the controlled synthesis of nanomaterials and their applications in electronics and optoelectronics.

Johnny C. Ho received his B.S. with high honors in Chemical Engineering in 2002 and his M.S. and Ph.D. in Materials Science and Engineering from the University of California, Berkeley, in 2005 and 2009, respectively. From 2009 to 2010, he worked as a postdoctoral research fellow in the nanoscale synthesis and characterization group at Lawrence Livermore National Laboratory, California. Currently, he is an Associate Professor of Materials Science and Engineering at City University of Hong Kong. His research interests focus on the synthesis, characterization, integration, and device applications of nanoscale materials for various technological applications, including nanoelectronics, sensors, and energy harvesting.

method can be selected for the operation on any flat-surface substrate. For instance, the colloidal nanospheres can be densely deposited onto the substrate by spin-coating, while

**ADVANCED
SCIENCE NEWS**

www.advancedsciencenews.com

**ADVANCED
MATERIALS
TECHNOLOGIES**

www.advmattechnol.de

Figure 1. Schematic illustration of various colloidal self-assembly strategies. A) Drop-coating, B) dip-coating, C) spin-coating, D) electrophoretic deposition, E) self-assembly at the gas/liquid interface, and F) transfer from the gas/liquid to the gas/solid interface. Reproduced with permission.[1] Copyright 2011, Elsevier Ltd.
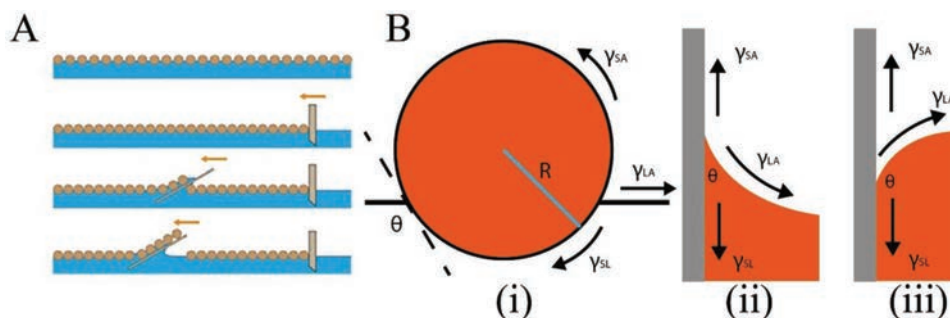
the quality of assembled colloidal film is mainly manipulated by the concentration of colloidal suspension, spin-coating speed, substrate wettability, etc (Figure 1C).[47] By using electrophoretic deposition, the charged nanospheres would move toward the electrodes under direct current fields or alternating current fields, leading to the self-assembly of colloidal spheres on the electrode surface, as displayed in Figure 1D.[48,49] Both Figure 1E and F show the self-assembly of colloidal spheres at the gas/liquid interface which is a facile and cost-effective route toward the large-area coatings.[3,50] These highly ordered and uniform nanosphere monolayers

can be obtained via the spreading of colloidal suspension onto a liquid surface, and then these floating monolayers are readily transferred onto varied substrates. After the evaporation of solvent in the suspension, the dense nanosphere existed in a single monolayer format without any variation in its thickness would remain on the substrate surface. In particular, utilizing this technique, MCCs can be efficiently synthesized by the self-assembly of PS nanospheres at the gas/deionized water (DI water) interface, in which they are subsequently transferred onto other substrates. Nevertheless, there is not a champion method for the self-assembly of colloidal spheres, where the colloidal materials and their dimensions as well as the substrate materials and their surface roughness would dictate the proper method for the controllable formation of large-scale MCCs.

On the other hand, Langmuir–Blodgett (LB) assembly method is a very simple and powerful technique for the fabrication of highly ordered monomolecular films with a densely packed structure, a high reproducibility, and a large-area uniformity.[51–53] In this method, the colloidal nanoparticles (e.g., silica and PS nanospheres) are usually employed to form self-assembled monolayers with the hydrophobic surface as shown in **Figure 2**A. The general working principle is quite straightforward and commonly used with surfactants, such as oil. Importantly, this method can be applied to colloidal materials as well, as long as they allow the formation of a monolayer at an interface. When a colloidal suspension is dispersed onto a surface, the colloids would spread as far as possible, forming a spaced monolayer on the surface. The film is then compressed through a barrier, which reduces the available surface area, resulting in an increased surface tension. When a substrate is then "scooped" through this compressed film, the lower surface tension provided by the substrate would then cause the colloids to transfer onto it from the interface.

It is interesting that the assembled films can only be picked up on the upstroke of the substrate. In order to figure out and quantify this phenomenon of hydrophobic particles assembled film, researchers have provided expressions to describe the energy required by extracting a particle from the air/water interface in the upward direction and forcing a particle into the water, separately.

These expressions can be described as follows with details given in Figure 2B[54]

Figure 2. Fluidic deposition of the colloidal self-assembly: Langmuir–Blodgett (LB) method. A) Schematic demonstration of the LB method. Reproduced with permission.[51] Copyright 2018, Elsevier Ltd. B) Forces at the solid/liquid/air interface, (i) a particle at the air/water interface, (ii) hydrophilic surface (θ is acute angle), (iii) hydrophobic surface (θ is obtuse angle), γ_{SA}, γ_{LA}, and γ_{SL} are interfacial tensions between solid, liquid, and air, respectively. Reproduced with permission.[50] Copyright 2010, Wiley-VCH Verlag GmbH & Co. KGaA.

$$E_{OUT} = \pi R^2 \gamma_{LA} \left(1 + \cos\theta\right)^2 \tag{1}$$

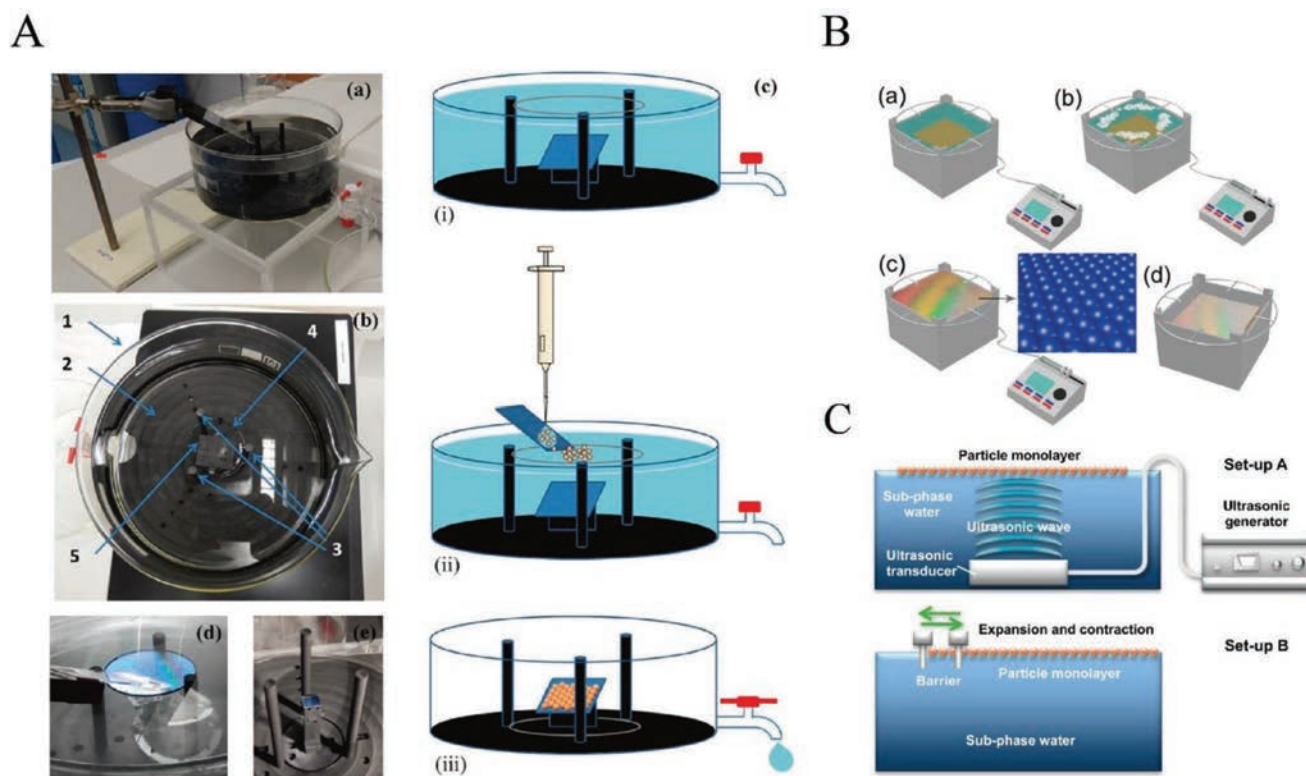$$E_{IN} = \pi R^2 \gamma_{LA} \left(1 - \cos\theta\right)^2 \tag{2}$$

where R is the radius of the particle, γ_{LA} is the interfacial tension between liquid and air, and θ is the obtuse angle. Furthermore, the ratio of E_{OUT}/E_{IN} can be presented by Equation (3)[55]

$$E_{OUT}/E_{IN} = \cot^4\left(\theta/2\right) \tag{3}$$

This ratio is quite small for any value of θ, which indicates that the required energy to move a particle upward is much less than the required energy to move a particle downward. These investigations can evidently provide a theoretical basis for the fact that the nanospheres based monolayer is only deposited on the upstroke.

Figure 3 demonstrates several improved methods of LB assembly schemes. A container with a hole and a tap for water discharge can be designed to dispense the colloidal spheres using a tilted glass slide and allow the self-assembly formation of monolayers at the air/water interface (Figure 3A).[56] The nitrile butadiene rubber ring floating on the water surface is then employed to confine the self-assemble area, avoiding the monolayer damage or disruption during transfer. The self-assembly of colloidal spheres process is also sketched in Figure 3A(c) in details. After water draining out in the glass container, a dense monolayer is left on the substrate. At the same time, Figure 3B presents a low-cost and high-throughput micropropulsive injection (MPI) method based on a large-area self-assembly of colloidal PS nanospheres.[57] The self-assemble process is shown as the following series of steps: (i) presetting the substrates underneath the water and connecting the injectors with the MPI system (Figure 3B(a)); (ii) self-assembly of colloidal PS nanospheres on the water surface fabricated via the MPI system (Figure 3B(b)); (iii) formation of a dense self-assembled PS monolayer consisting of colloidal crystals on the entire water surface (Figure 3B(c)); transferring of PS monolayer onto the preset substrates (Figure 3B(d)). In order to decrease the defect concentration of the MCCs fabricated by LB method, two

Figure 3. A) Self-assembly of colloidal spheres at air/water interface by surface confinement and water discharge. (a) Photograph of the overall setup. (b) Detail of (1) glass container with tap, (2) circular plate, (3) cylindrical rods, (4) nitrile butadiene rubber ring, and (5) sample holder. (c) Sketch of the procedure: (i) installation of the substrate in the container, (ii) dispensation and self-assembly of colloidal spheres, and (iii) monolayer transfer onto the substrate after water discharge. (d) Photograph of the self-assembly monolayer at air/water interface confined within the area of the ring. (e) Photograph of a sample after transfer. Reproduced with permission.[56] Copyright 2016, American Chemical Society. B) Schematics of the micro-propulsive injection (MPI) systems and the formation processes for large-area PS nanosphere arrays. (a) An MPI system with one injector and four nozzles. A substrate is preset underneath the water. (b) Initial stage for the injection of PS colloids over the water surface. (c) The formation of hexagonally arranged PS monolayer upon the water surface once a defect-less and colorful interference pattern occurred under white light illumination. The inset image schematically shows the arranged PS monolayer. (d) Transfer of the PS monolayer onto the preset substrates by slowly declining the water level or raising the substrate. Reproduced with permission.[57] Copyright 2015, American Chemical Society. C) Schematic illustrations of the setup of Langmuir–Blodgett trough. Setup "A": ultrasonic irradiation to the particle monolayer. Setup "B": Barrier-sway process to the particle monolayer. Reproduced with permission.[58] Copyright 2015, American Chemical Society.

**ADVANCED
SCIENCE NEWS**
www.advancedsciencenews.com
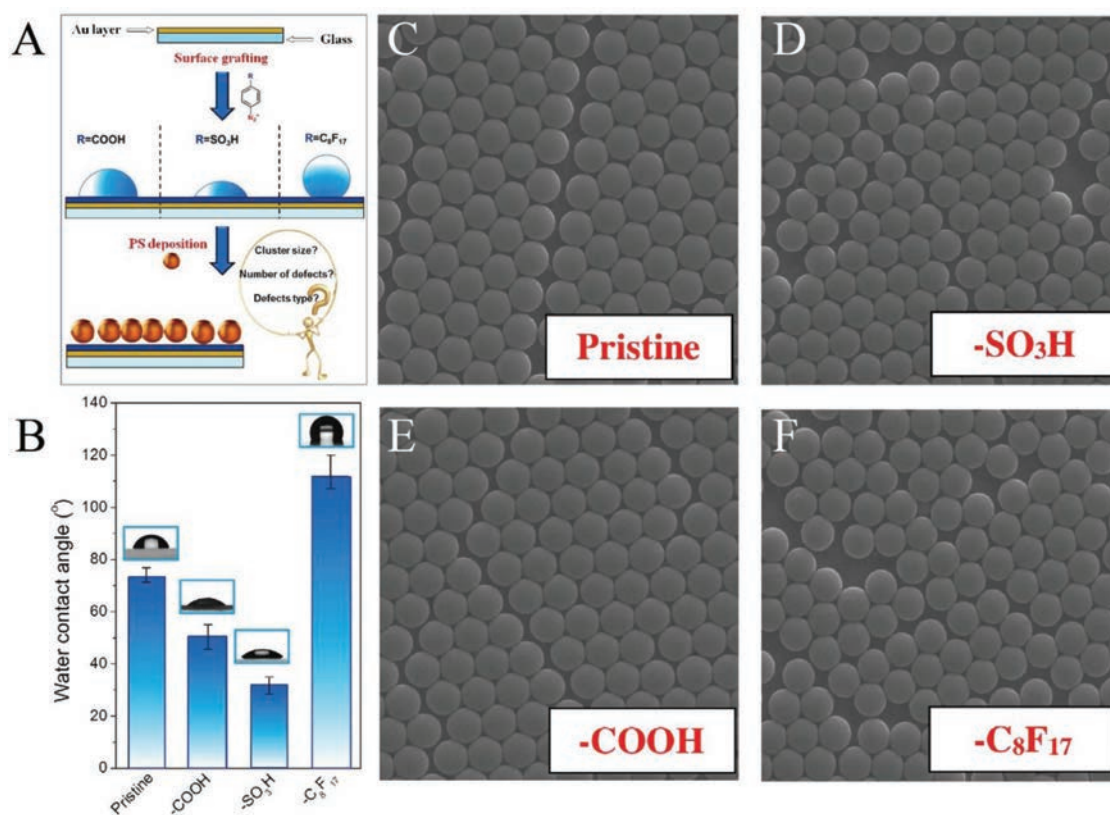
**ADVANCED
MATERIALS
TECHNOLOGIES**
www.advmattechnol.de

different techniques of the ultrasonic annealing and the barrier-sway can be employed as illustrated in Figure 3C.[58] The setup of "ultrasonic annealing" is consisted of an ultrasonic generator and a transducer. 1.2 to 1.5 MHz oscillation is irradiated from the transducer head to the water surface for 30 min at 20 °C. Meanwhile the colloidal silica spheres are dripped, and then spread on the water surface (Figure 3C, setup "A"). By contrast, the "barrier-sway" is a physical treatment process, leading to a sway forward and backward of the silica spheres on the water alternately at a frequency rate of 0.2 to 0.5 Hz with an amplitude of 25–35 mm at 20 °C by manipulating the barrier of LB trough (Figure 3C, setup "B"). All of these demonstrate the unique characteristics of different LB methods for the formation of controllable, uniform and large-scale monolayers of self-assembled colloids for practical utilizations.

Moreover, the hydrophilic or hydrophobic functional groups can be used to modify the quality of MCCs on the Au surface.[59] **Figure 4**A shows a thin Au layer, which can be covalently modified by different organic functional groups via diazonium chemistry with the aim to introduce hydrophilic or hydrophobic properties. The impact of the surface grafting on the wettability (i.e., contact angle) is systematically demonstrated in Figure 4B, while Figure 4C shows the colloidal PS spheres deposited onto the pristine Au surface with the dislocation-like defects. The same type of defects is also observed in the case of 4-carboxyphenyl-modified surface (Figure 4E). In the case of 4-sulfophenyl

functional groups, the Schottky-like defect becomes dominant (Figure 4D). The surface grafting by arenediazonium tosylates-C_8F_{17} can also significantly disrupt the ordering of PS sphere arrays (Figure 4F). Thus, the colloidal spheres cannot self-assemble into a perfect monolayer on the substrate surface with a high hydrophilicity. These findings can clearly indicate that controlling the surface hydrophobicity is crucial for the formation of high-quality self-assembled colloidal monolayer.
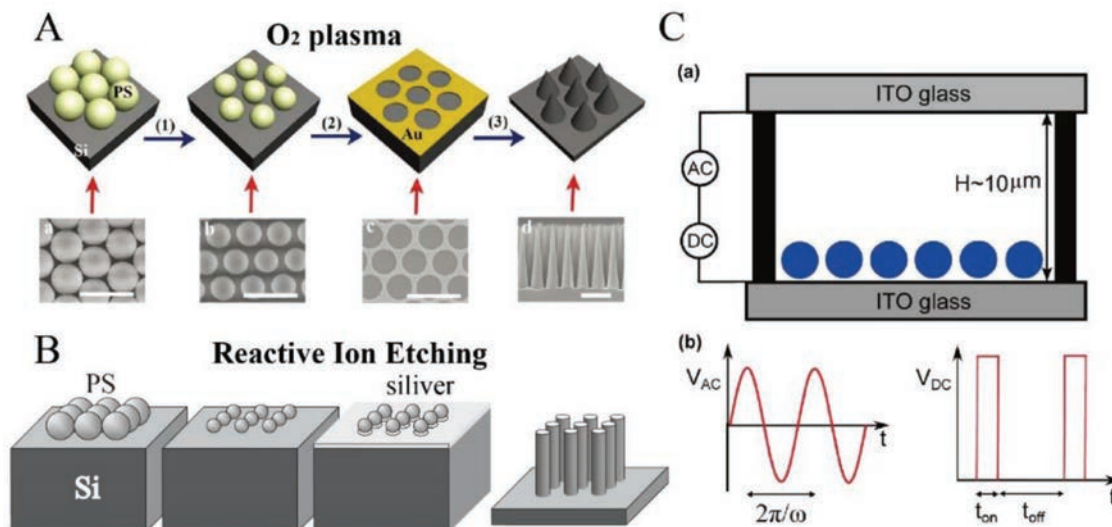
3. Construction of Various Large-Scale, Hierarchical, and Nanostructured Arrays

Once the large-scale and high-quality MCCs are obtained, they can then be acted as the mask for metal deposition after processing of O_2 plasma, reactive ion etching or combinations of various electric fields. In specific, the PS monolayer was subjected to O_2 plasma in order to reduce the diameter of PS spheres, and then Au film was deposited onto the substrate via thermal evaporation as shown in **Figure 5**A.[60] After removal of the PS spheres, nanocone arrays could be generated by using the method of metal-assisted chemical etching (MaCE), which is a well-developed chemical etching scheme to obtain highly anisotropic nanostructure in Si, GaAs, and others with designated metal catalysts.[63–65] Reactive ion etching process is another technique to reduce the diameter of the PS spheres, leading to

Figure 4. Au surface grafting and their properties tuning with the aim to investigate further the deposited PS array quality. A) Process schematics. B) Water contact angles measured on pristine Au surface and Au surfaces grafted with organic compounds ($-SO_3H$, $-COOH$, and $-C_8F_{17}$). C–F). Scanning electron microscope (SEM) images of PS spheres deposited on the pristine and grafted samples with organic compounds of $-SO_3H$, $-COOH$, and $-C_8F_{17}$, respectively. The scan area is 6×6 μm^2. Reproduced with permission.[59] Copyright 2018, Elsevier B.V.

**ADVANCED
SCIENCE NEWS**
www.advancedsciencenews.com

**ADVANCED
MATERIALS
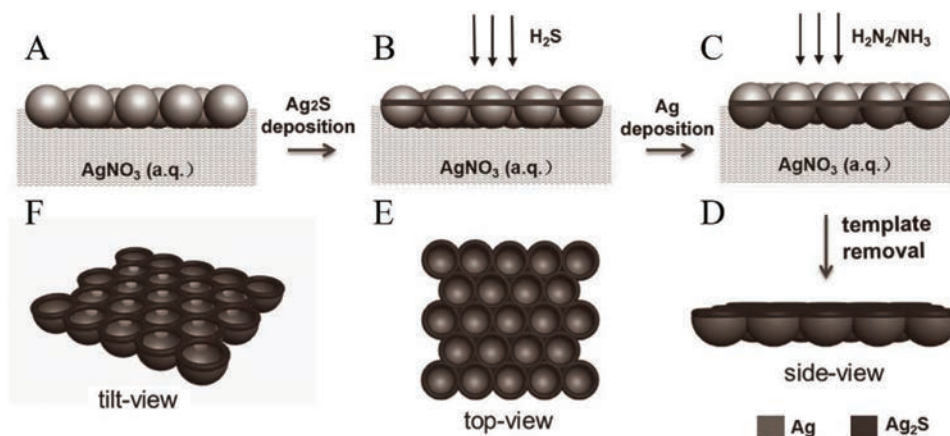TECHNOLOGIES**
www.advmattechnol.de

Figure 5. A) Oxygen plasma processed PS spheres for the fabrication of periodic nanocone arrays and their corresponding SEM images. The scale bar represents 1 μm. Reproduced with permission.[60] Copyright 2017, The Royal Society of Chemistry. B) Reactive ion etching processed PS spheres for the fabrication of periodic nanopillar arrays. Reproduced with permission.[61] Copyright 2007, Wiley-VCH Verlag GmbH & Co. KGaA. C) Cross-sectional view of the experimental setup (a). The electric field applied combines both a continuous alternating current and pulses of direct currents (b). Reproduced with permission.[62] Copyright 2017, American Chemical Society.
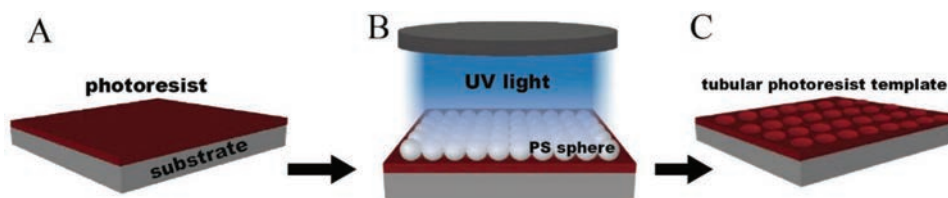
an unclose-packed array of colloidal PS spheres as presented in Figure 5B.[61] A silver film was next evaporated onto the silicon substrate as a catalyst. Simultaneously, Figure 5C presents an electric-field assisted self-assembly of colloidal spheres into the unclose-packed array due to the dipolar repulsion. The cross-sectional view of the setup is shown in Figure 5C(a). In explicit, a droplet of colloidal suspension was placed between two indium tin oxide (ITO) slides. First, an alternating-current (AC) electric field was applied between the two electrodes using a function generator. Then, a sequence of direct-current (DC) pulses together with a programmable DC power supply were applied, resulting in the separation of colloidal spheres

from each other at a constant distance because of the induced dipolar repulsion. Obviously, combining with different fabrication schemes, these MCCs can be utilized as the masks for the effective construction of various hierarchical nanostructured arrays.[62]

In addition, **Figure 6** shows that the unique Ag_2S–Ag heterostructured nanobowl arrayed structure can also be realized by the nanosphere lithography method.[66] In details, the MCCs self-assembled on the surface of aqueous $AgNO_3$ solution was employed as the template as presented in Figure 6A. Next, the Ag_2S nanonet film was obtained due to the preferential deposition of Ag_2S at gas–liquid interface under the H_2S gas

Figure 6. The template of PS monolayer for the fabrication of Ag_2S–Ag heterostructured and periodic nanobowl arrays by two-step nanosphere lithography at the gas–liquid interface. A) Self-assembly of PS spheres on the surface of aqueous $AgNO_3$ solution. B) Ag_2S nanonet film was obtained under the H_2S gas. C) Introducing the N_2H_4/NH_3 gas mixture would lead to the reduction of Ag^+ ions while the preferential deposition of metallic Ag is taken place at the bottom of each PS spheres. D) Formation of 2D ordered arrays of Ag_2S–Ag heterostructured nanobowls after the template removal. E,F) Top- and tilt-schematic view of the obtained arrays which consist of Ag_2S nanonets lying on Ag nanobowl arrays. Reproduced with permission.[66] Copyright 2017, Wiley-VCH Verlag GmbH & Co. KGaA.

**ADVANCED
SCIENCE NEWS**
www.advancedsciencenews.com

**ADVANCED
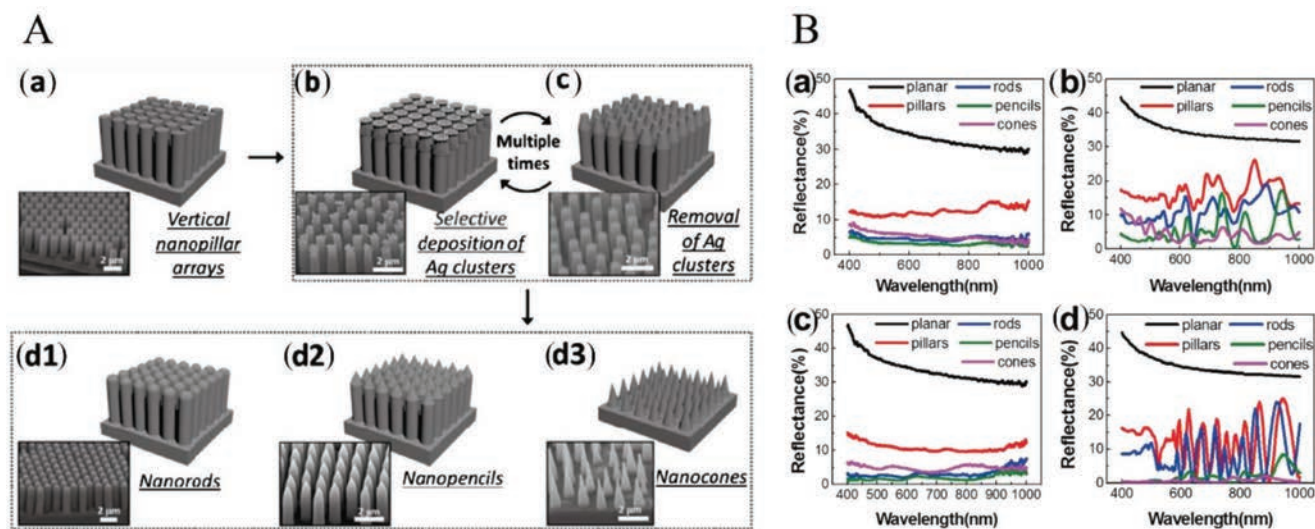MATERIALS
TECHNOLOGIES**
www.advmattechnol.de

Figure 7. A schematic illustration of the photolithography-assisted process for the fabrication of periodic nanoarrays: A) spin-on deposition of photoresist on a substrate, B) a monolayer of silica or PS spheres formed on top of the photoresist under UV light exposure. C) The patterned photoresist nanohole obtained after removing the spheres and developing of photoresist.

(Figure 6B). Subsequently, when the N_2H_4/NH_3 gas mixture is diffused into the system, it would lead to the reduction of Ag^+ ions and the preferential deposition of metallic Ag at the bottom of each PS spheres (Figure 6C). After removal of the MCC template, the periodic and heterostructured Ag_2S–Ag nanobowl arrays were obtained with a high uniformity in a large scale, consisting of connected Ag_2S rings lying on the edge of Ag bowls with some cavities on the lateral walls (Figure 6D–F). These unique Ag_2S–Ag heterostructured nanobowl arrays have already been demonstrated with the effective resistance switching characteristics and superior photoresponses, being promising for potential utilizations in both electronic devices and photocatalysis, etc.[66,67]

Except functioning as the masks and the templates, the MCCs deposited on the photosensitive materials, such as photoresist, could also be served as the optical lens.[68] Explicitly, photoresists could be spun onto substrates, and then dipped into the developer solution for a few seconds after soft bake (**Figure 7**A). In this case, the hydrophilic surface of photoresist was obtained, which could facilitate the subsequent self-assembly of the colloidal silica or PS spheres on top of the photoresist (Figure 7B). After that, the samples were exposed under ultraviolet (UV) irradiation by using a conventional photolithography technique. Notably, the exposure profile of the

photoresist could be precisely controlled by the size of spheres, the thickness of photoresist layer and the duration of irradiation. Eventually, the nanohole arrays were simply obtained on the photoresist layer after removal of colloidal spheres and development in the developer solution (Figure 7C).

Apart from the pattern obtained in the photoresist layer, various hierarchical and periodic silicon nanostructures with the excellent optical properties could also be fabricated by employing the MCCs as the mask.[69–71] **Figure 8**A shows the fabrication procedures of silicon (Si) nanopillar, nanorod, nanopencil, and nanocone arrays constructed by using the MaCE method. Briefly, MCCs were assembled on boron-doped p-type Si (100) substrates by using the LB approach. The substrates were first pretreated with mild oxygen plasma to induce hydrophilic surfaces for the facilitation of uniform nanosphere coating. Utilizing these colloidal spheres as the mask, a 1.5/20 nm thick Ti/Au was then deposited through thermal evaporation. Subsequently, the hierarchical and periodic Si nanopillars with a controllable diameter and periodicity could be achieved via metal catalytic etching in HF/H_2O_2 solution (Figure 8A(a)). These Si nanopillars were used as the template, which could be further treated with a mixture of $AgNO_3$, HF, and HNO_3 or H_2O_2. Ag clusters in this mixture would preferentially deposit on the tips of nanopillars and at the same
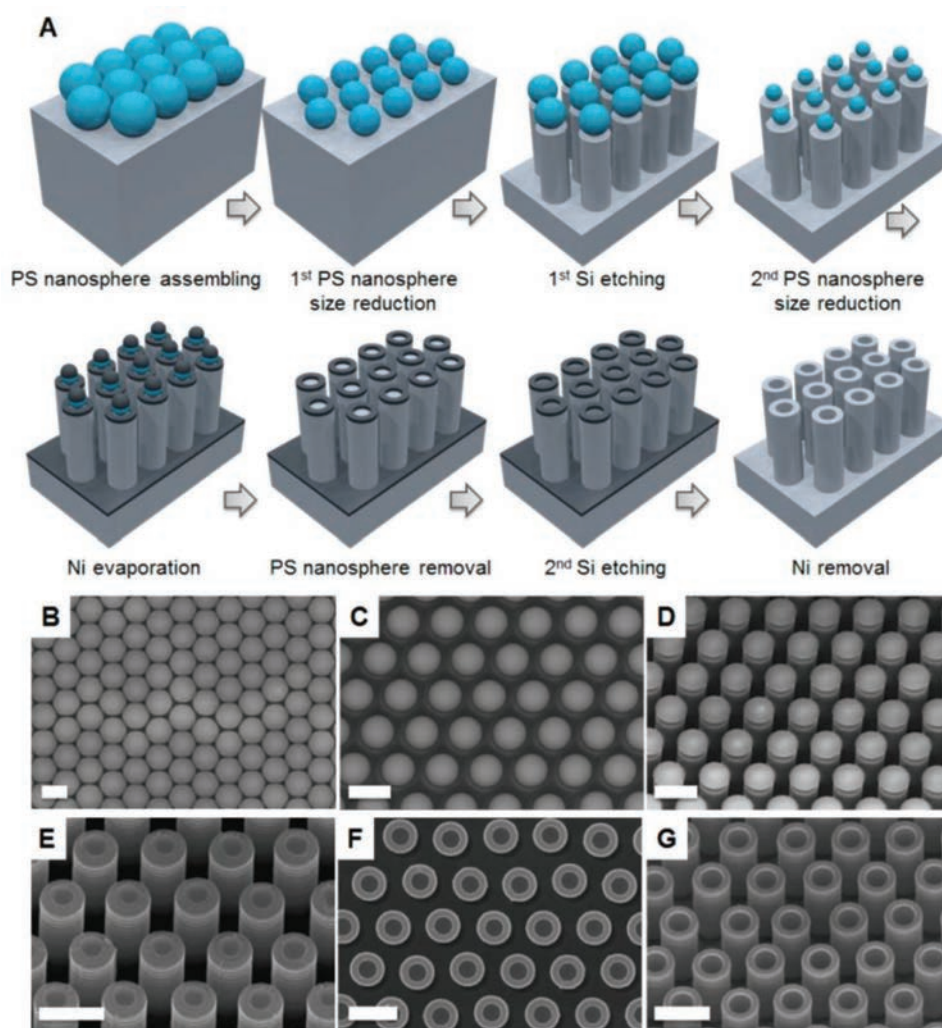

Figure 8. A) Schematics for the fabrication of different morphological Si nanoarrays. The insets show the representative SEM images of the correspondingly obtained nanoarrays. Reproduced with permission.[69] Copyright 2013, The Royal Society of Chemistry. B) Comparison of the reflectance spectra of various nanostructured arrays between experimental measurement and optical simulation. (a) Experimental and (b) simulated spectra of different nanostructures with the geometrical pitch of 1.27 µm. (c) Experimental and (d) simulated spectra of different nanostructures with the geometrical pitch of 0.6 µm. Reproduced with permission.[72] Copyright 2014, American Chemical Society.
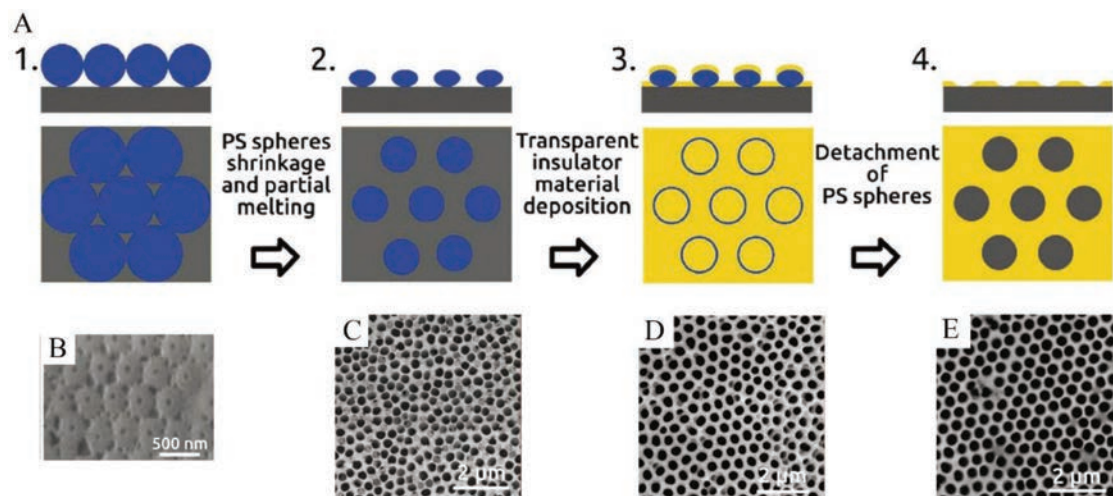
**ADVANCED
SCIENCE NEWS**
www.advancedsciencenews.com

**ADVANCED
MATERIALS
TECHNOLOGIES**
www.advmattechnol.de

time perform Si etching. This way, the subsequent removal of Ag clusters by HNO₃ washing would give fresh nanopillar tips as shown in the process schematic in Figure 8A(b),(c). Due to the repeated deposition and removal processes of these Ag clusters, different morphological nanopillar arrays (i.e., nanorods, nanopencils, and nanocones) tailored under well-controlled chemical conditions were generated (Figure 8A(d1)–(d3)). It is noted that the morphologies, dimensions, and aspect ratios of these hierarchical and periodic nanostructures could be controlled accurately with this simple wet-chemistry anisotropic etching technique. Impressively, these Si hierarchical and periodic nanostructures also demonstrated with the superb antireflection performance under ultraviolet–visible (UV–vis) spectroscopy, where the pencil and cone nanostructured arrays exhibited the best optical absorption characteristics

here among all samples, as shown in Figure 8B. These excellent broadband optical absorption behaviors could be attributed to the increasing material filling ratio changing from the tip to the basal plane of the nanoarrays, enhancing the mean free time of photons and trapping the photons within the hierarchical structure.[72] All of these hierarchical structures would contribute to the ideal configuration for next-generation photovoltaic devices.

Furthermore, **Figure 9**A presents the fabrication steps of the 3D Si nanotube arrays in large scale by multiple-patterning NSL (MP-NSL) based on the PS MCCs.[73] The SEM images of the products processed right after several key steps are shown as Figure 9B–G. First, a monolayer act as the mask for MP-NSL was formed at water/air surface by using the drop cast method, and then transferred to a 2 cm × 2 cm Si substrate underneath

Figure 9. Self-aligned multiple-patterning nanosphere lithography for Si nanotube arrays. A) A schematic illustration of the process. Step 1: the monolayer of close-packed (PS) nanospheres formed at water/air interface, and then transferred onto a Si wafer. Step 2: oxygen plasma processing. Step 3: Si nanopillars fabricated by deep reactive ion etching with the nanospheres as masks. Step 4: a second oxygen plasma processing. Step 5: deposition of Ni on PS nanospheres and Si nanopillars. Step 6: removal of PS nanospheres by oxygen plasma etching. Step 7: Si holes formed by deep reactive ion etching Step 8: 3D Si nanotube arrays achieved after the removal of Ni by HCl. SEM images of key intermediates: B) monolayer of closed-packed PS nanospheres formed on a Si wafer, C) PS nanospheres on Si wafer after first oxygen plasma processing, D) PS nanospheres on top of periodic Si nanopillar arrays, E) PS nanospheres after the second oxygen plasma processing, F) Ni nanorings on top of Si nanopillars, and G) Si nanotube arrays with the Ni nanorings. All Scale bars are 1 μm. Reproduced with permission.[73] Copyright 2017, American Chemical Society.
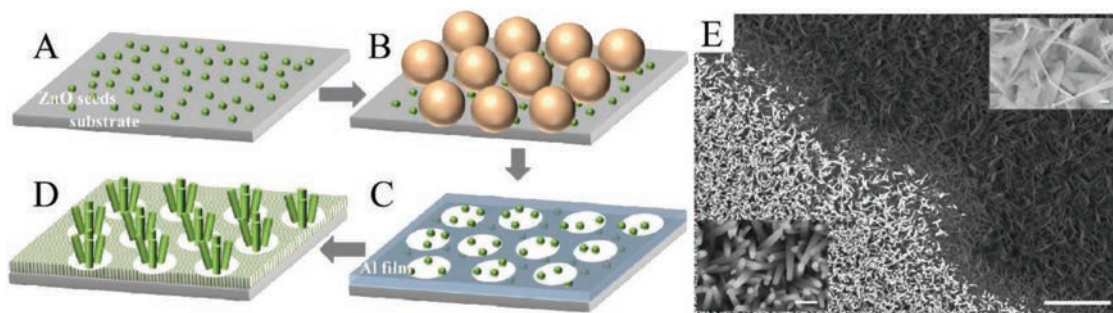
Figure 10. A) Schematic illustration of the four fabrication steps of the SiO$_2$ patterned Al foil. B) Hexagonally patterned SiO$_2$ layer with distances of 460 and 600 nm on the Al foil after detaching the PS spheres. Top-view SEM images of the AAO film grown in a 0.1 M phosphoric acid electrolyte applying 195 V after: C) first anodization of electropolished Al foil, D) second anodization, E) anodization of Al foil with prepatterned structures. Reproduced with permission.[76] Copyright 2018, The Royal Society of Chemistry.
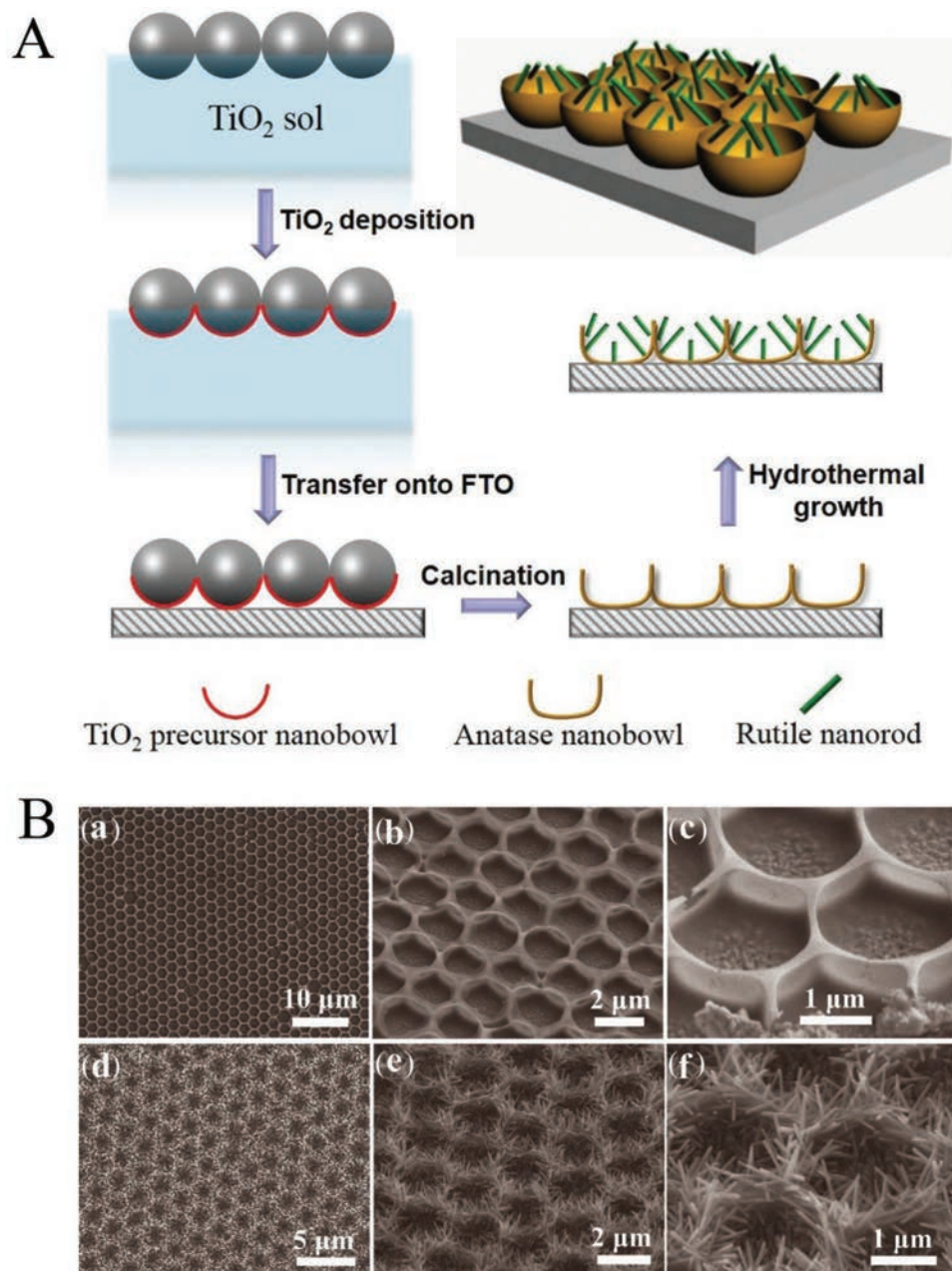
the water/air interface by gently removing the liquid as illustrated in Figure 9B. It is noted that the pitch of the final Si nanotube arrays can be tailored from several hundred nanometers to several micrometers depending on original size of the PS nanospheres. Next, the diameters of the polystyrene nanospheres are reduced by the oxygen plasma etching, which can define the outer diameter of the Si nanotubes as given in Figure 9C. By using the deep reactive ion etching (DRIE) technique, Figure 9D presents the fabricated Si nanopillar arrays with high-aspect ratio, while the PS nanospheres still remain on the top of these nanopillars. Then, a second oxygen plasma etching was employed to reduce the size of PS nanospheres on top of the pillars as illustrated in Figure 9E. Similarly, the smaller nanospheres remained on the center of Si nanopillars would serve as masks for the subsequent DRIE. Furthermore, the Ni layer with the thickness of 20 nm was deposited on the sample surface by electron-beam evaporation, acting as the anti-etching layer during the DRIE process. After removal of PS nanospheres, the Ni nanorings with the exposed Si surface at the central part were obtained as shown in Figure 9F.

Finally, Figure 9G displays the finished Si nanotube arrays achieved after the removal of Ni by the chemical etch treatment (5% HCl).

Besides the MaCE method and DRIE technique, the nanosphere lithography based on the MCCs could as well be combined with the bottom-up technique to fabricate periodic anodic aluminum oxide (AAO), which was usually employed as the template to prepare various nanostructures. The porous AAO with the uniform dimension of nanopores was successfully synthesized on different substrates, such as glass or ITO surface.[74,75] However, it was rarely reported the fabrication of periodic AAO. **Figure 10**A shows the fabrication process of the SiO$_2$ nanohole arrays on Al foil. The top-view SiO$_2$ monolayer on the Al foil after the removal of PS spheres was presented in Figure 10B. For comparison, an electropolished Al foil without any pre-patterning and an Al foil submitted to a preliminary first anodization for 24 h anodized under the same conditions were selected. The top-view SEM images of first anodization of electropolished Al foil and second anodization with preliminary first anodization were presented in Figure 10C,D

Figure 11. Schematic illustration of ZnO nanowire/nanosheet synthesis. A) ZnO seeds were formed on the substrate. B) A monolayer of PS spheres was deposited on top of the ZnO seeds. The size of the sphere can be adjusted with dry etching. C) Al nanohole arrays were fabricated using the PS spheres as the masks. D) Patterned ZnO nanowires/nanosheets grown from the same growth solution. E) SEM image of the boundary between the ZnO nanowire area (bottom-left) and nanosheet area (top-right). The scale bar is 5 µm in length. Inset: magnified SEM images of nanowires (bottom-left) and nanosheets (top-right). The scale bar in either inset is 200 nm. Reproduced with permission.[81] Copyright 2015, The Optical Society.
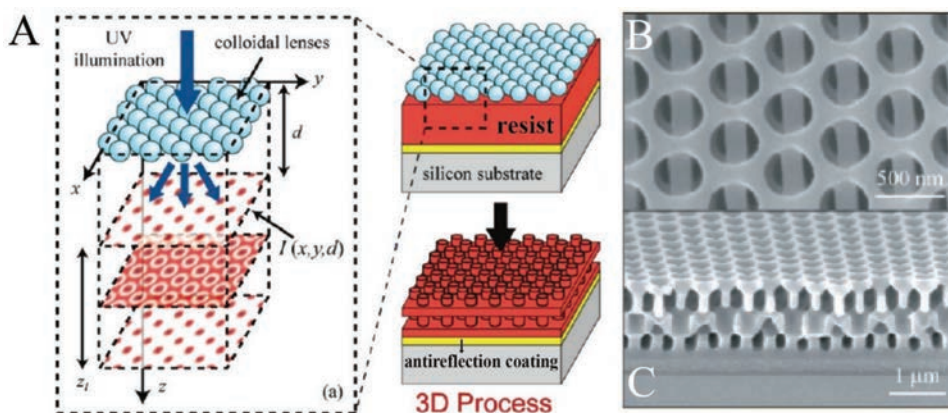
Figure 12. A) Schematic illustration of the preparation process of TiO_2 NR@NB arrays. B) SEM images of (a–c) TiO_2 NB arrays and (d–f) TiO_2 NR@NB arrays obtained after 5 h of hydrothermal growth. Reproduced with permission.[82] Copyright 2016, Wiley-VCH Verlag GmbH & Co. KGaA.

respectively. Obviously, the periodic AAO nanostructures with well-controlled and large interpore distances were obtained by the nanospheres lithography prepatterning and one-step anodization process (Figure 10E). This unique hierarchical structure can open up lots of potential applications in various technology domains.[76]

It is noted that the hydrothermal method is one of the most popular approaches in the nanomaterial synthesis due to its simplicity and flexibility in the morphology control.[77–80] The nanosphere lithography with MCCs can then be combined with the hydrothermal method to generate numerous interesting hierarchical and periodic nanoarrays.[81] **Figure 11** demonstrates

the ZnO nanowire/nanosheet arrays synthesized on ITO glass substrates by hydrothermal method combined with nanosphere lithography scheme. In particular, the ZnO seed layer was first synthesized on the ITO glass substrates by spin-coating of the Zn precursor colloidal suspension as presented in Figure 11A. After drying and annealing of the seed layer in ambient air, a monolayer of PS spheres was prepared on top of the ZnO seeds/ITO glass substrates (Figure 11B). Then, the Al film of 50 nm in thickness was deposited onto the PS monolayer by using electron-beam deposition. After removal of the PS monolayer, the periodic Al nanohole arrays were obtained with the Zn seeds in the holes (Figure 11C). Finally, the hierarchical

**ADVANCED
SCIENCE NEWS**
www.advancedsciencenews.com

**ADVANCED
MATERIALS
TECHNOLOGIES**
www.advmattechnol.de

Figure 13. A) Schematic illustration of the proposed approach, where a hexagonal array of nanospheres is illuminated by an UV laser to generate a 3D intensity distribution. The x–y intensity pattern is a function of propagation distance d (right). The volumetric intensity distribution can be recorded by assembling the nanospheres directly on a substrate spin-coated with thick photoresist (left). B) The structure contains alternating 2D hexagonal holes array and 1D grating lines due to laser polarization. C) Cross-section view of fabricated nanostructure with λ = 351 nm, D = 350 nm, and γ = 0.67. Reproduced with permission.[89] Copyright 2011, American Chemical Society.
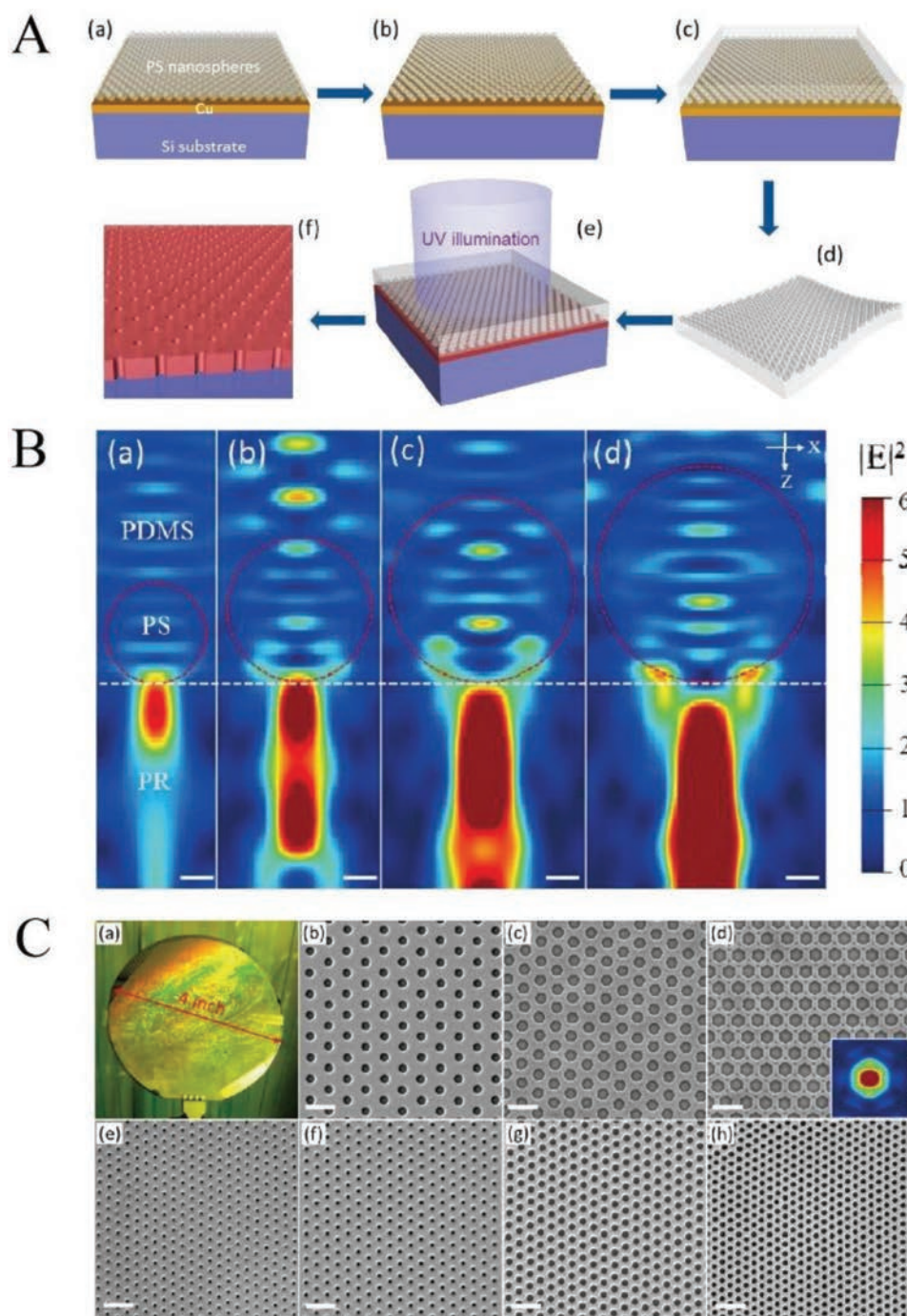
and periodic ZnO nanowires/nanosheets were prepared on the ITO glass substrate via hydrothermal routes (Figure 11D). Figure 11E shows an SEM image of the ZnO nanowire area, the nanosheet area, and the boundary between them. The nanowires were directly grown on cleaned ITO substrate because of the ZnO seed. By contrast, the ZnO nanosheets were grown onto the Al thin film.

Similarly, **Figure 12**A presents the fabrication process of hierarchical and periodic TiO_2 nanorod@nanobowl (NR@NB) arrays synthesized by combinations of nanosphere lithography and hydrothermal growth.[82] The MCCs based template was first self-assembled onto the surface of TiO_2 sol–gel, leading to the deposition of a thin layer of amorphous TiO_2 precursor onto the bottom of each PS sphere. Then, the as-formed MCCs with TiO_2 on the bottom was transferred to the fluoride-doped tin oxide (FTO) substrate. After removal of PS spheres via calcination process, the anatase TiO_2 nanobowl arrays were achieved with excellent electrical properties.[83–85] Furthermore, the TiO_2 nanobowl arrays on FTO were successively employed as a patterned substrate for the hydrothermal growth of rutile TiO_2 nanorods, resulting in the formation of hierarchical and periodic TiO_2 NR@NB arrays. These hierarchical TiO_2 NR@NB arrays with large surface area and the rutile/anatase phase junction were demonstrated with the significantly enhanced photocatalytic properties for water splitting.[86–88] In order to confirm their structural details, Figure 12B shows the SEM images of obtained TiO_2 NB arrays and NR@NB arrays on the FTO substrate. The top-view image of the NB arrays indicates that the formation of large area and periodic nanobowl arrays was achieved, retaining the periodic structure of the MCCs based template as given in Figure 12B(a). The corresponding tilt-view and high-magnification SEM images are also shown in Figure 12B(b),(c), while construction of hierarchical and periodic TiO_2 NR@NB arrays is evidently confirmed on FTO as presented in the SEM images in Figure 12B(d)–(f).
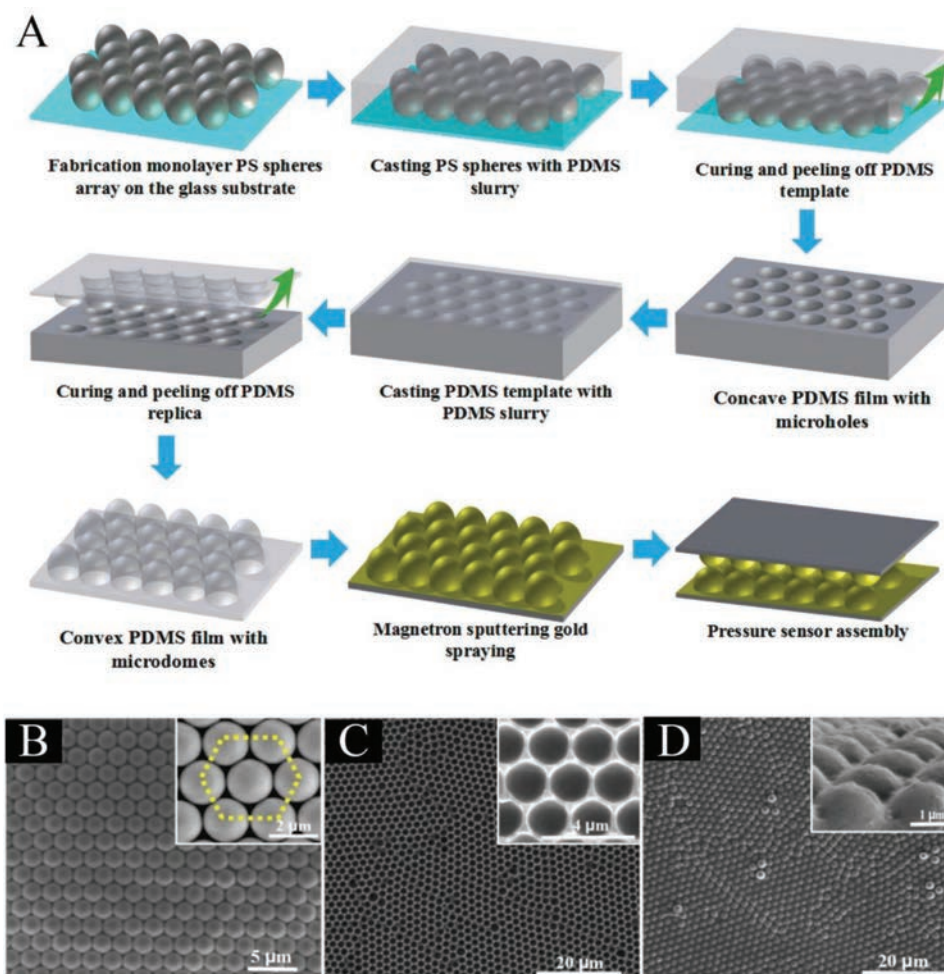
In addition to perform as masks and templates for 2D patterning, the MCCs can also be employed as the optical lens to generate 3D hierarchical and periodic nanostructures directly.[24,89] As presented in **Figure 13**A, the MCCs assembled

on the photoresist could serve as optical lens and then were illuminated with normal incident UV light. Because the self-assembled PS spheres is periodic, the diffracted light passing through the spheres would exhibit the Talbot effect, resulting in a repeated intensity with an axial period along the propagation distance.[90] The right schematic in Figure 13A shows the fabrication process of 3D nanostructures. The top-view SEM image of hierarchical and periodic 3D nanostructure with alternating layers of nanohole arrays and grating lines is also depicted in Figure 13B. The grating lines could be attributed to the polarized incident light during the exposure process. Figure 13C gives the cross-section geometry of the obtained 3D periodic nanostructures. It is obvious that these periodic nanostructures can be easily obtained and their dimensions can be precisely tuned by this simple colloidal self-assembly enabled fabrication process, which facilitate lots of practical utilizations requiring high surface-to-volume ratio, including energy storage, catalysis, and others.

However, in most cases, during the processing, the colloidal spheres are served as the sacrificial masks and cannot be reused as the optical lens, which is highly unfavorable for scalable cost-effective fabrications.[2,91] To shed light solving this problem, a novel photolithographic method by first replicating the geometrical features of self-assembled nanospheres onto the surface of a soft polymer film and then employing the film as reusable photomasks for nanopattern generations was developed.[92,93] In this special technique, highly ordered micro-/nanosphere arrays were interlinked and confined by a soft transparent polymer (e.g., polydimethylsiloxane, PDMS), and then acted as photomasks for area-selective exposures of photoresist in contact.[94] The fabrication process of soft photomask is illustrated in **Figure 14**A. First, a thin layer (30 nm) of Cu was coated on the surface of silicon wafer by magnetron sputtering. Then, a thin layer of Ti (3–5 nm) was sputtered under the same condition before the Cu deposition for the enhancement of the adhesion between the Cu and the Si substrate (Figure 14A(a)). The PS MCCs were assembled on the substrate via the LB method, and then etched by oxygen plasma to reduce the size of PS nanospheres (Figure 14A(b)).

Figure 14. A) Deposition of PS nanospheres based monolayer on the Cu-coated Si substrate (a). Shrinking the nanospheres by oxygen plasma etching (b). Casting PDMS prepolymer over the nanospheres (c). Peeling off the cured PDMS film with the confined nanospheres monolayer (d). Attaching the PDMS soft mask to a photoresist layer and illuminating with flood UV light (e). Detaching the PDMS mask and developing the exposed photoresist to obtain nanopatterns (f). B) FDTD calculations of the electric field intensity ($|E|^2$) distributions. The diameters of the PS spheres in (a), (b), (c), and (d) are 500, 700, 900, and 1100 nm, respectively; and the corresponding pitches are 600, 800, 1000, and 1200 nm, respectively. The regions inside the red dashed circles denotes PS spheres; the outside circles and above the white dashed-dotted lines are PDMS matrix. The regions below the white dashed-dotted lines are photoresist (PR). All scale bars are 200 nm. C) Colloidal mask assisted optical patterning using positive photoresist (AZ5206E). (a) Digital photograph and (b)–(d) SEM images of photoresist patterns fabricated using an 1150/1280 (diameter/pitch, nm) colloidal mask. Exposure time for (b), (c), and (d) are 1, 3, and 5 s, respectively. Inset: calculated electric field intensity distribution at a depth of 300 nm under the photoresist surface. (e)–(g) SEM images of patterns fabricated using a 700/800 colloidal mask, with exposure time of 1, 2, and 4 s, respectively. (h) SEM image of pattern fabricated using a 500/600 colloidal mask, with exposure time of 4 s. Scale bars in (b)–(h) are 2 μm. Reproduced with permission.[92] Copyright 2014, American Chemical Society.
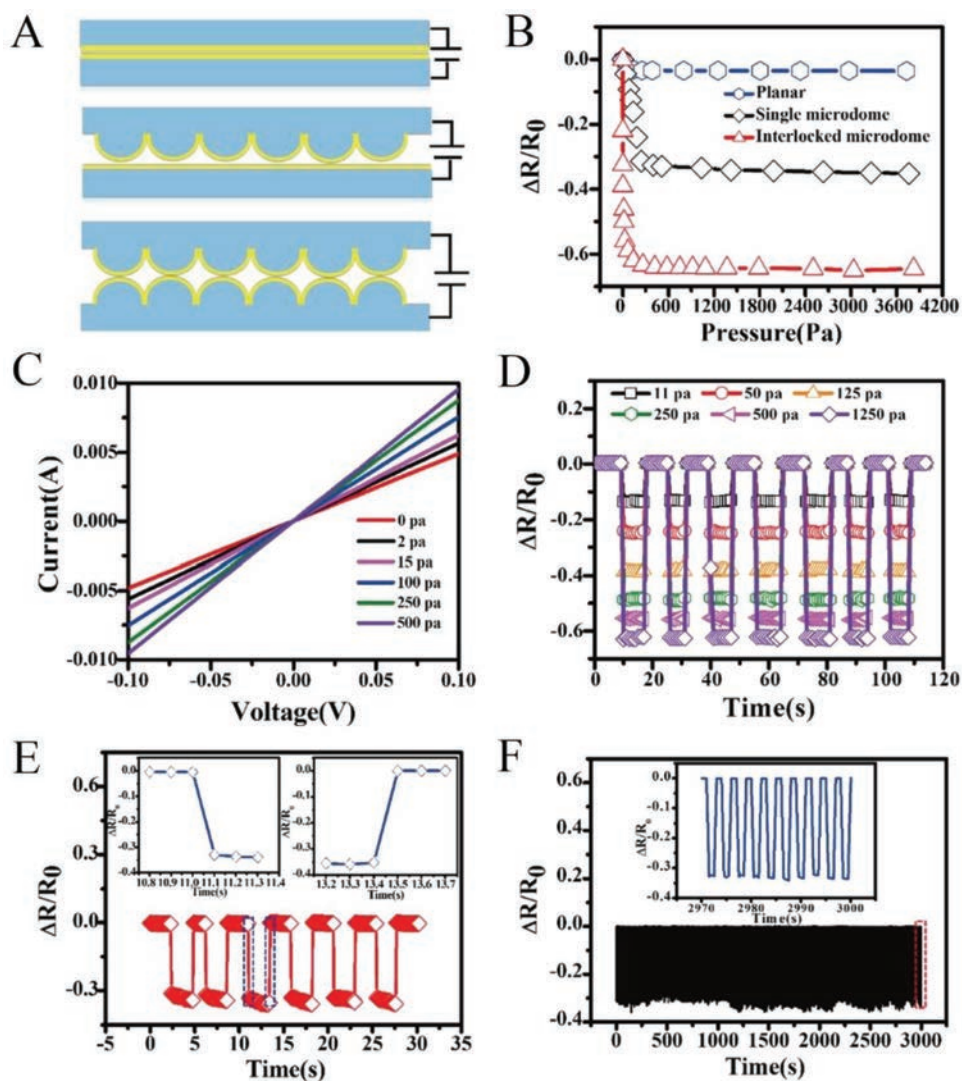
Figure 15. A) Schematic illustration of the fabrication process of PDMS films with microdome arrays and the corresponding pressure sensors. B) SEM image of the PS MCCs with a diameter of 2 µm. C) SEM image of the concave PDMS film with microbowls. D) SEM image of the convex PDMS film with microdome arrays. The inset shows the enlarged image of the corresponding microstructures. Reproduced with permission.[95] Copyright 2017, American Chemical Society.

PDMS prepolymers were casted over the sample in a Petri dish and cured at 60 °C for 2 h, as shown in Figure 14A(c). Finally, the cured PDMS film was peeled off manually from the substrate as shown in Figure 14A(d). Then, the PDMS soft mask was gently pressed against the surface of the photoresist layer to allow the conformable contact, and then was illuminated by UV light to fabricate the photoresist nanoholes, as presented in Figure 14A(e–f). The finite difference time-domain (FDTD) simulations were employed to further investigate the optical properties of the as-fabricated composite films. Figure 14B presents the intensity profile of the simulated UV light (365 nm) for the masks and the photoresist layer with PS sphere diameters from 500 to 1100 nm. It is clearly noted that the incident light can be efficiently focused underneath the PS nanospheres, demonstrating that these soft polymer films can serve as photomasks to produce subwavelength patterns.

After the exposure, the soft mask was detached from the substrate, rinsed with DI water and dried with nitrogen gas. These soft masks could be reused for many times without any geometrical degradation because of the mechanical robustness of

embedded PS sphere within the tip region of the soft mask. Evidently, Figure 14C(a) shows the photograph of the fabricated photoresist nanoholes on a 4-in. wafer by using a 1150/1280 (diameter/pitch) soft colloidal mask. Figure 14C(b)–(d) presented the photoresist nanoholes by using positive photoresist. The inset of Figure 14C(d) shows the FDTD calculated light-intensity distribution in a horizontal plane at the depth of 300 nm below the photoresist surface. Moreover, the feature size and geometry can be finely tuned by changing the exposure time. With the increase of the exposure time, the size of holes became enlarged, and meanwhile, the shape changed from round to hexagonal. The shape change may result from the multiple light scattering among the spheres that were well-packed in a hexagonal lattice. Figure 14C(e)–(h) displays the SEM images of patterns fabricated using the masks of smaller colloidal particle sizes (700/800 and 500/600, diameter/pitch, nm) and different exposure parameters, showing excellent control of sizes/pitches of the features over wide dimension ranges. All these results can clearly reveal the versatility and the reproducibility of this unique fabrication scheme.

**ADVANCED
SCIENCE NEWS**
www.advancedsciencenews.com

**ADVANCED
MATERIALS
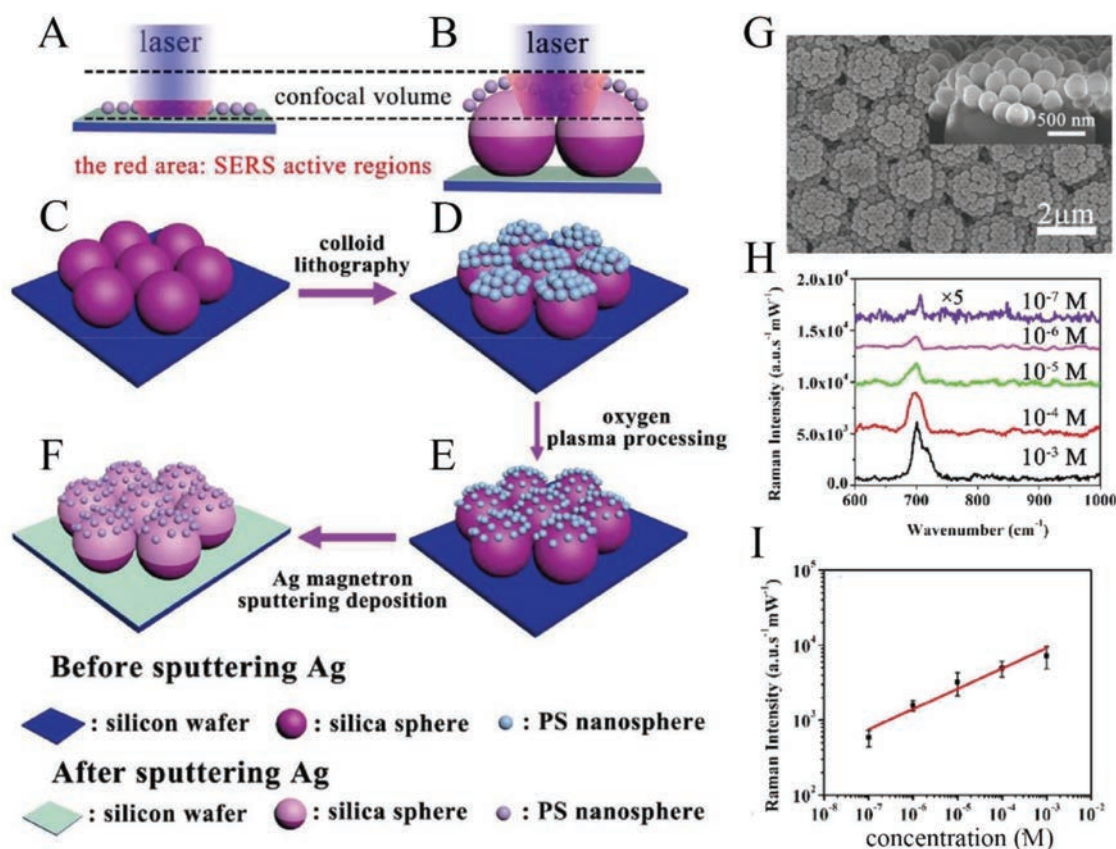TECHNOLOGIES**
www.advmattechnol.de

Figure 16. A) The diagram of three different sensor structures. B) The comparison of pressure sensitivities of different sensor structures: the planar film, single microdome film, and the interlocked microdome film. C) Current–voltage (I–V) curves of the pressure sensor with different applied pressures. D) Time-resolved static resistance change response of the sensor under repeated mechanical loads with pressures ranging from 11 to 1250 Pa. E) Response time of the pressure sensor with an applied pressure of 100 Pa. The insets show the section of the curve within the dashed lines which corresponds to the loading of pressure. F) Relative resistance changes of the sensor with repetition of 1000 loading/unloading cycles by 100 Pa. The inset shows the resistance change curves of the sensor extracted from the red part. Reproduced with permission.[95] Copyright 2017, American Chemical Society.

4. Other Practical Utilizations for Various Application Domains

Due to the features of simplicity, cost-effectiveness and well-controlled morphology, the self-assembly of colloidal spheres has been extensively applied to fabricate hierarchical and periodic 2D or 3D nanostructures, and subsequently applied in many technological fields such as the sensors and surface-enhanced Raman scattering (SERS).[95–98] **Figure 15**A shows the fabrication process of a flexible pressure sensor based on self-assembly of colloid PS microspheres and PDMS–PDMS pattern transfer technology. The 2 µm PS microspheres were self-assembled on glass to form MCCs and then covered with PDMS slurry (Figure 15B, SEM image of PS monolayer). After

peeling off from the glass substrate, the concave PDMS layer was obtained and acted as a template for the casting of PDMS slurry (Figure 15C, the corresponding SEM image). Finally, the convex PDMS with microdomes was achieved after the PDMS slurry form the concave PDMS layer. The SEM image of corresponding PDMS film with convex microdomes replicated from the concave PDMS is shown as the Figure 15D. The flexible pressure sensor is consisted of two pieces of PDMS films with microdome arrays, as displayed in Figure 15A.

The flexible pressure sensor with interlocking microdomes based on 2 µm PS spheres is presented in **Figure 16**A. As compared with the planar type and the planar/single microdome type, the response of the interlocked microdome sensor is very sensitive as illustrated in Figure 16B. The remarkable sensing
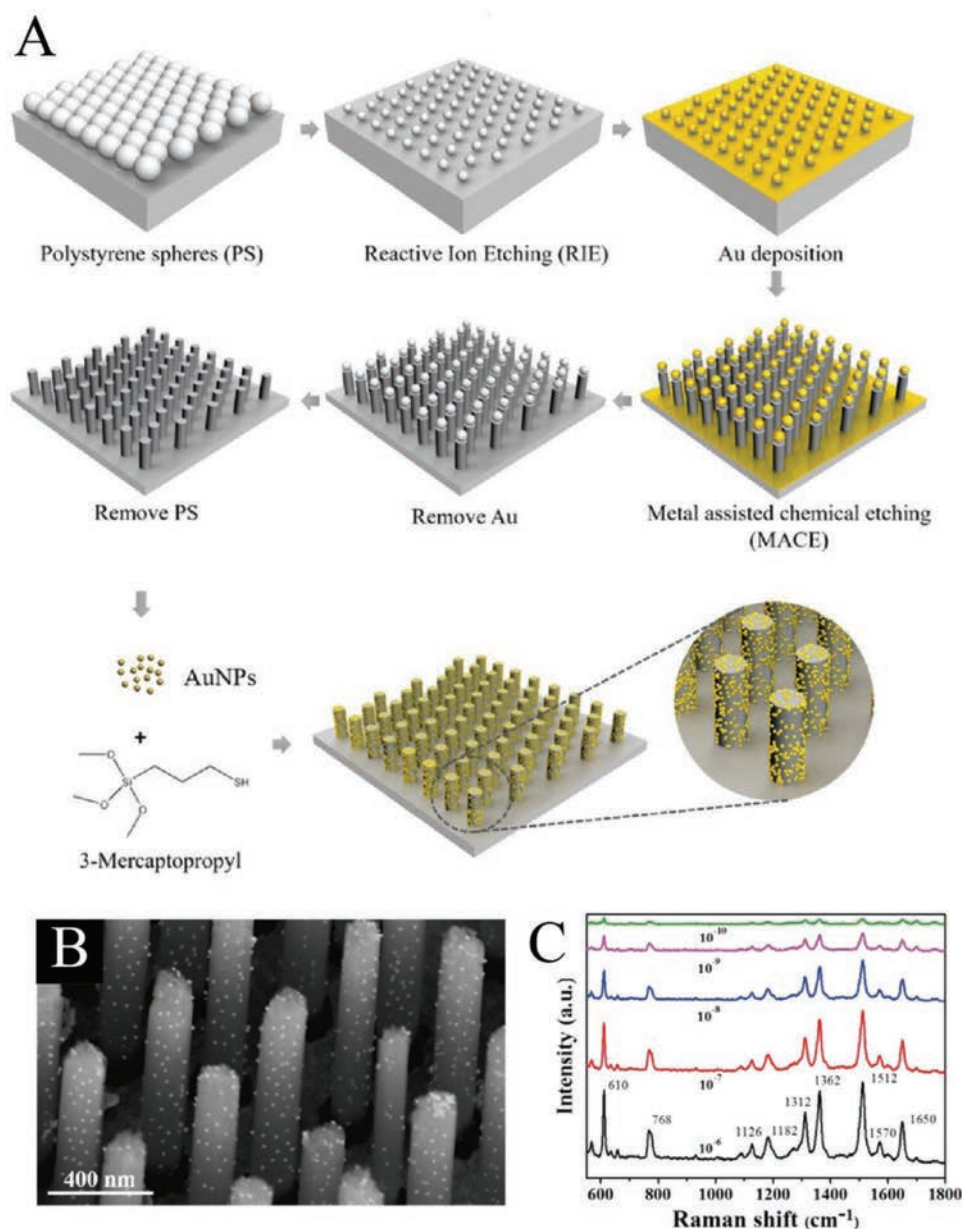
Figure 17. Schematic illustration of the preparation of SLNAs-Ag on clean Si wafers. A,B) The comparison between the planar and 3D microstructures. The "SERS active regions" were marked respectively with the red shadows. C) The silica spheres templates (denoted with red big spheres) prepared by spin-coating. D) A monolayer close-packed hexagonal structure of polystyrene (PS) particles (denoted with blue spheres) transferred onto the surface of silica spheres using colloid lithography. E) PS nanospheres were etching via oxygen plasma etching. F) Ag film deposition on etched PS nanospheres templates. G) SEM images of sunflower-like" nanoarrays decorated with Ag nanoparticles under the etching time of 5 min. H) SERS spectra of melamine with various concentrations ranging from 10^{-3} to 10^{-7} M. I) The calibration curve of normalized Raman intensity at 701 cm^{-1} versus the concentration of melamine. Reproduced with permission.[99] Copyright 2017, The Royal Society of Chemistry.

performance of this interlocked microdome sensor can be attributed to the change of the contact area, caused by the deformation of the microstructure. In addition, the electrical characteristics of the pressure sensor were also investigated. As given in Figure 16C, the current–voltage (I–V) curves of the pressure sensor under different weights were recorded. It is noted that the slope of the I–V curves increases with the increasing of the applied load under the constant voltage, indicating the resistance decrease as the external pressure rises. This linear characteristic of the I–V curves demonstrates that the device behavior obeys Ohm's contact behaviors. The reproducibility and stability properties of the pressure sensor under series of external pressures ranging from 11 to 1250 Pa were as well investigated. As depicted in Figure 16D, it is obvious that relative changes in resistance repeatedly take place under various external pressures, indicating the stable sensing performance and the great reproducibility of the pressure sensor upon various pressures regardless of low pressure, medium pressure, or high pressure. It also demonstrates that the pressure sensor can rapidly respond to the loading/unloading applied force without hysteresis. Figure 16E shows the response and relaxation time upon the application of a repeated pressure of 100 Pa. The similar

relative changes in resistance for the 6 cycles indicates a cycling stability of the flexible sensor under the pressure of 100 Pa. The insets indicate that the instant response time of sensor is impressively less than 100 ms. Meanwhile, the same value of relative resistance changes after 1000 loading/unloading cycles (Figure 16F) further demonstrate a high durability of the pressure sensor, which can be attributed to the excellent elasticity of the PDMS microdomes. This finding would confirm the double layer PDMS structure serving as a good preliminary platform for the fabrication of highly efficient pressure sensors.

Beside pressure sensors, **Figure 17** presents the application of self-assembly of colloidal spheres in the field of SERS.[99] The 3D hierarchical sunflower-like nanoarrays decorated with Ag nanoparticles (SLNAs-Ag) could be obtained by combining binary colloidal spheres (i.e., SiO$_2$ and PS spheres) and then decorating with Ag nanoparticles. First, Figure 17A,B shows the comparison of SERS active regions between the planar and 3D microstructures. The fabrication procedures of 3D SLNAs-Ag is then schematically illustrated in Figure 17C–F. Particularly, the monolayer of silica spheres was prepared on the substrate, and then acted as the basement for deposition of PS nanospheres via a spin-coating method (Figure 17C,D.

**ADVANCED
SCIENCE NEWS**
www.advancedsciencenews.com

**ADVANCED
MATERIALS
TECHNOLOGIES**
www.advmattechnol.de

Figure 18. A) Schematic illustration of Au nanoparticles (AuNPs)-conjugated Si nanorod (Si NR) arrays fabricating process. B) SEM images of AuNPs conjugated SiNR array. C) Raman spectra of Rhodamine 6G (R6G) molecules from 10^{-6} to 10^{-10} M on AuNPs@SiNR substrates. Reproduced with permission.[100] Copyright 2017, American Chemical Society.

After oxygen plasma etching, the Ag film was evaporated onto the sunflower-like nanoarrays consisting of silica nanospheres and PS nanospheres to generate an SERS substrate (Figure 17E,F), followed by the deposition of Ag on the SLNAs with etching time of 5 min. The SEM image of the SLNAs-Ag was presented in Figure 17G, and it can be clearly seen that there are obvious gaps between the adjacent PS nanospheres. After that, the SLNAs-Ag was dipped into different melamine water solutions with concentrations ranging from 10^{-3} to 10^{-7} M for SERS measurement. Figure 17H shows the SERS spectrums of various concentration levels of melamine from 10^{-3} to 10^{-7} M. The characteristic SERS spectra peaks at 701 cm^{-1} of melamine can be evidently observed for all concentration levels

of melamine. It is also noted that the SERS sensitivity at 701 cm^{-1} increases linearly with the increasing of the concentration of melamine (Figure 17I), demonstrating a high performance and low-cost SERS sensor of the SLNAs-Ag. The excellent control in the dimension of obtained hierarchical and periodic nanostructures enabled by colloidal self-assembly assisted fabrication techniques can further manipulate the detection peak and other SERS features for lots of other related applications.

The Si nanorod arrays fabricated by nanosphere lithography and metal-assisted chemical etching also can be applied in the area of SERS as shown in **Figure 18**.[100] As schematically depicted in Figure 18A, the SiNR arrays can be obtained from the following process: (i) self-assembly of a PS monolayer on

the Si surface, (ii) reduction of diameter of PS nanospheres by RIE processing; (iii) deposition of the Au layer on the substrate; (iv) metal-assisted chemical etching; (v) removal of Au and PS nanospheres; (vi) conjugation of AuNPs. In order to achieve the conjugation with AuNPs, 3-mercaptopropyltrimethoxysilane (MPTS) was used due to its simple structure, easily removed by photolysis and no disturbance in the Raman spectra of target molecules.[101] The MPTS consists of three $-OCH_3$ and sulfhydryl, the former can be connected with silicon hydroxyl by a chemical reaction, while the latter can link to AuNPs on the other side. Therefore, abundant AuNPs (diameter 20 nm) can be decorated on the surface of SiNRs as displayed in Figure 18B. The SERS measurement of the AuNPs@SiNR was further investigated by varying the concentration of R6G molecules from 10^{-6} to 10^{-10} M. As presented in Figure 18C, the Raman intensity increases gradually with the increasing of R6G concentration. It can be seen that the distinguishable signals at the concentration of 10^{-10} M can still be observed, in which all these demonstrate an excellent Raman sensitivity of AuNPs@SiNR.

5. Conclusions and Outlook

In summary, nanosphere lithography enabled with self-assembly of colloidal spheres, modification of monolayer colloidal crystals and other lithographic processes can evidently serve as a cost-effective and large-scale surface patterning method as well as a straightforward one-step 3D fabrication scheme. In this review, the current up-to-date status on the research and development of self-assembly of colloidal spheres for the fabrication of various hierarchical and periodic nanostructures are summarized. To be specific, we focus on the fundamentals of colloidal self-assembly, the functions of obtained monolayers of colloidal spheres and the successive construction of numerous nanostructures. The applications of as-fabricated hierarchical and periodic nanostructures are also introduced. In spite of the great success of self-assembly of colloidal spheres and the subsequent fabrication of nanostructures, there are still several issues associated with nanosphere lithography, which remains to be addressed in the near future for their practical utilizations. First, the defects in the monolayer colloidal crystals will be entailed to the subsequent nanostructures, resulting the deterioration of the devices based on these nanostructures. Thus, the defects-free of these self-assembled colloids in large-scale should be further achieved. Second, although there are various assembly methods developed, such as the Langmuir–Blodgett scheme, their processing time is somewhat longer than required. Therefore, continual development of rapid assembly of monolayer colloidal crystals would be essential for their successive deployments to the industry. Third, the polystyrene or silica spheres are frequently used to function as masks, templates or optical lens. More colloidal materials configured in spherical shapes with the better dimension, surface and mechanical property control should be developed in order to fulfill different requirements for other technological domains. Fourth, these nanosphere lithography techniques can also be combined with two or more different fabrication techniques to generate more sophisticated hierarchical and periodic

nanostructures, especially for 3D configured geometries. This would enable the simple fabrication approach for the realization of complex structures, which cannot be easily achieved by various newly developed 3D printing schemes. Finally, substantial efforts should be input into the practical applications of hierarchical and periodic nanostructures facilitated by these nanosphere lithography enabled fabrication routes. All these fabricated structures would contain unexceptionally large surface-to-volume ratio, which are advantageous for lots of utilizations in photovoltaics, photonics, energy storage, catalysis, and others. With all the reviewed features and promising properties of nanolithography based on these self-assembly of colloidal spheres, we anticipate this technique bringing promising applications in the near future.

Conflict of Interest

The authors declare no conflict of interest.

[1] X. Ye, L. Qi, *Nano Today* **2011**, *6*, 608.
[2] J. Zhang, Y. Li, X. Zhang, B. Yang, *Adv. Mater.* **2010**, *22*, 4249.
[3] S. M. Yang, S. G. Jang, D. G. Choi, S. Kim, H. K. Yu, *Small* **2006**, *2*, 458.
[4] J. Tian, J. Jin, F. Zheng, H. Zhao, *Langmuir* **2010**, *26*, 8762.
[5] U. C. Fischer, H. P. Zingsheim, *J. Vacuum Sci. Technol.* **1981**, *19*, 881.
[6] K. Satoh, M. Matsuda, K. Nagai, M. Kamigaito, *Nat. Nanotechnol.* **2007**, *2*, 145.
[7] Z. Ning, O. Voznyy, J. Pan, S. Hoogland, V. Adinolfi, J. Xu, M. Li, A. R. Kirmani, J. P. Sun, J. Minor, *Nat. Mater.* **2014**, *13*, 822.
[8] X. Liang, Y. Cheng, X. Xu, R. Dong, D. Li, Z. Zhou, R. Wei, G. Dong, S. W. Tsang, J. C. Ho, *Appl. Surf. Sci.* **2018**, *451*, 250.
[9] X. Liang, L. Shu, H. Lin, M. Fang, H. Zhang, G. Dong, S. Yip, F. Xiu, J. C. Ho, *Sci. Rep.* **2016**, *6*, 34139.
[10] D. S. Dolzhnikov, H. Zhang, J. Jang, J. S. Son, M. G. Panthani, T. Shibata, S. Chattopadhyay, D. V. Talapin, *Science* **2015**, *347*, 425.

**ADVANCED
SCIENCE NEWS**

www.advancedsciencenews.com

**ADVANCED
MATERIALS
TECHNOLOGIES**

www.advmattechnol.de

[11] Y. Shirasaki, G. J. Supran, M. G. Bawendi, V. Bulović, *Nat. Photonics* **2013**, *7*, 13.

[12] B. Kowalczyk, I. Lagzi, B. A. Grzybowski, *Curr. Opin. Colloid Interface Sci.* **2011**, *16*, 135.

[13] Y. Hu, Y. Liu, H. Qian, Z. Li, J. Chen, *Langmuir* **2010**, *26*, 18570.

[14] S. Nie, S. R. Emory, *Science* **1997**, *275*, 1102.

[15] K. Kneipp, Y. Wang, H. Kneipp, L. T. Perelman, I. Itzkan, *Phys. Rev. Lett.* **1997**, *78*, 1667.

[16] P. J. Dowding, B. Vincent, *Colloids Surf., A* **2000**, *161*, 259.

[17] R. J. Ansell, K. Mosbach, *J. Chromatogr., A* **1997**, *787*, 55.

[18] S. Omi, M. Saito, T. Hashimoto, M. Nagai, G. H. Ma, *J. Appl. Polym. Sci.* **1998**, *68*, 897.

[19] J. M. Desimone, E. E. Maury, Y. Z. Menceloglu, J. B. Mcclain, T. J. Romack, J. R. Combes, *Science* **1994**, *265*, 356.

[20] M. Peer, A. Qajar, R. Rajagopalan, H. C. Foley, *Carbon* **2013**, *51*, 85.

[21] Z. Z. Gu, H. Chen, S. Zhang, L. Sun, Z. Xie, Y. Ge, *Colloids Surf., A* **2007**, *302*, 312.

[22] Q. He, X. Cui, F. Cui, L. Guo, J. Shi, *Microporous Mesoporous Mater.* **2009**, *117*, 609.

[23] T. Qiu, B. Luo, M. Giersig, E. M. Akinoglu, L. Hao, X. Wang, L. Shi, M. Jin, L. Zhi, *Small* **2015**, *10*, 4136.

[24] X. A. Zhang, J. Elek, C. H. Chang, *ACS Nano* **2013**, *7*, 6212.

[25] Y. Wang, N. Lu, H. Xu, G. Shi, M. Xu, X. Lin, H. Li, W. Wang, D. Qi, Y. Lu, *Nano Res.* **2010**, *3*, 520.

[26] J. Yoo, *Sol. Energy* **2010**, *84*, 730.

[27] C. J. Heo, S. H. Kim, S. G. Jang, S. Y. Lee, S. M. Yang, *Adv. Mater.* **2009**, *21*, 1726.

[28] R. Walter, A. Tittl, A. Berrier, F. Sterl, T. Weiss, H. Giessen, *Adv. Opt. Mater.* **2015**, *3*, 398.

[29] J. C. Li, Y. L. Chen, S. Y. Lu, *U.S. Patent Application 14/791*, 241, **2015**.

[30] Y. Zhang, T. Wei, Z. Xiong, L. Shang, *Appl. Phys. Lett.* **2014**, *105*, 013108.

[31] C. L. Haynes, R. P. Van Duyne, *J. Phys. Chem. B* **2001**, *105*, 5599.

[32] J. C. Hulteen, R. P. Van Duyne, *J. Vac. Sci. Technol., A* **1995**, *13*, 1553.

[33] J. H. Moon, W. S. Kim, J.-W. Ha, S. G. Jang, S. M. Yang, J. K. Park, *Chem. Commun.* **2005**, 4107.

[34] M. H. Wu, C. Park, G. M. Whitesides, *J. Colloid Interface Sci.* **2003**, *265*, 304.

[35] A. Douvas, P. Argitis, K. Misiakos, D. Dimotikali, P. S. Petrou, S. E. Kakabakos, *Biosens. Bioelectron.* **2002**, *17*, 269.

[36] C. Vieu, F. Carcenac, A. Pépin, Y. Chen, M. Mejias, A. Lebib, L. Manin-Ferlazzo, L. Couraud, H. Launois, *Appl. Surf. Sci.* **2000**, *164*, 111.

[37] J. Taniguchi, K. Koga, Y. Kogo, I. Miyamoto, *Microelectron. Eng.* **2006**, *83*, 940.

[38] A. Kosiorek, W. Kandulski, H. Glaczynska, M. Giersig, *Small* **2005**, *1*, 439.

[39] L. Ji, Y. F. Chang, B. Fowler, Y. C. Chen, T. M. Tsai, K. C. Chang, M. C. Chen, T. C. Chang, S. M. Sze, E. T. Yu, *Nano Lett.* **2014**, *14*, 813.

[40] H. Ceylan, M. Urel, T. S. Erkal, A. B. Tekinay, A. Dana, M. O. Guler, *Adv. Funct. Mater.* **2013**, *23*, 2100.

[41] S. Cataldo, J. Zhao, F. Neubrech, B. Frank, C. Zhang, P. V. Braun, H. Giessen, *ACS Nano* **2012**, *6*, 979.

[42] S. W. Lee, K. S. Lee, J. Ahn, J. J. Lee, M. G. Kim, Y. B. Shin, *ACS Nano* **2011**, *5*, 897.

[43] W. Wu, M. Hu, F. S. Ou, Z. Li, R. S. Williams, *Nanotechnology* **2010**, *21*, 255502.

[44] B. Cui, T. Veres, *Microelectron. Eng.* **2007**, *84*, 1544.

[45] A. S. Dimitrov, K. Nagayama, *Langmuir* **1996**, *12*, 1303.

[46] X. Li, J. Wang, J. Zhang, X. Yan, X. Zhang, D. Zhu, W. Li, X. Zhang, B. Yang, *Langmuir* **2010**, *26*, 2930.

[47] P. Jiang, M. J. McFarland, *J. Am. Chem. Soc.* **2004**, *126*, 13778.

[48] S. O. Lumsdon, E. W. Kaler, O. D. Velev, *Langmuir* **2004**, *20*, 2108.

[49] M. Trau, D. Saville, I. Aksay, *Science* **1996**, *272*, 706.

[50] M. Bardosova, M. E. Pemble, I. M. Povey, R. H. Tredgold, *Adv. Mater.* **2010**, *22*, 3104.

[51] R. van Dommelen, P. Fanzio, L. Sasso, *Adv. Colloid Interface Sci.* **2018**, *251*, 97.

[52] L. J. Cote, F. Kim, J. Huang, *J. Am. Chem. Soc.* **2009**, *131*, 1043.

[53] H. Du, Y. Bai, Z. Hui, L. Li, Y. Chen, X. Tang, T. Li, *Langmuir* **1997**, *13*, 2538.

[54] J. H. Clint, S. E. Taylor, *Colloids Surf.* **1992**, *65*, 61.

[55] M. Bardosova, P. Hodge, V. Smatko, R. Tredgold, D. Whitehead, *Acta Phys. Slovaca* **2004**, *54*, 409.

[56] V. Lotito, T. Zambelli, *Langmuir* **2016**, *32*, 9582.

[57] P. Gao, J. He, S. Zhou, X. Yang, S. Li, J. Sheng, D. Wang, T. Yu, J. Ye, Y. Cui, *Nano Lett.* **2015**, *15*, 4591.

[58] K. Shinotsuka, Y. Kajita, K. Hongo, Y. Hatta, *Langmuir* **2015**, *31*, 11452.

[59] V. Burtsev, V. Marchuk, A. Kugaevskiy, O. Guselnikova, R. Elashnikov, E. Miliutina, P. Postnikov, V. Svorcik, O. Lyutakov, *Appl. Surf. Sci.* **2018**, *433*, 443.

[60] F. Teng, N. Li, D. Xu, D. Xiao, X. Yang, N. Lu, *Nanoscale* **2017**, *9*, 449.

[61] Z. Huang, H. Fang, J. Zhu, *Adv. Mater.* **2007**, *19*, 744.

[62] J. Gong, N. Wu, *Langmuir* **2017**, *33*, 5769.

[63] X. Li, *Curr. Opin. Solid State Mater. Sci.* **2012**, *16*, 71.

[64] Z. Huang, N. Geyer, P. Werner, J. de Boor, U. Gosele, *Adv. Mater.* **2011**, *23*, 285.

[65] C. Chartier, S. Bastide, C. Lévy-Clément, *Electrochim. Acta* **2008**, *53*, 5509.

[66] Y. Li, X. Ye, Y. Ma, L. Qi, *Small* **2015**, *11*, 1183.

[67] L. Xu, Z. Yin, S. W. Cao, Z. Fan, X. Zhang, H. Zhang, C. Xue, *Chem. - Eur. J.* **2014**, *20*, 2742.

[68] W. Wu, A. Katsnelson, O. G. Memis, H. Mohseni, *Nanotechnology* **2007**, *18*, 485302.

[69] H. Lin, H. Y. Cheung, F. Xiu, F. Wang, S. Yip, N. Han, T. Hung, J. Zhou, J. C. Ho, C. Y. Wong, *J. Mater. Chem. A* **2013**, *1*, 9942.

[70] H. Lin, M. Fang, H. Y. Cheung, F. Xiu, S. Yip, C. Y. Wong, J. C. Ho, *RSC Adv.* **2014**, *4*, 50081.

[71] F. Xiu, H. Lin, M. Fang, G. Dong, S. Yip, J. C. Ho, *Pure Appl. Chem.* **2014**, *86*, 557.

[72] H. Lin, F. Xiu, M. Fang, S. Yip, H. Y. Cheung, F. Wang, N. Han, K. S. Chan, C. Y. Wong, J. C. Ho, *ACS Nano* **2014**, *8*, 3752.

[73] X. Xu, Q. Yang, N. Wattanatorn, C. Zhao, N. Chiang, S. J. Jonas, P. S. Weiss, *ACS Nano* **2017**, *11*, 10384.

[74] A. Pakes, G. Thompson, P. Skeldon, P. Morgan, *Corros. Sci.* **2003**, *45*, 1275.

[75] S. Z. Chu, K. Wada, S. Inoue, S. Todoroki, *J. Electrochem. Soc.* **2002**, *149*, B321.

[76] I. Minguez-Bacho, F. Scheler, P. Buttner, K. Bley, N. Vogel, J. Bachmann, *Nanoscale* **2018**, *10*, 8385.

[77] N. T. Suen, S. F. Hung, Q. Quan, N. Zhang, Y. J. Xu, H. M. Chen, *Chem. Soc. Rev.* **2017**, *46*, 337.

[78] Z. W. Seh, J. Kibsgaard, C. F. Dickens, I. Chorkendorff, J. K. Norskov, T. F. Jaramillo, *Science* **2017**, *355*, eaad4998.

[79] M. Fang, G. Dong, R. Wei, J. C. Ho, *Adv. Energy Mater.* **2017**, *7*, 1700559.

[80] M. Fang, W. Gao, G. Dong, Z. Xia, S. Yip, Y. Qin, Y. Qu, J. C. Ho, *Nano Energy* **2016**, *27*, 247.

[81] K. Chen, D. D. Thang, S. Ishii, R. P. Sugavaneshwa, T. Nagao, *Opt. Mater. Express* **2015**, *5*, 353.

[82] W. Wang, J. Dong, X. Ye, Y. Li, Y. Ma, L. Qi, *Small* **2016**, *12*, 1469.

[83] G. K. Mor, K. Shankar, O. K. Varghese, C. A. Grimes, *J. Mater. Res.* **2004**, *19*, 2989.

[84] J. R. Jennings, A. Ghicov, L. M. Peter, P. Schmuki, A. B. Walker, *J. Am. Chem. Soc.* **2008**, *130*, 13364.

[85] N. Negishi, K. Takeuchi, T. Ibusuki, *J. Mater. Sci.* **1998**, *33*, 5789.

1800541 (18 of 19)

[86] J. Buckeridge, K. T. Butler, C. R. A. Catlow, A. J. Logsdail, D. O. Scanlon, S. A. Shevlin, S. M. Woodley, A. A. Sokol, A. Walsh, *Chem. Mater.* **2015**, *27*, 3844.

[87] D. O. Scanlon, C. W. Dunnill, J. Buckeridge, S. A. Shevlin, A. J. Logsdail, S. M. Woodley, C. R. Catlow, M. J. Powell, R. G. Palgrave, I. P. Parkin, *Nat. Mater.* **2013**, *12*, 798.

[88] L. W. Zhang, Y. J. Wang, H. Y. Cheng, W. Q. Yao, Y. F. Zhu, *Adv. Mater.* **2009**, *21*, 1286.

[89] C. H. Chang, L. Tian, W. R. Hesse, H. Gao, H. J. Choi, J. G. Kim, M. Siddiqui, G. Barbastathis, *Nano Lett.* **2011**, *11*, 2533.

[90] C. R. Worthington, J. T. Winthrop, *J. Opt. Soc. Am.* **1965**, *55*, 373.

[91] J. Zhang, B. Yang, *Adv. Funct. Mater.* **2010**, *20*, 3411.

[92] M. Fang, H. Lin, H. Y. Cheung, F. Xiu, L. Shen, S. Yip, E. Y. Pun, C. Y. Wong, J. C. Ho, *ACS Appl. Mater. Interfaces* **2014**, *6*, 20837.

[93] M. Fang, H. Lin, H. Y. Cheung, S. Yip, F. Xiu, C. Y. Wong, J. C. Ho, *Adv. Opt. Mater.* **2014**, *2*, 855.

[94] T. Y. Jeon, H. C. Jeon, S. Y. Lee, T. S. Shim, J. D. Kwon, S. G. Park, S. M. Yang, *Adv. Mater.* **2014**, *26*, 1421.

[95] Y. Zhang, Y. Hu, P. Zhu, F. Han, Y. Zhu, R. Sun, C. P. Wong, *ACS Appl. Mater. Interfaces* **2017**, *9*, 35968.

[96] Y. Luo, X. Jiang, L. Liu, G. Si, *Nanosci. Nanotech. Let.* **2018**, *10*, 1.

[97] H. S. Lee, J. Chung, G. T. Hwang, C. K. Jeong, Y. Jung, J. H. Kwak, H. Kang, M. Byun, W. D. Kim, S. Hur, *Adv. Funct. Mater.* **2014**, *24*, 6914.

[98] C. Pang, G. Y. Lee, T. I. Kim, S. M. Kim, H. N. Kim, S. H. Ahn, K. Y. Suh, *Nat. Mater.* **2012**, *11*, 795.

[99] X. Zhang, X. Xiao, Z. Dai, W. Wu, X. Zhang, L. Fu, C. Jiang, *Nanoscale* **2017**, *9*, 3114.

[100] D. Lin, Z. Wu, S. Li, W. Zhao, C. Ma, J. Wang, Z. Jiang, Z. Zhong, Y. Zheng, X. Yang, *ACS Nano* **2017**, *11*, 1478.

[101] I. Choi, Y. S. Huh, D. Erickson, *Microfluidics Nanofluidics* **2012**, *12*, 663.